NBSIR 82-2629

1981 Annual Report: Optical Measurements for Interfacial Conduction and Breakdown

U.S. DEPARTMENT OF COMMERCE
National Bureau of Standards
National Engineering Laboratory
Center for Electronics and Electrical Engineering
Electrosystems Division
Washington, DC 20234

January 1983

Prepared for:
Department of Energy
Division of Electric Energy Systems
Washington, DC 20585

NBSIR 82-2629

1981 ANNUAL REPORT: OPTICAL MEASUREMENTS FOR INTERFACIAL CONDUCTION AND BREAKDOWN

R. E. Hebner, Jr., E. F. Kelley, and J. N. Hagler

U.S. DEPARTMENT OF COMMERCE
National Bureau of Standards
National Engineering Laboratory
Center for Electronics and Electrical Engineering
Electrosystems Division
Washington, DC 20234

January 1983

Prepared for:
Department of Energy
Division of Electric Energy Systems
Washington, DC 20585

U.S. DEPARTMENT OF COMMERCE, Malcolm Baldrige, *Secretary*
NATIONAL BUREAU OF STANDARDS, Ernest Ambler, *Director*

TABLE OF CONTENTS

LIST OF FIGURES

LIST OF FIGURES (cont.)

LIST OF FIGURES (cont.)

LIST OF TABLES

Executive Summary

Power system apparatus employs composite insulation. For example, in a transformer, paper pressboard and transformer oil provide the necessary electrical insulation. Economic considerations provide incentives to reduce the size of the apparatus, yet retain the same voltage rating. This serves to increase the electric field stress on the composite insulation which increases the probability of failure unless steps are taken to make the insulation more reliable. In order to improve the electrical characteristics of composite insulation, it is important to determine what factors influence its electrical breakdown.

Space or surface charge and contaminants affect the breakdown strength of single component insulation and composite insulation systems. Charge distributions modify the electric field from what would be calculated from geometrical considerations alone and thereby produce regions of field intensification which can increase breakdown probability. Particle or chemical contaminants may also decrease the electrical strength of a system. These factors need to be investigated throughout the temperature range which can exist in practical apparatus.

Before space-charge measurements are performed on composite insulation systems via electro-optical techniques, it is necessary to understand the role of space charge in transformer oil by itself under a variety of contaminants and temperatures. Kerr-effect measurements are reported here for contaminated transformer oil from room temperature to 68°C, and for clean oil the measurements are extended to 107°C. In all the observed cases, the field intensifications due to space charge are less than 10% of the average field and usually less than 5%.

In order to supplement the space-charge measurements in composite insulation systems, mathematical and computer modeling of space and surface charge was included in order to anticipate the effects of charges. Substantial charge densities were found to be necessary in order to modify the electric field in such a way that a change in the breakdown strength could be anticipated.

Breakdown tests were performed on a paper-oil interfacial system where a paper sample is held parallel to the field and touching both electrodes. This study helps to understand what factors influence the reduction of breakdown strength and should give insight to the electro-optical measurements. It was determined that the handling of the paper samples was critical to the tendency for the breakdown to occur along the paper. When contaminated oil was used, it appeared that large particle contaminants lowered the breakdown strength but did not cause the breakdown to prefer the interface.

The work done so far has served to eliminate factors which would readily account for a lower electrical strength of composite insulation than the strength of each component insulant by itself. This information focuses attention on other factors such as water and particle contamination as being possible sources of space charge or failure, and it forces our attention to higher temperatures.

1981 ANNUAL REPORT: OPTICAL MEASUREMENTS FOR INTERFACIAL CONDUCTION AND BREAKDOWN

R. E. Hebner, Jr., E. F. Kelley, and J. N. Hagler

Abstract

This report presents measurements and calculations contributing to the understanding of space and surface charges in practical insulation systems. Calculations are presented which indicate the size of charge densities necessary to appreciably modify the electric field from what would be calculated from geometrical considerations alone. Experimental data is also presented which locates the breakdown in an electrode system with a paper sample bridging the gap between the electrodes. It is found that with careful handling, the breakdown does not necessarily occur along the interface even if heavily contaminated oil is used.

The effects of space charge in the bulk liquid are electro-optically examined in nitrobenzene and transformer oil. Several levels of contamination in transformer oil are investigated. Whereas much space charge can be observed in nitrobenzene, very little space charge, if any, can be observed in the transformer oil samples even at temperatures near 100°C.

Key words: breakdown; composite insulation; dielectrics; electric field calculation; electro-optics; high voltage; insulation; interfaces; Kerr effect; liquids; solids.

I. INTRODUCTION

The objectives of this investigation are to develop apparatus and appropriate procedures for the optical measurement of interfacial electric field and space-charge density of materials for electric power equipment and systems; to understand the interfacial prebreakdown and breakdown processes in specific insulating systems; and to demonstrate the applicability of the developed instrumentation and procedures in future development and design of systems involving liquid-solid dielectrics.

Because space-charge effects are evident in gaseous composite systems [1,2], it is tempting to extend those results to explain the behavior of liquids. The results reported here caution presuming too much of a role of space charge in modifying the prebreakdown electric fields in liquid and liquid/solid systems. Specific experimental models using transformer oil, paper, or pressboard are studied so that these results are applicable to the power industry.

This report first discusses the quantitative effects of surface charge on an interface in modifying the electric field. This extends the mathematical modeling done in the last annual report in that an estimation technique is developed to place an upper bound on field distortions. Additionally, computer solutions to the electrostatic problem of a charged interface are presented.

An experimental study is next presented which indicates the contribution of the interface to breakdown. This work extends previous results in that it includes the effects of contaminated transformer oil and documents the handling of the paper interface.

Finally, electro-optical measurements are presented which contrast the space-charge effects found in nitrobenzene with the findings in transformer oil. The transformer oil measurements were extended to include contaminated transformer oil, and the clean transformer oil measurements were extended to over 100°C.

II. RESEARCH PLAN

Power system apparatus employs solid insulation for structural support and electrical insulation. As in the case of many transformers, an insulating liquid fills the remaining volume of the apparatus. In order to reduce the size of the apparatus (with obvious economic advantages), yet retain the same voltage capability, the composite insulation must be subjected to higher electrical stresses. Unless steps are taken to increase the breakdown strength, such a reduction in size will increase the probability of failure of the apparatus. This economic incentive strongly suggests that the behavior of composite insulation systems be characterized at a fundamental level.

The presence of space or surface charge in a composite insulation system will change the electric field from what it would be if such charge were absent. Thus if a uniform field (as provided by the geometry of two parallel

plates) were modified by space charge while the voltage on the plates is held constant, the uniformity of the field would be destroyed and field intensification would occur in some region between the plates. The probability of breakdown would be increased due to the increase in the local electric field, and the apparatus would be more likely to fail. For this reason, it is important that the role of space charge in composite insulation systems be determined, its source be identified, and its control be attempted. Other factors such as particle or chemical contamination may influence either the breakdown probability or the existence of space charge in composite insulation systems. Hence such contaminants need to be investigated.

To obtain fundamental understanding of interfacial breakdown, mathematical modeling is combined with experiments. In the mathematical model phase of the study, the distortion of the electric field, in typical geometries due to interfacial space charge, is calculated. Experimental techniques to measure the electric field are also being developed to verify the applicability of the mathematical model to practical systems. Electro-optical measurements, in this case based on the Kerr effect, were selected because they offer high temporal and spatial resolution and do not perturb the system under investigation. Additionally, in order to be directly applicable to practical power system apparatus, these experimental observations must cover the range of temperature possible in such apparatus, i.e., from room temperature to over 150°C.

Before the field modifying effects of an interface can be inferred from electro-optical measurement, it is necessary to document the space-charge behavior in transformer oil alone over a range of temperatures and contaminations. Only after such characterizations are made upon the oil can the effects of an interface be distinguished from the nature of oil. This is the emphasis of the electro-optical measurements reported here.

The measurement of breakdown characteristics of an interfacial system is carried out upon a paper-oil system where the paper is held parallel to the electric field and touching both electrodes. This system is subjected to various handling procedures to identify the factors which contribute to the breakdown probability. Both clean and contaminated oil are used. The purpose of such an investigation is to isolate those factors which contribute to decreasing the breakdown strength of a composite system.

Earlier in this work, some effort was directed toward understanding dielectrophoretic phenomena because it was presumed that dielectrophoretic forces on particles and/or bubbles may make a significant contribution to interfacial breakdown. Although that work was very well done and expanded the understanding and the control of dielectrophoretic effects, our investigation failed to establish a direct connection between these effects and interfacial breakdown. That phase of the investigation, therefore, was not continued.

In summary, the research proceeds by studying model systems in which interfacial breakdown is produced. Techniques are being developed to measure and to calculate the electric field distribution in the vicinity of the interfaces. This approach is intended to provide a quantitative understanding of interfacial breakdown. It is anticipated that this improved understanding will lead to improved tests on, and

standards for, insulating materials and systems. In addition, this work should yield measurement techniques which will help other researchers in the development of improved apparatus.

III. INTERFACIAL PHENOMENA

A. EFFECTS OF SURFACE AND SPACE CHARGE

It may be speculated that a primary cause of breakdown (flashover) is the intensification of the electric field due to an accumulation of space or surface charge within a system. However, carefully controlled experiments have shown that this flashover can occur quite far from where charge is assumed to be accumulating [3].

Here we present the results of the investigation into the role which space and surface charge play in enhancing an electric field. Using mathematical models, we have estimated the enhancement of the magnitude of the electric field in two situations.

Section 1 contains an analysis of the effect of accumulation of surface charge on an interface placed at right angles to (and between) two parallel electrodes upon which a potential difference has been applied. Different dielectric materials are assumed on either side of the interface. Such a model would be suggested by sandwiching a thick pressboard spacer between parallel plates where the spacer only fills half the region between the plates. The remaining half might be filled with transformer oil. Or it could describe a solid-gas interfacial system. In either case, the effect of surface charge is of interest. We use Fourier series techniques to obtain an estimate of the field enhancement due to the surface charge and show that this enhancement decreases exponentially with the distance from the interface.

In section 2, we outline the results of a preliminary investigation into the effect of introducing a thin cylinder of charge into the gap between two spheres. Such a model is useful in considering the effects of charged particles electrohydrodynamically confined in a columnar region between two electrodes [4]. This study was carried out using a computer code (resident at NBS) for solving two dimensional elliptic boundary value problems. We derive the following result: given two spheres each of radius 8 cm separated by a gap of 2 cm with a potential difference of 20 kV placed upon them, and with a thin cylinder of charge (total charge 1.2×10^4pC) introduced in the gap; then the enhancement 3 cm from the axis of symmetry is at most 2%.

1. Surface Charge on Interface

As a first example of the effect of space or surface charge accumulation on the electric field, consider the following problem: two parallel electrodes are located at $z = 0$ (cm) and $z = 1$ (cm). The space between the electrodes is divided into two regions: the region $y < 0$ is filled with an insulator with permittivity $\varepsilon_1 = \kappa_1 \varepsilon_0$ and the region $y > 0$ is filled with an insulator $\varepsilon_2 = \kappa_2 \varepsilon_0$. (Thus, we assume an interface located at $y = 0$.)

Assume further that a potential difference V is placed across the plates and a surface charge density $\rho(z)$ exists on the interface (see fig. 1). (The derivation of the series solution presented below was considered first in [3].)

Laplace's equation for the potential ϕ in the regions bounded by the electrodes is

$$\nabla^2 \phi\,(y,z) = 0, \tag{1}$$

with the following boundary conditions:

$$\phi(y,0) = 0, \quad \phi(y,1) = V, \tag{2}$$

$$\lim_{y \to \pm\infty} \phi(y,z) \neq \infty, \tag{3}$$

$$\phi \text{ is continuous at } (0,z) \text{ for } 0 \leq z \leq 1, \tag{4}$$

$$\varepsilon_1 \phi_y(0^-,z) - \varepsilon_2 \phi_y(0^+,z) = \rho(z) \quad \text{for } 0 \leq z \leq 1 . \tag{5}$$

Here, ϕ_y denotes the partial derivative of ϕ with respect to y.

First, assume V = 0. We solve eqs (1) - (3) separately in the regions $y < 0$ and $y > 0$ and use conditions (4) and (5) to find the general solution.

Using the usual procedure of separation of variables and eqs (1) - (3), we obtain solutions to Laplace's equation

$$\phi_n(y,z) = \begin{cases} e^{-n\pi y} \sin(n\pi z), & y > 0 \\ e^{n\pi y} \sin(n\pi z), & y < 0. \end{cases}$$

So, for $y > 0$, the resulting potential may be written as

$$\phi(y,z) = \sum_{n=1}^{\infty} a_n e^{-n\pi y} \sin(n\pi z), \tag{6}$$

and for $y < 0$,

$$\phi(y,z) = \sum_{n=1}^{\infty} b_n e^{n\pi y} \sin(n\pi z), \tag{7}$$

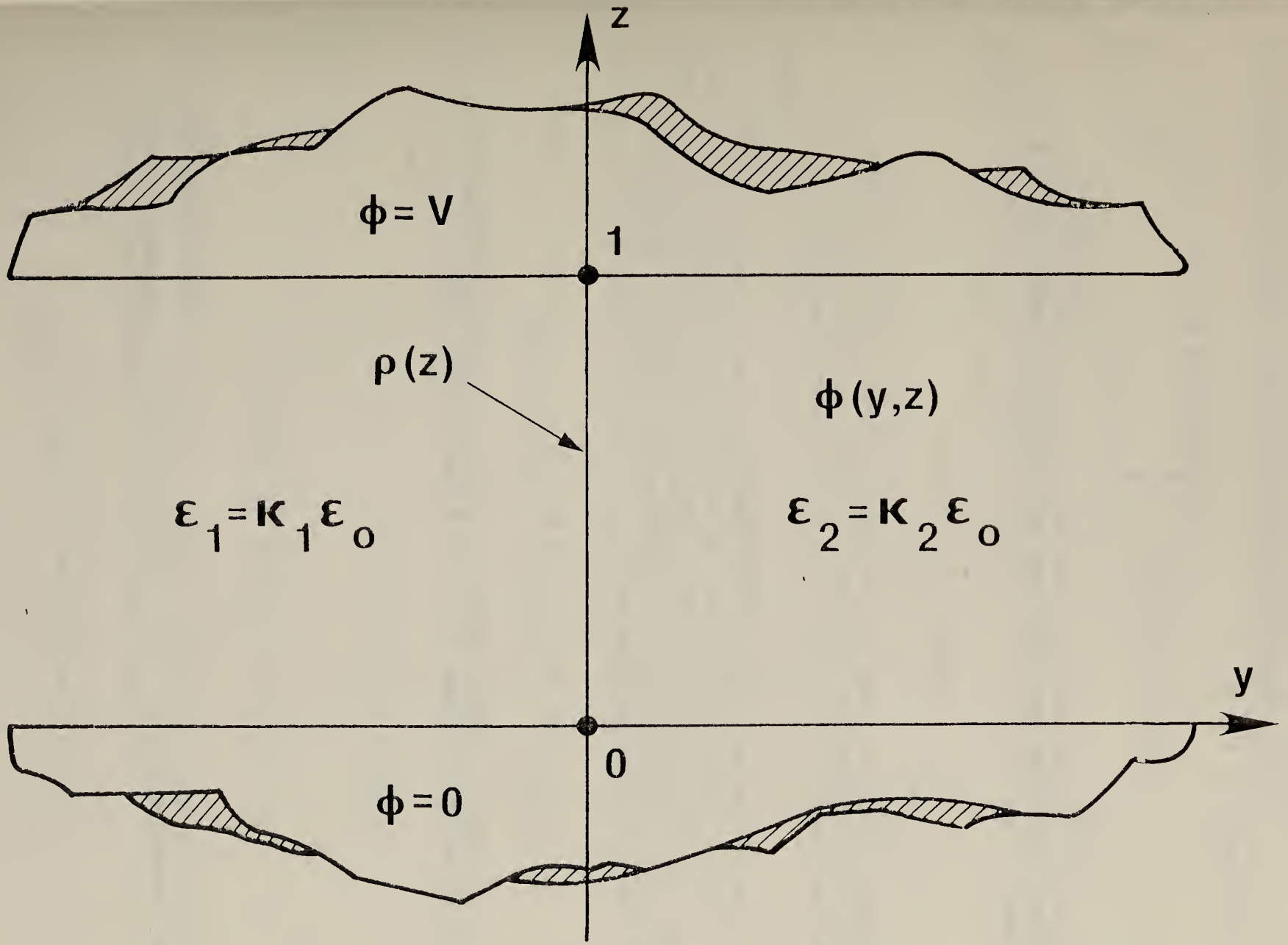

Fig. 1. Surface charge at the interface of two regions of differing permittivity between parallel plates having a potential difference of V.

for some sequences (a_n) and (b_n).

The orthogonality conditions for the sequence of functions $\sin(n\pi z)$, $n=1,2,..$ on $0 \leq z \leq 1$ is

$$\int_0^1 \sin(n\pi z)\sin(m\pi z)dz = \begin{cases} 1/2 \text{ if } m = n \\ 0 \text{ if } m \neq n \end{cases} . \qquad (8)$$

Let $y \to 0^+$ in eq (6) and $y \to 0^-$ in eq (7). The continuity condition (4) says that these two limits must be identical for each z, $0 \leq z \leq 1$. Thus

$$\sum_{n=1}^{\infty} a_n \sin(n\pi z) = \sum_{n=1}^{\infty} b_n \sin(n\pi z).$$

Integrating each of these series against $\sin(n\pi z)$, $n = 1,2,...$ and using the orthogonality relations (8) yields $a_n = b_n$, $n = 1,2,...$. So, for some numbers C_n, $n = 1,2,...$the potential may be expressed as

$$\phi(y,z) = \sum_{n=1}^{\infty} C_n e^{-n\pi|y|} \sin(n\pi z). \qquad (9)$$

Note that the potential $\phi(y,z)$ is a symmetric function about the y axis, i.e., $\phi(y,z) = \phi(-y,z)$. In particular, $\phi_y(0^-,z) = -\phi_y(0^+,z)$ for $0 \leq z \leq 1$. We obtain, using eq (5),

$$\phi_y(0^-,z) = \rho(z)/(\varepsilon_1+\varepsilon_2) \text{ for } 0 \leq z \leq 1. \qquad (10)$$

To obtain the coefficients C_n, differentiate the series in eq (9) term by term with respect to y for $y<0$ and let $y \to 0^-$. Then

$$\phi_y(0^-,z) = \sum_{n=1}^{\infty} n\pi C_n \sin(n\pi z),$$

or

$$\rho(z)/(\varepsilon_1+\varepsilon_2) = \sum_{n=1}^{\infty} n\pi\, C_n \sin(\pi z).$$

Integrating each side against $\sin(n\pi z)$, $n = 1,2,....$ and using eq (8) once again, we obtain

$$\int_0^1 [\rho(z)/(\varepsilon_1+\varepsilon_2)]\sin(n\pi z) = n\pi C_n/2.$$

This allows us to express the C_n in terms of the charge density

$$C_n = (G/n\pi) \int_0^1 \rho(z)\sin(n\pi z)dz, \tag{11a}$$

where

$$G = 2/(\varepsilon_1+\varepsilon_2). \tag{11b}$$

This completes the derivation in the case where the potential is "zero" on both electrodes. If the potential on the top electrode is now assumed to be V, then we easily obtain the solution

$$\phi(y,z) = Vz + \sum_{n=1}^{\infty} C_n e^{n\pi|y|}\sin(n\pi z), \tag{12}$$

where the C_n's are given by (11).

Before considering some of the consequences of this derivation, we recall briefly some elementary mathematical facts. The proofs of these assertions are standard and can be found in many books which discuss Fourier series and infinite series. (For example, see [5,6].)

(1) The sum of a geometric series: If $|x| < 1$, then

$$\sum_{n=1}^{\infty} x^n = x/(1-x).$$

(2) The Schwartz inequality: If $\sum_{n=1}^{\infty} a_n^2 < \infty$ and $\sum_{n=1}^{\infty} b_n^2 < \infty$ then

$$|\sum_{n=1}^{\infty} a_n b_n| < \infty$$

and

$$|\sum_{n=1}^{\infty} a_n b_n| \leq (\sum_{n=1}^{\infty} a_n^2)^{1/2}(\sum_{n=1}^{\infty} b_n^2)^{1/2}.$$

(3) Parseval's identity:

Since the sequence of functions $\sin(n\pi z)$, $n=1,2,\ldots$ is a complete orthogonal system on $0 \leq z \leq 1$, the following holds:
If

$$\int_0^1 |f^2(z)|dz < \infty,$$

and if

$$a_n = \int_0^1 f(z)\sin(n\pi z)dz, \quad n = 1, 2, \ldots ,$$

then

$$\int_0^1 |f^2(z)|\,dz = 2\sum_{n=1}^{\infty} |a_n|^2.$$

We are now ready to proceed with our estimate of the magnitude of the electric field E_0 due to the surface charge. So let us assume that both electrodes satisfy $\phi = 0$. Also we impose the restriction that the surface charge density $\rho(z)$ is square integrable on the interval $0 \leq z \leq 1$, i.e.,

$$\int_0^1 \rho^2(z)dz < \infty .$$

Defining

$$a_n = \int_0^1 \rho(z)\sin(n\pi z)dz,$$

then the coefficients (eq (11)) in the expansion for the potential may be written as

$$C_n = 2a_n/[n\pi(\varepsilon_1+\varepsilon_2)] = Ga_n/n\pi,$$

and the potential becomes

$$\phi(y,z) = (G/\pi)\sum_{n=1}^{\infty} (a_n/n)e^{-n|y|}\sin(n\pi z). \tag{13}$$

Since the potential is symmetric about the y axis, we restrict the remainder of this discussion to the region $y > 0$. Differentiating the series (13) term by term yields the negative of the electric field components produced by the charge density

$$\phi_y(y,z) = -G\sum_{n=1}^{\infty} a_n e^{-n\pi y}\sin(n\pi z),$$

and

$$\phi_z(y,z) = G\sum_{n=1}^{\infty} a_n e^{-n\pi y}\cos(n\pi z).$$

Noting that the electric field due to the charge density is

$$E_0 = (|\phi_y|^2+|\phi_z|^2)^{1/2}, \tag{14}$$

we can obtain an upper bound for E_0. Since $|\sin(n\pi z)| \leq 1$ and $|\cos(n\pi)| \leq 1$, E_0 is bounded by

$$E_0 \leq (\sqrt{2})G \sum_{n=1}^{\infty} |a_n| e^{-n\pi y}.$$

Using the Schwartz inequality this can be written as

$$E_0 \leq (\sqrt{2})G\left(\sum_{n=1}^{\infty} a_n^2\right)^{1/2}\left(\sum_{n=1}^{\infty} (e^{-2\pi y})^n\right)^{1/2}.$$

Using Parseval's identity and the expression for the sum of a geometric series, the decaying exponential bound for E_0 can be seen

$$E_0 \leq G\left(\int_0^1 \rho^2(z)dz\right)^{1/2}[e^{-\pi y}/(1-e^{-2\pi y})^{1/2}], \qquad (15)$$

where, as previously defined, $G = 2/(\varepsilon_1+\varepsilon_2)$.

To illustrate the uses of this estimate, we consider the following experimental situation: a potential of 25 kV is applied to the top electrode and various surface charge densities are assumed on the interface. The right side is vacuum $\varepsilon_2 = \varepsilon_0$, and the permittivity of the insulator is $\varepsilon_1 = 20\varepsilon_0$.

Of course, in an experimental situation the extent of the electrodes and the interface is finite. However, our mathematical model can serve as an indicator of the possible field enhancement. Let us apply here our estimate (15) to two different surface charge densities on the interface.

Case 1: A uniform space-charge density. Assume $\rho_1(z) = \rho_0$, for $0 \leq z \leq 1$, where $\rho_0 = 10^{-5}$ C/m^2. If no surface charge were present, then the electric field would have a constant magnitude E = 25 kV/cm. The integration over the square of the charge density in eq (15) simply gives ρ_0, so the change in the magnitude of the electric field satisfies (at the point (y,z) between the electrodes with $y > 0$)

$$E_0 \leq (1.076)[e^{-\pi y}/(1-e^{-2\pi y})/^{1/2}](kV/cm).$$

For y = 0.5 cm, for instance, we obtain $E_0 \leq 0.22$ kV/cm and $E_0/E \leq 0.009$. Thus, at a point 0.5 cm from the interface, the field enhancement is less than 1%. For y = 1 cm, we obtain

$$E_0 \leq 0.047 \text{ kV/cm and } E_0/E \leq 0.002,$$

so the field enhancement is at most 0.2%.

Case 2: A nonuniform space-charge density. Assume

$$\rho_2(z) = \begin{cases} 0, & 0 \leq z \leq 1/3 \\ (1.5z - 0.5)\rho_0, & 1/3 \leq z \leq 1, \end{cases}$$

where $\rho_0 = 10^{-5}$ C/m^2. Figure 2 shows the graph of $\rho_2(z)$. Most of the charge is concentrated near the top electrode. A simple calculation shows that

$$\left[\int_0^1 \rho^2(z)dz\right]^{1/2} = (\sqrt{2})\rho_0/3 < 0.5\rho_0.$$

A simple analysis as in case (1) shows that $E_o/E \leq 0.5\%$ on the line $y = 0.5$ cm and $E_o/E \leq 0.1\%$ on the line $y = 1$ cm. Figure 3 shows equipotential lines for the case where $\rho(z) = \rho_1(z)$, and figure 4 shows these lines when $\rho(z) = \rho_2(z)$. The line $y = 0$ is centered in each picture.

2. Cylindrical Space Charge Between Spheres

In this section, we use a computer model to study the following electrostatic problem: a potential difference is placed on two spheres separated by a small gap. A thin cylinder of charge is assumed in the gap between the spheres (see fig. 5). We are interested in the change in the magnitude of the electric field due to this charge.

More precisely, two spheres of each of radius R have their centers at the points $(0,0,c)$ and $(0,0,-c)$ with $R < c$ but so that the gap between the spheres, $d = 2(c-R)$, is "small." A potential $\phi = +V$ is put on the top sphere, and $\phi = -V$ on the bottom. We assume further that a thin cylinder of space charge exists in the gap and that the space charge density ρ, at a distance r from the z-axis, is given by

$$\rho(r) = \begin{cases} A\cos^2(\pi r/2a), & \text{for } 0 \leq r \leq a,\ |z| \leq c, \\ & \text{and } r^2+(z-c)^2 \geq R^2 \\ 0, & \text{otherwise,} \end{cases} \tag{16}$$

where A and a are small relative to R. A standard calculation shows that the total charge in this cylinder is (ignoring the slightly spherical shape of the top and bottom of the cylinder)

$$\int_{R-c}^{c-R}\int_0^{2\pi}\int_0^a A\cos^2(\pi r/2a)r\,dr\,d\theta\,dz \tag{17}$$

$$= [(\pi^2-4)/2\pi]a^2Ad \simeq 0.934a^2Ad\ ,$$

so that we can control the total amount of charge in the cylinder by adjusting A once a and d are known.

To study the solution to this problem we used a program which solves two-dimensional elliptic boundary value problems with fairly general boundary conditions over fairly general bounded geometries using an adaptive finite element technique [7].

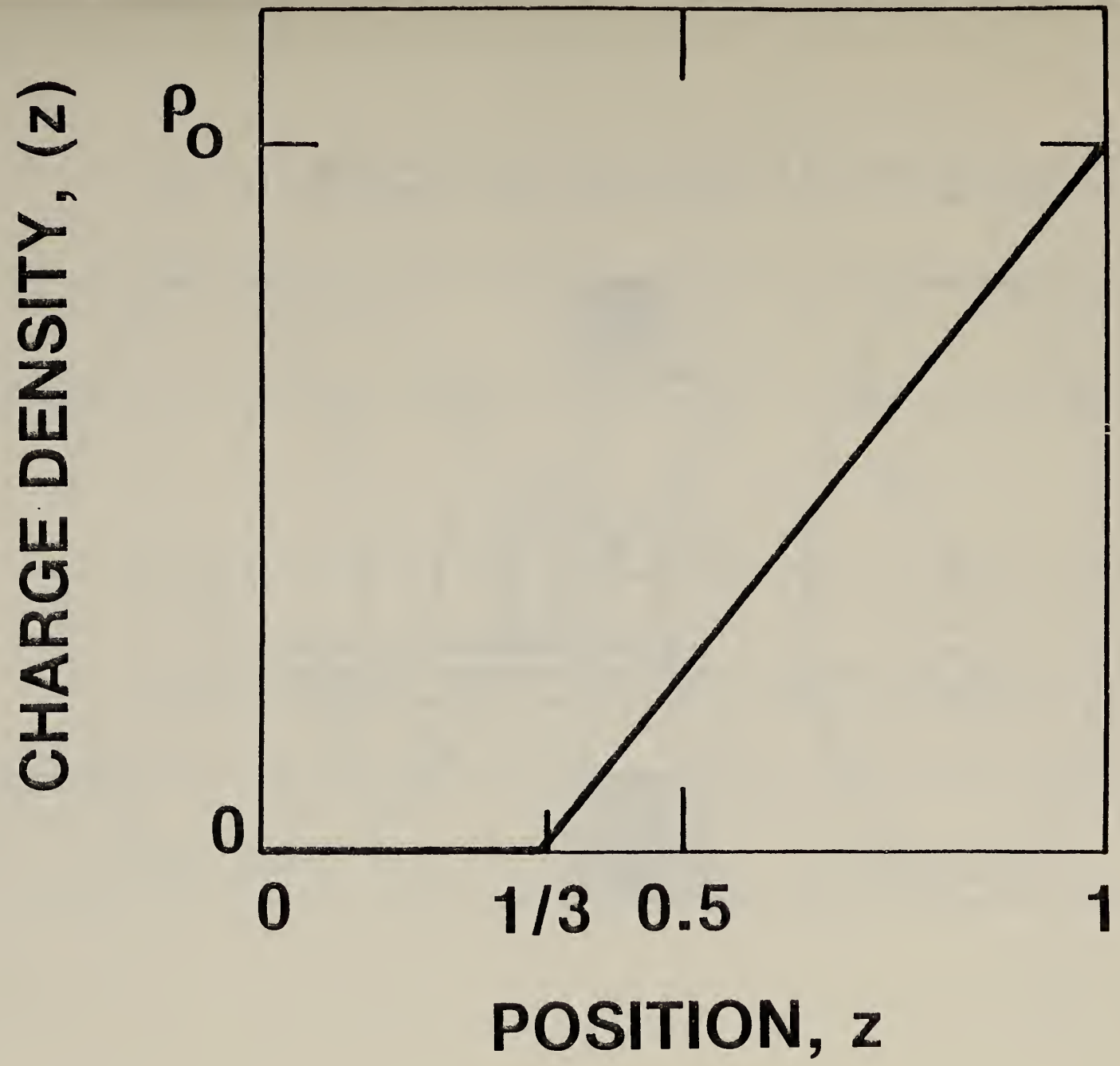

Fig. 2. Surface charge density along the interface, ρ (z).

Fig. 3. Equipotential lines between parallel plates for a uniform interfacial surface charge density, $\rho_1(z)$, and with no voltage applied to the plates, $V = 0$.

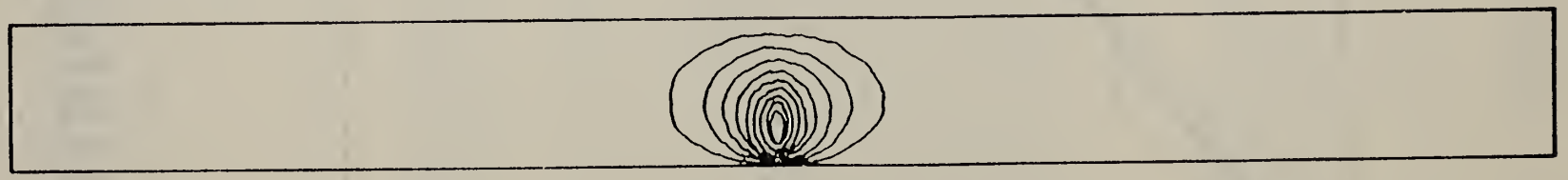

Fig. 4. Equipotential lines between parallel plates for the nonuniform interfacial surface charge density, $\rho_2(z)$, and with $V = 0$.

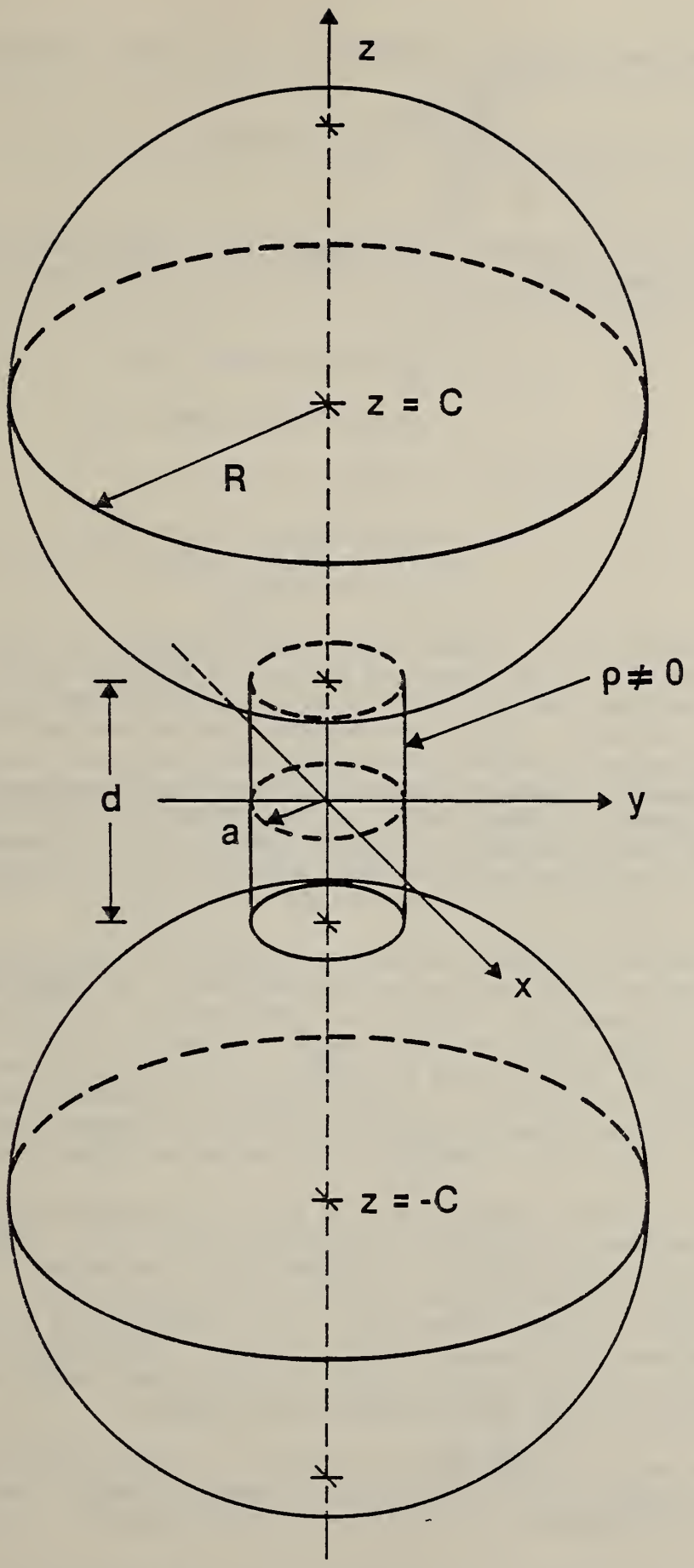

Fig. 5. Cylindrical space charge between two spheres. The upper sphere is at $\phi = +V$ and the lower sphere is at $\phi = -V$.

Using the cylindrical symmetry in this problem, Poisson's equation in the variables r and z reduces to

$$-(\phi_{rr} + \phi_r/r + \phi_{zz}) = \rho(r)/Eo, \tag{18}$$

where $\rho(r)$ is given by (16).

The specific geometry and dimensionless spacing we chose is shown in figure 6; specifically, R = 8, C = 9, d = 2, and we used a = 0.5. For the boundary conditions we use

$$\phi = \begin{cases} +V \text{ on the top semicircle} \\ -V \text{ on the bottom semicircle} \end{cases} \tag{19}$$

$$\partial\phi/\partial n = 0, \text{ for } r = 0 \text{ and } -1 \leq z \leq 1 \tag{20}$$

$$\phi = \phi \text{ induced on the lines from } (8,9) \text{ to } (13,9), (13,9) \text{ to } (13,-9) \text{ and } (13,-9) \text{ to } (8,-9). \tag{21}$$

Some explanation is in order about conditions (20) and (21). In (20), n denotes the unit outer normal to the region and (20) is equivalent to stipulating that the equipotential lines intersect the z axis at right angles. The three lines on the boundary and referenced in condition (21) are assumed to be far enough away from the z axis that the potential is unaffected by moderate amounts of space charge centered along the axis of symmetry. Specifically, we use 10 terms of the series of Legendre functions for the potential where no space charge is present. (Note: We checked our solution using 10 terms with one using 30 or more terms, and found no significant difference in our results.)

A word of caution is necessary before we present our results. The values for the field vectors were generated by the computer program. This program generates the graph of the potential $\phi(r,z)$ as being piecewise linear, and the field vector at the point (r,z) is found by computing the normal to the plane which coincides with the graph of $\phi(r,z)$ at the point $(r,z,\phi(r,z))$. This procedure, we believe, has reasonable accuracy in this case, but certainly suffers somewhat from the inherent loss of accuracy in a numerical differentiation procedure.

Table 1 shows the total charge and the maximum charge density in the gap between the spheres as specified in eq (16). Various radii and spacing are chosen where it is assumed that a potential of 10 kV is placed on the top sphere and -10 kV on the bottom sphere. Table 2 shows the percent increase or decrease in field intensity at a point with dimensionless coordinates r and z. To obtain coordinates in centimeters for each of the various situations, multiply the r and z coordinates by d/2, where d is the spacing between the spheres.

The main conclusion to be observed from these tables is that at a distance three units from the axis of symmetry only a small (i.e., less than 2%) enhancement of the electric field occurs.

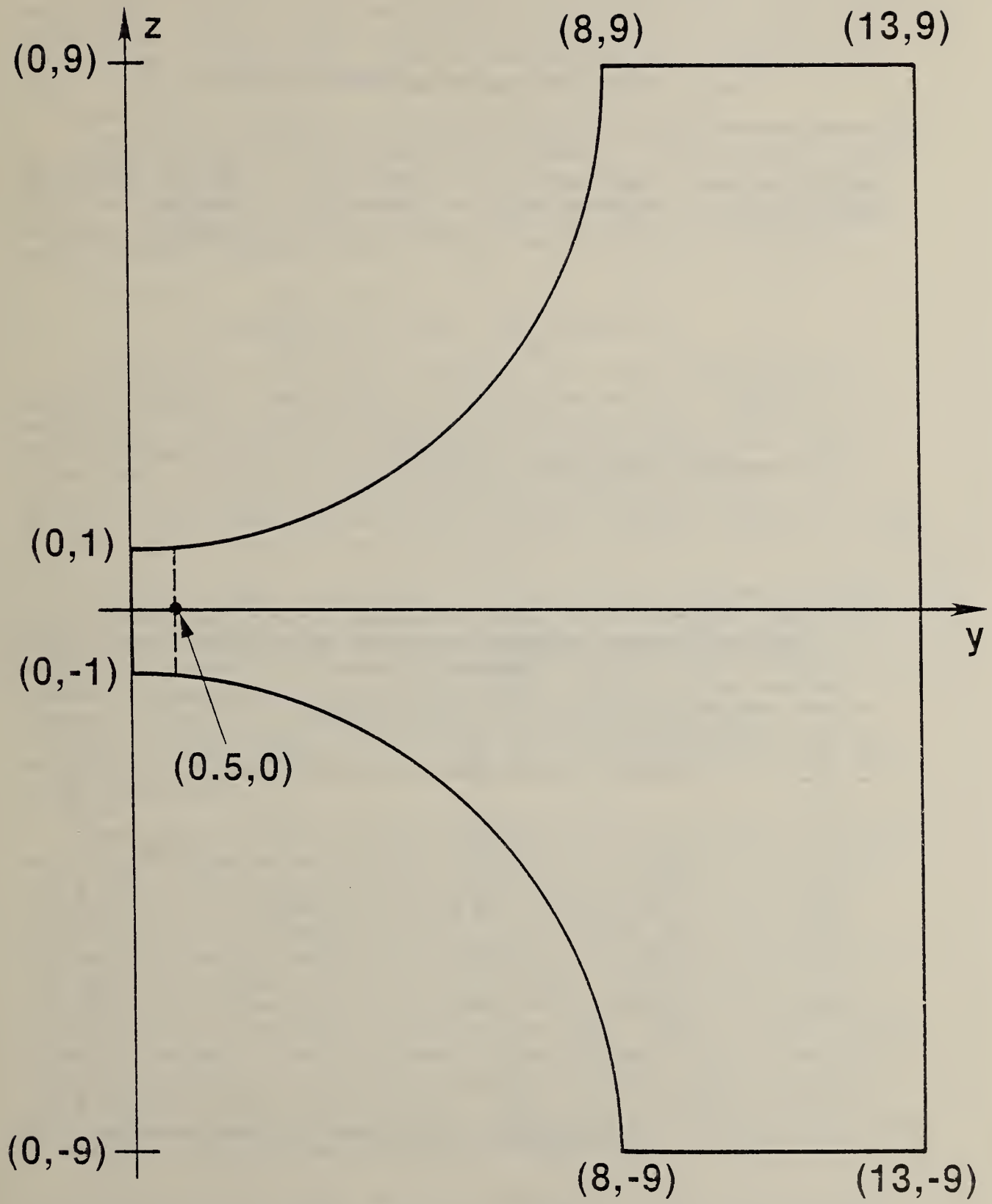

Fig. 6. Geometry and coordinates used in the program PLTMG.

Table 1. Space charge in gap between spheres

Spacing between spheres (cm)	Radii of spheres (cm)	Total charge (pC)	Maximum charge density (pC/cm^3)
1	4	6.04×10^3	1.03×10^5
2	8	1.21×10^4	2.58×10^4
5	20	3.02×10^4	4.13×10^3

Table 2. Percent increase (decrease) in field density, gap d = 2

z	r = 1.5	2.0	2.5	3.0
1.5				(3.96)
1.0	(15.2)	(11)	(14.2)	1.5
0.5	(24.6)	(5.5)	(8.5)	0.9
0.0	12.2	5.9	3.9	1.1
-0.5	16 5	4.6	5.3	1.2
-1.0	11.6	7.2	3.8	1.1
-1.5				1.9

Figures 7 through 9 were drawn using the program PLTMG. The first of these shows a typical high level triangulation used in the finite element calculation. Figure 8 shows equipotential lines for the case where no space charge is present and figure 9 shows equipotential lines for the case with space charge to which the data above refers.

The analyses presented here show that even for large charge densities the resulting perturbations of the ideal geometric field are surprisingly small. Especially for distances beyond the gap spacing, we find that field modifications are typically less than 10% in the case of a cylinder of charge between spherical electrodes and less than 1% for sheets of charge between parallel plates.

B. BREAKDOWN LOCATION -- CONTAMINATED OIL

On the basis of the above discussion it is clear that substantial amounts of space or surface charge are required before a significant modification of the electric field arises. Such a result indicates that when breakdown occurs at an interface, it may not be because of field distortions arising from space charge, but some other phenomena may increase the probability of breakdown at the interface. This is not to say that space charge does not exist or cannot influence breakdown in some way other than a modification of the field.

A previous report [8] showed that for a clean, well-characterized system, breakdown does not necessarily occur at an oil-paper interface. Equivalently, it was shown that the presence of an interface does not necessarily reduce the breakdown strength of a system. Such results strongly indicated that space-charge field intensifications were not present in carefully cleaned and prepared interfacial systems or that they made no difference. The question of liquid purity became important at this point and prompted us to repeat these interfacial breakdown tests using contaminated oil.

The electrodes used for this study were two discs (diameter 2.5 cm) with rounded edges which provided a uniform field. The discs were split along their diameter to clamp the paper sample parallel to the electric field. 60-Hz ac voltage was applied at a ramping rate of 3 kV/s until the electrode system broke down. The paper samples were sufficiently thin so that the split edge did not significantly enhance the field where the paper was clamped. The fact that the split electrode edge did not enhance the breakdown probability appreciably was shown by separating the electrode split halves the thickness of the paper (0.007 cm), and running several breakdowns without any paper in the system. The position of the breakdowns continued to distribute themselves randomly about the uniform field region and not prefer the small split. This indicated that the split electrode geometry would not be responsible for driving the breakdown to the paper interface when the paper is installed.

Obtaining statistically meaningful data is a time-consuming process since the breakdown usually destroys the interface. When the breakdown occurs at the interface it burns away a portion of the paper. However, even if the breakdown does not occur at the interface, the shockwave from

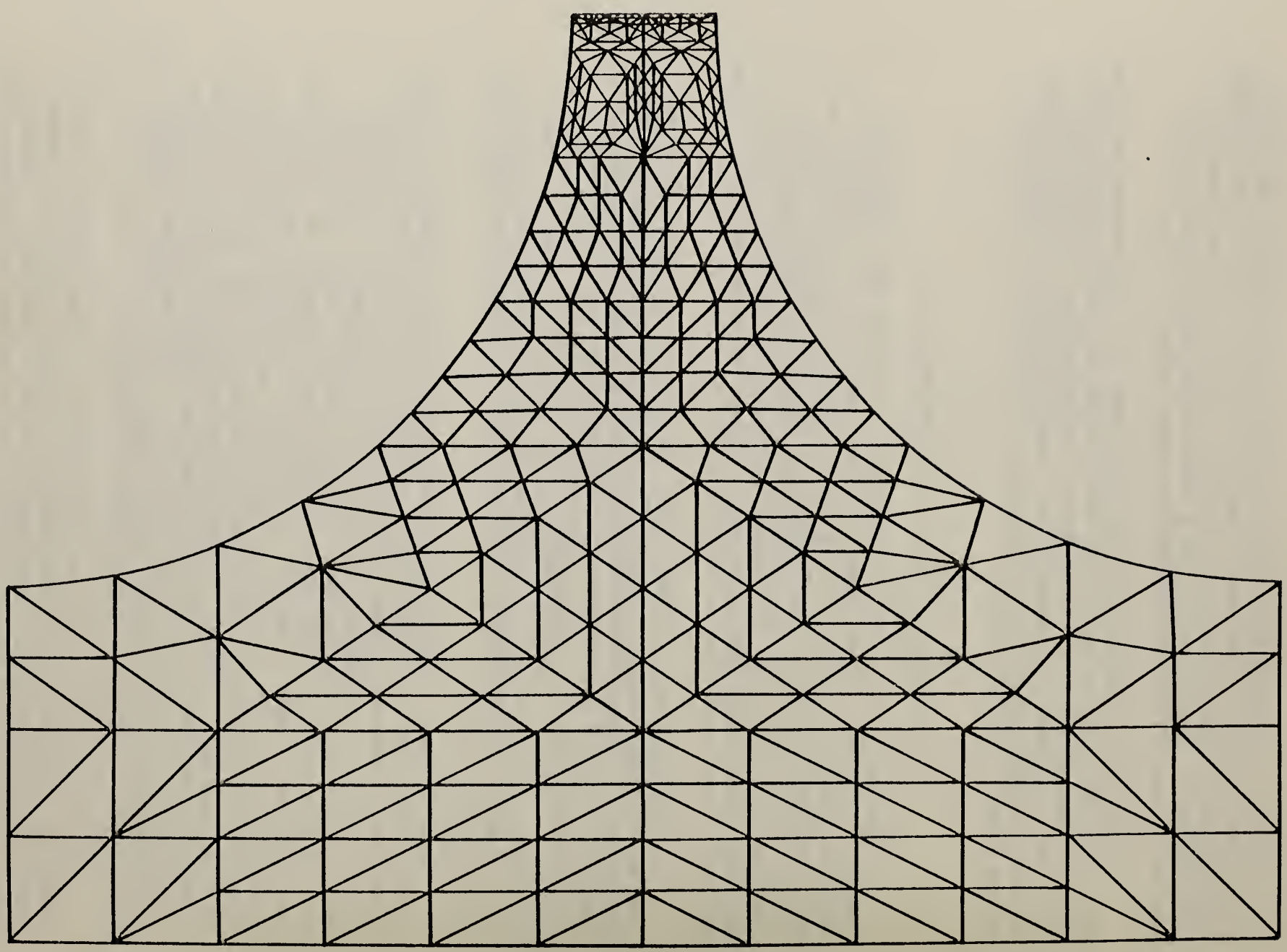

Fig. 7. Triangulation employed by program PLTMG.

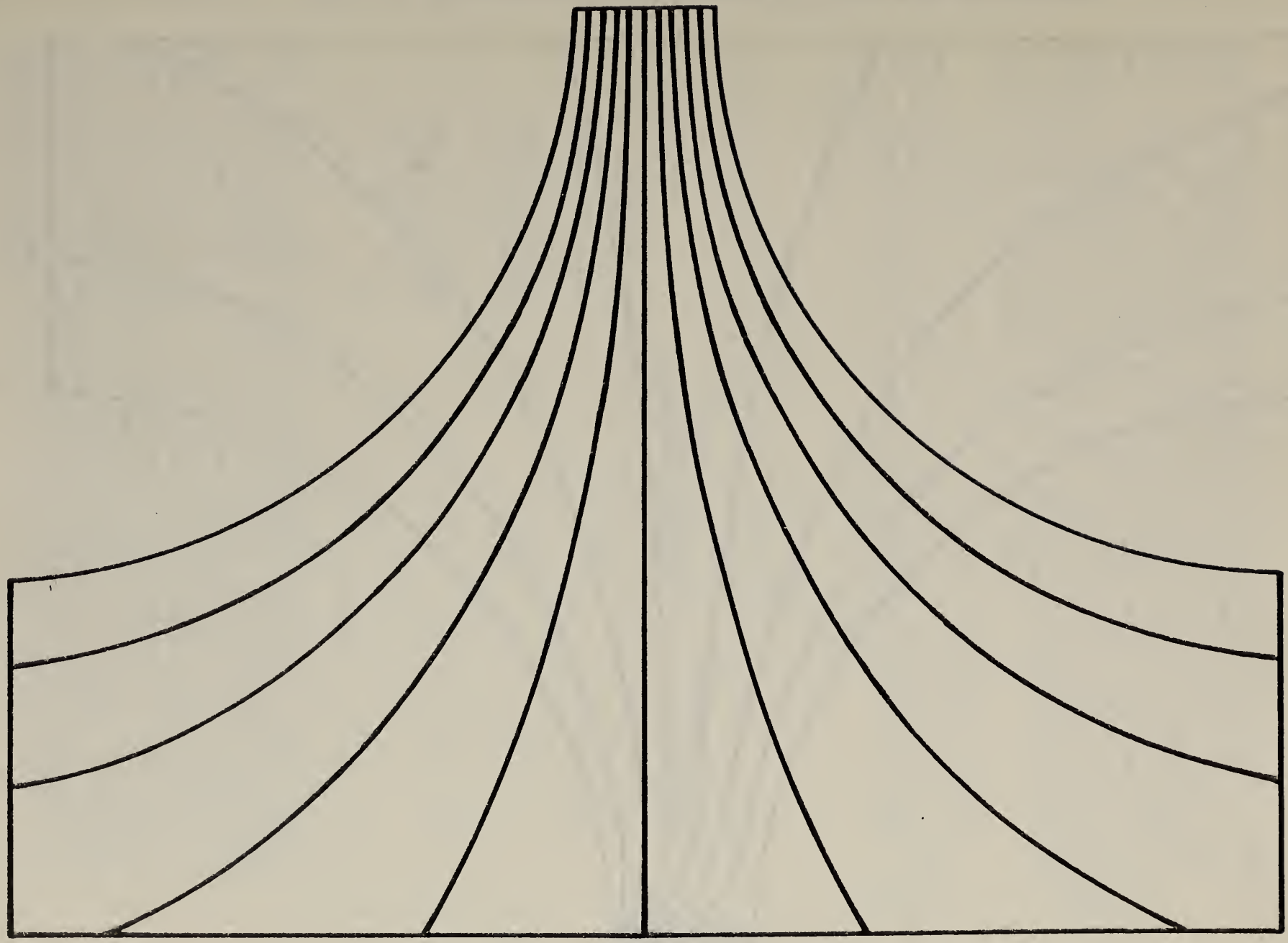

Fig. 8. Equipotential lines obtained via PLTMG with no space charge present.

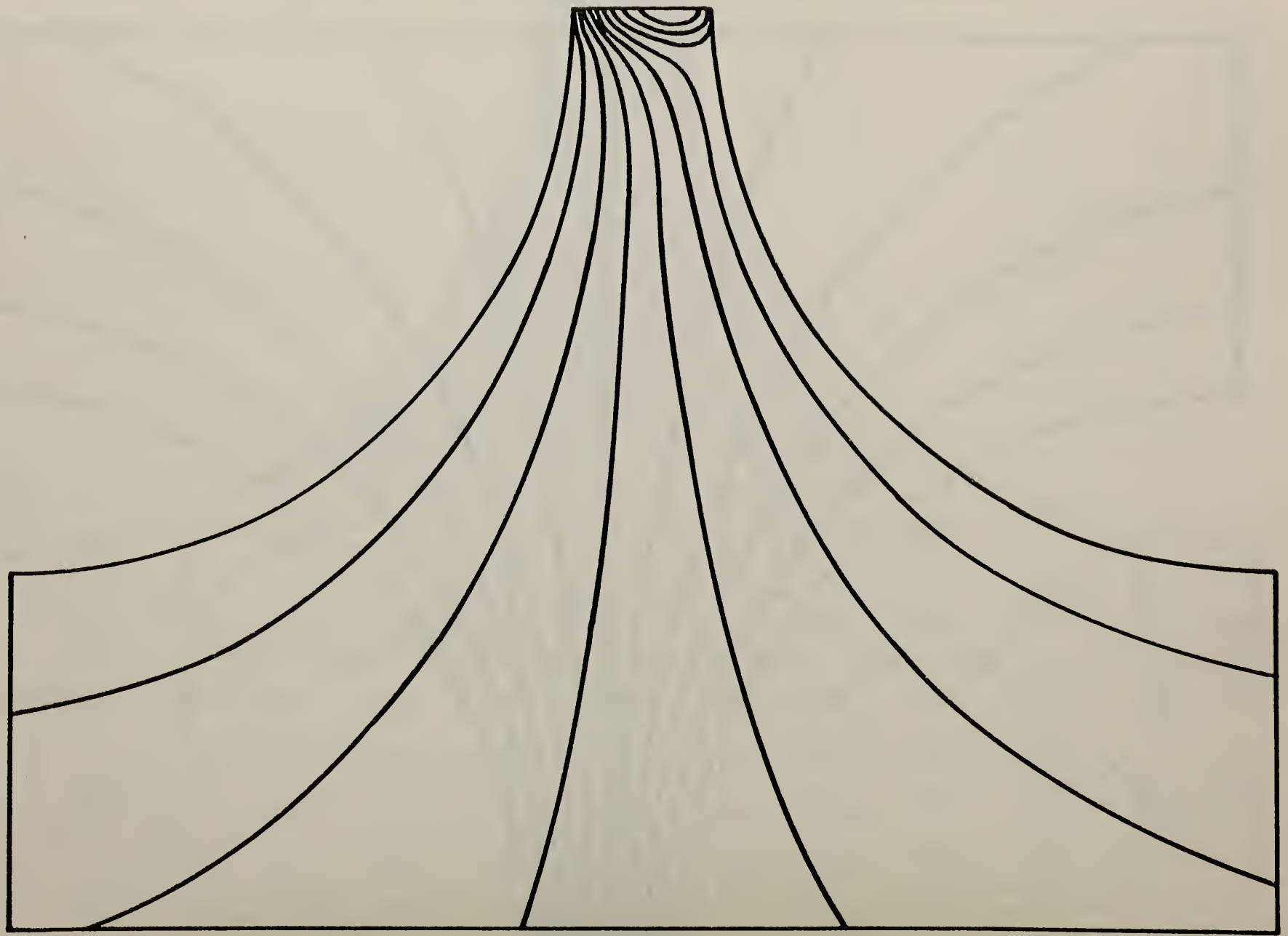

Fig. 9. Equipotential lines obtained via PLTMG with space charge present (see eq 16).

the breakdown usually rips the paper. Thus, the apparatus must be opened and a new interface installed after each breakdown. To minimize the amount of time expended, we felt that surveying interfacial breakdowns under several different conditions with relatively few breakdowns for each condition was preferred to many breakdowns under only one condition. Even so, it took more than 150 breakdown tests before the handling procedures could be established and consistent data obtained. These results strongly suggest that there is no fundamental electric field perturbation introduced by the paper interface, but that the interface's contribution to lowering the breakdown voltage possibly rests in either entrapped gasses in the interface material (bubbles) or dirt, or both.

To determine the influence of oil purity on breakdown location, measurements were first performed using clean oil (mechanically filtered and degassed) and then severely contaminated oil was used. The contaminated oil had been removed from a commercial transformer which had failed. The data obtained using clean oil is presented in table 3.

Table 3. Clean oil data

Condition	Number of breakdowns recorded	Breakdown voltage (2.5 mm gap)
No interface	15	76 ± 10 kV
Interface present	10	68 ± 11 kV
Interface present but breakdown not at interface	7	74 ± 7 kV
Interface present and breakdown at interface	3	56 ± 9 kv

The variations associated with the breakdown voltages are the standard deviations about the mean value. Throughout these experiments, whether or not the breakdown occurs at the interface is determined in two ways: optical observations during breakdown and observation of burned areas on the interface. The results in table 3 show that 70% of the time the breakdown did not occur at the interface, and the breakdown voltage was essentially the same as the breakdown voltage without an interface. The 30% of the time the breakdowns occurred at the interface, the breakdown voltage was substantially lower than without an interface. Because of the difficulty in handling the paper interface, we hypothesize that the breakdowns at the interface were caused either by bubbles embedded in the paper or perhaps by particles introduced with the paper or a combination of both.

The results obtained using contaminted oil are shown in figure 10. The contaminated oil contained small particles which would eventually precipitate out of the oil. Since the particles presumably influence breakdown, the oil reservoir was initially shaken to suspend these particles. The first five breakdowns or "shots" were made without an interface present, and the resulting average breakdown voltage was 53 ± 7 kV -- significantly below the 76 ± 10 kV recorded for clean oil. The second five measurements were taken with a paper interface present and provided a higher breakdown voltage, 65 ± 12 kV, where three of the five breakdowns occurred at the interface. Suspecting that the suspended particles were dominating the breakdown behavior, the system was allowed to sit overnight, which would permit the larger particles to precipitate out from the oil. The next morning five breakdowns were recorded without an interface whereby the average breakdown voltage was 74 ± 7 kV -- about the same as for clean oil.

At this point a series f 10 shots was taken, five with an interface and five without. Only now the oil reservoir was shaken before each shot so that the oil in the cell contained the larger particles which had previously precipitated out. Using this method the breakdowns without an interface occurred at an average of 34 ± 5 kV and with an interface at 39 ± 8 kV -- essentially the same. Note, however, only two of the breakdowns occurred at the interface. From these data, it is postulated that although the oil contamination, especially particulate contamination, decreases the breakdown voltage of the system, it does not have a dramatic effect on the interfacial phenomena since the breakdown, as before, does not necessarily occur at the interface even with heavily contaminated oil.

The first 100 or so breakdowns are not reported in table 3 or figure 10. When interfaces were installed during these shots, they always broke down at much lower voltages compared to the breakdown voltage without an interface. The procedure used to load the interface into the cell was as follows: a paper interface which had been under oil in a vacuum was placed in the split electrode system and then sealed in the cell. The cell was evacuated for at least one minute and then loaded with oil while the vacuum was maintained above the oil. After the cell was filled with oil, the system was brought to atmospheric pressure with dry nitrogen. A problem arises during the filling process. When the oil enters the cell under vacuum, it outgasses, producing small bubbles, some of which lodge upon the interface. These bubbles are suspected of lodging in the fiber structure of the paper interface thereby weakening its ability to withstand voltage. The above hypothesis fits the observations well, for the loading procedure can be changed so that the interface is found to withstand as much voltage as the liquid, at least 50% of the time and perhaps more.

The procedure which resulted in the most breakdown resistant interfaces was: to load a new interface into the cell and to evacuate the cell for one minute. Because the oiled paper supply was stored under vacuum, it is possible to get a few bubbles on or near the interface only during installation. These bubbles are easily removed during the cell's evacuation. The cell was pressurized with dry nitrogen to atmospheric pressure and then slowly filled with oil to avoid producing small bubbles.

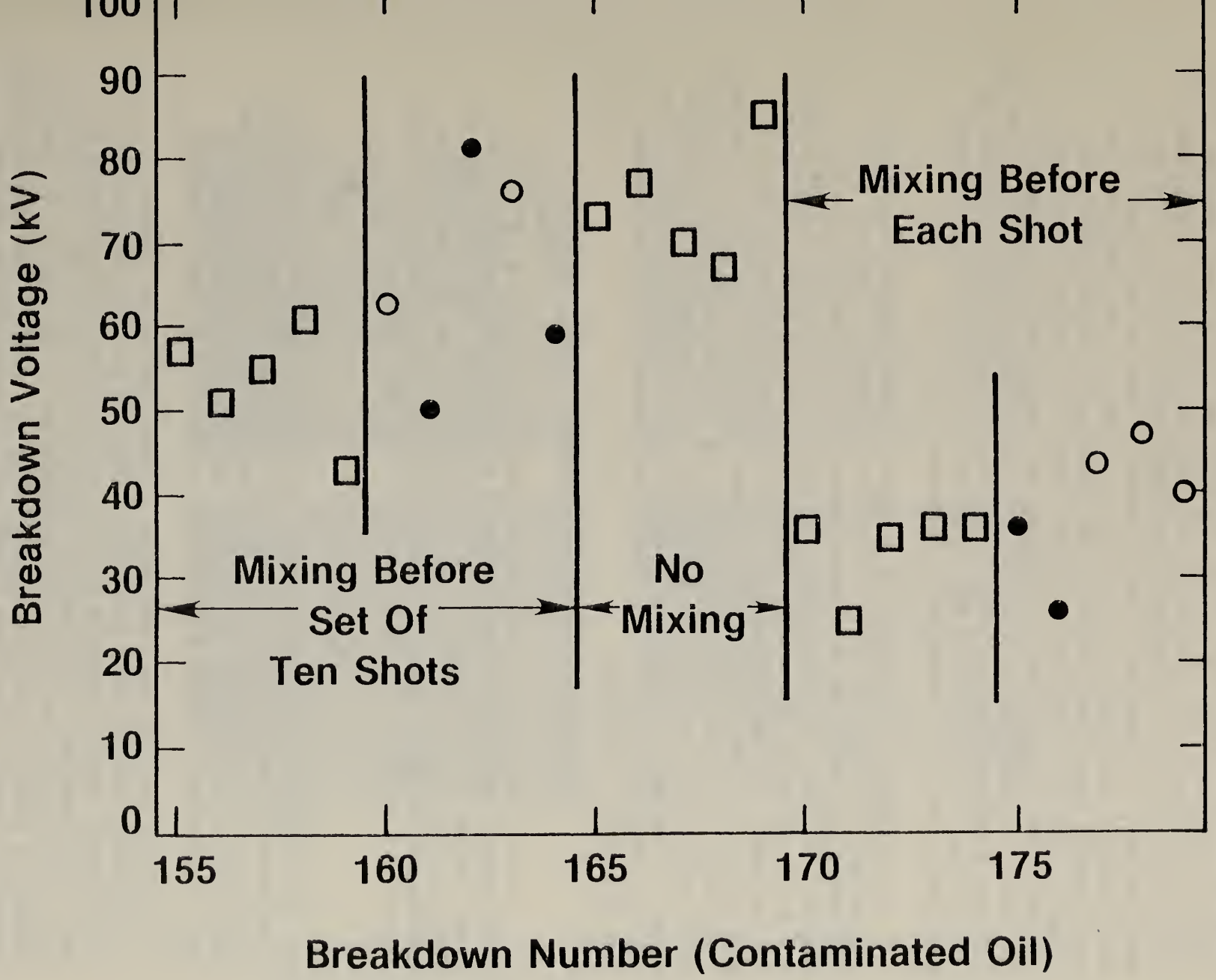

Fig. 10. Summary of breakdown voltage measurements using contaminated oil. The open circles indicate breakdown away from the interface while the solid circles denote interfacial breakdown. The squares represent data on oil only (no paper in the system).

The bubbles which managed to attach themselves to the interface during loading were always sufficiently large that they could be pushed away by slowly circulating the oil through the cell and along the interface. The difference between this procedure and the first is that the interface is pressurized after all the bubbles have been removed from its surface. When the cell is loaded with the oil under vacuum, we postulate that small bubbles impregnate the interface. If the oil were degassed, we would expect even these bubbles to be dissolved if enough time were allowed. However, since the breakdown occurs shortly after loading the cell, the procedure which produces the fewest number of bubbles in the paper is suspected of producing the most breakdown resistant interface. The data reported here (in table 3 and fig. 10), therefore, employed the second loading process where the interface is pressurized and the cell is loaded with oil at atmospheric pressure.

To illustrate the problem of bubbles, we show several microscope photographs of the paper material used in figure 11. The top left photograph, A, shows the oil soaked paper before subjecting it to a vacuum. The top right photograph, B, shows the effects of vacuum pumping for a few minutes. The vacuum pumping clearly makes a great difference in the number of bubbles remaining in the paper. The bottom left photograph, C, shows that extended vacuum pumping (several hours) removes more, but not all, of the bubbles; note the one bubble marked. Overnight this bubble dissolved into the liquid and is not observed in the bottom right photograph, D, taken the next morning. These results point to the physical characteristics of the paper interface as a critical element in the interfacial breakdown.

IV. ELECTRIC FIELD MEASUREMENTS -- SPACE CHARGE

In this section we review Kerr-effect electro-optical, field measurements, and the equipment used to make those measurements. The space charge in nitrobenzene which develops between parallel plates is then observed and quantified. These methods are then applied to the measurement of space charge in transformer oil. Dramatically different results are observed for transformer oil than for nitrobenzene.

A. THEORY

The electric field measurements reported here are made using the electro-optic Kerr effect. Such measurements provide non-contact means of observing the electric field, since only light is used to probe the field region of interest. Kerr-effect measurements are described in detail elsewhere, so only a brief description will be given here [9].

Certain liquids, when subjected to electric fields, become birefringent, meaning that polarized light will pass through the liquid at different speeds depending upon the polarization angle relative to the field direction. Light polarized parallel to the field will move more slowly than light polarized perpendicular to the field. If parallel plates are used to provide a uniform field in a cell filled with a liquid exhibiting a Kerr effect, and if the cell is placed between crossed polarizers so that the uniform field direction is at an angle of 45° with

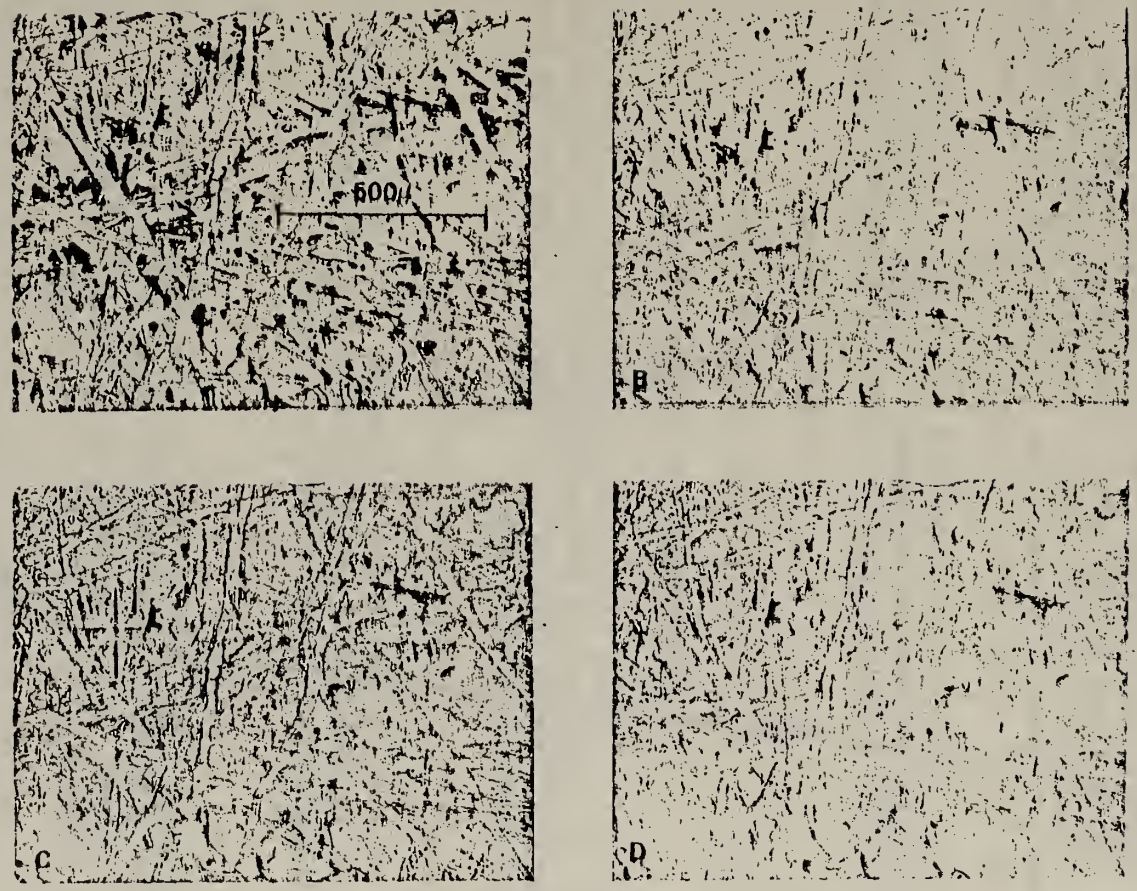

Fig. 11. Microscope photographs showing removal of bubbles in the paper used for interfaces. The line in the upper left photograph denotes 0.5 mm (500 μm).

respect to the polarization axes, then the transmitted light will be found to be a function of the field between the plates E and the length of the plates ℓ

$$I/I_m = \sin^2(\pi B E^2 \ell), \tag{22}$$

where I is the transmitted intensity of the observed light ray, I_m is the maximum amount of light which can be transmitted along that ray path (as if the polarizer were aligned), and B is the Kerr constant of the liquid used. At room temperatures, the Kerr constant for nitrobenzene is $B = 3.2 \times 10^{-10}$ cm/V^2, and typically for transformer oil $B = 3.2 \times 10^{-13}$ cm/V^2. For uniform fields, the electric field is related to the applied voltage by $E = V/d$, where d is the plate spacing. Fringe fields are neglected throughout this report since they contribute less than a 1% correction [10].

Whenever the entire area surrounding the plates is illuminated, a two-dimensional Kerr pattern is produced. The light and dark regions found in such a Kerr pattern are usually described in terms of fringe numbers

$$n = (E/E_m)^2 = \begin{cases} 0,2,4,6,\ldots\text{.for dark fringes} \\ 1,3,5,7,\ldots\text{.for light fringes} \\ \text{non-integer for between fringes,} \end{cases} \tag{23}$$

where $E_m = (2B\ell)^{-1/2}$ is the field intensity required to produce the first fringe. E_m contains the Kerr-effect sensitivity information and the plate length. Then eq (22) may be written in terms of the fringe number or a relative electric field

$$I/I_m = \sin^2(n\pi/2) = \sin^2[(\pi/2)(E/E_m)^2]. \tag{24}$$

In order to infer the electric field strength from the light intensity information, it is necessary to keep track of the fringe number. By introducing the previous fringe number, an integer

$$N = \text{int}(n)\,, \tag{25}$$

(where $n-1 < N \leq n$), eq (24) may then be inverted to express the relative field strength in terms of the light intensity

$$E/E_m = \{2[N-\text{int}(N/2)] + (-1)^N(2/\pi)\sin^{-1}[(I/I_m)^{1/2}]\}^{1/2}. \tag{26}$$

A plot of this function is shown in figure 12. Whenever a parallel-plate geometry Kerr pattern shows several fringes (as is the usual case with nitrobenzene) the field strength may be determined using eq (26).

Consider a parallel-plate geometry where the plates are parallel to the x-y plane and placed with surfaces at $z = \pm d/2$ giving a plate separation or gap of d. Let the length of the plates be ℓ in the x-direction which also will be the direction of the light beam. This system is placed between crossed polarizers. Because of the Kerr effect, a two-dimensional pattern will be observed in the y-z plane. That is, for each ray (y,z) parallel to the x-axis there will be an observed intensity I(y,z) which is related

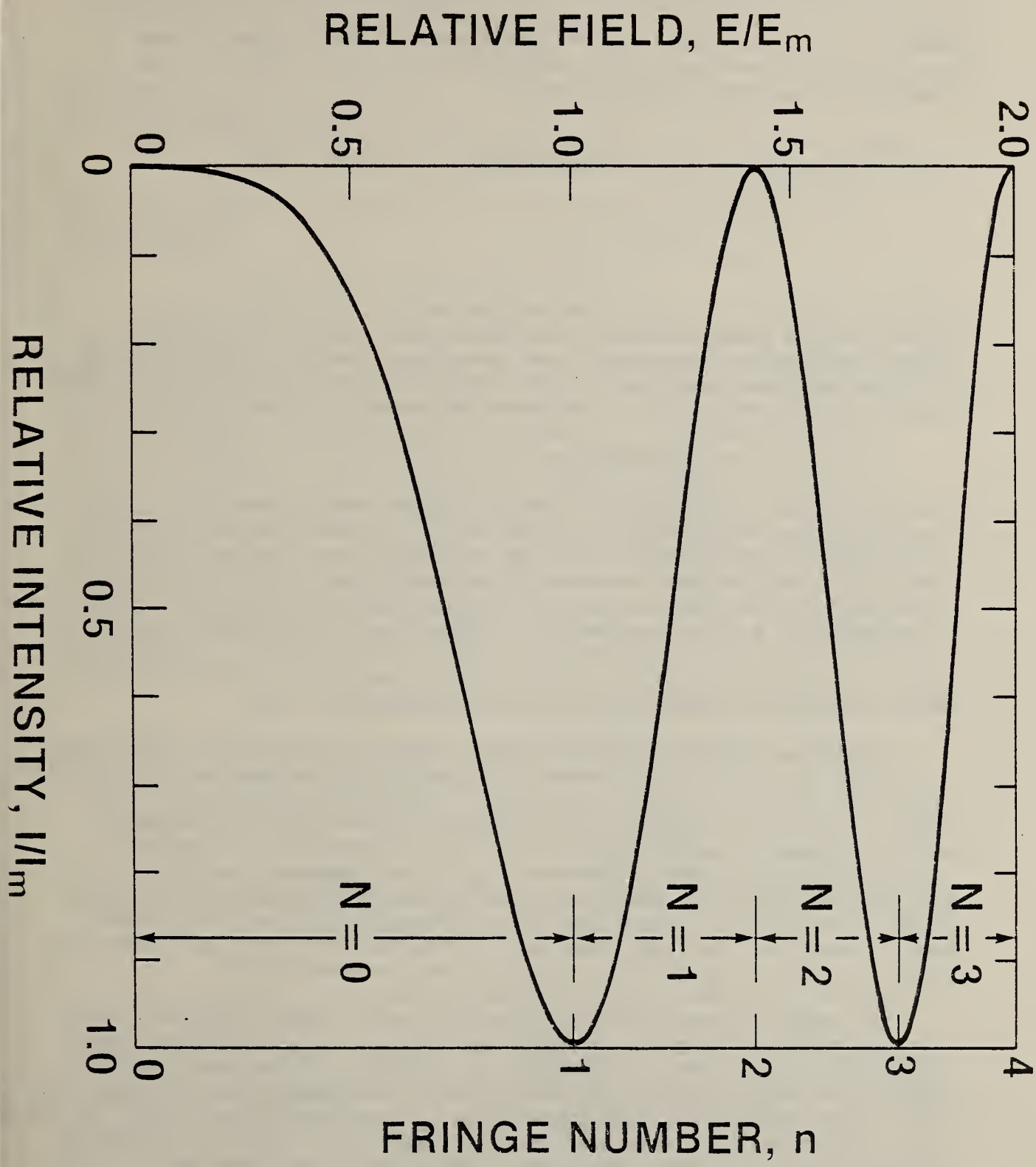

Fig. 12. The relative field strength expressed as a function of relative transmitted light intensity and previous fringe number N.

to the incident intensity $I_m(y,z)$ by eq (24). Describing the incident intensity $I_m(y,z)$ in this manner allows us to account for imperfections in the optical system or light source (usually a laser) which produces a nonuniform incident beam. For this reason reference is usually made to the relative transmitted light intensity $I(y,z)/I_m(y,z)$ to avoid the problems arising from imperfections.

There are two factors which determine the electric field $E(y,z)$. The voltage applied to the plates gives

$$\int_{-d/2}^{d/2} E(y,z)dz = V, \qquad (27)$$

where the plate at $z = d/2$ is the cathode and $z = -d/2$ is the anode. Secondly, space charge can influence the electric field according to Poisson's equation. By symmetry and assuming a linear, isotropic medium, the space charge density can, at most, be a function of z so that Poisson's equation may be written as a simple derivative of the electric field

$$\rho = \rho(z) = \pm\varepsilon dE/dz \ , \qquad (28)$$

where $\varepsilon = \kappa\varepsilon_0$ is the dielectric constant of the liquid, where κ is the electric susceptibility and $\varepsilon_0 = 8.85 \times 10^{-14}$ F/cm is the permittivity of free space. The plus (minus) sign is used if the direction of the field is (is not) in the direction of increasing z. If there is no space charge between the plates, then $\rho = 0$, $dE/dz = 0$, and the electric field is uniform $E(z) = V/d$ = constant. In such a case, the relative transmitted intensity will be uniform, given by eq (22), $I(y,z)/I_m(y,z)$ is constant. Thus, any nonuniformity of the electric field because of space charge will be manifested by a nonuniformity in the transmitted light.

With liquids like nitrobenzene which exhibit a large Kerr coefficient, it is easy to observe space-charge field modifications because a sufficiently large field can be applied to the liquid which will produce many fringes. Space-charge field distortions will become manifest by the presence of several fringes in regions where the relative intensity would be uniform if the field were uniform. However, if a liquid does not exhibit a large Kerr coefficient, then it may not be possible to observe the first bright fringe ($n = 1$) before the liquid between the plates breaks down. Such is the case with transformer oil if the plates are not made awkwardly long so that $E_m = (2B\ell)^{-1/2}$ is less than the breakdown field.

For example, if we assume E_m is on the order of the breakdown fields in transformer oil under the application of dc, say, $E_m = 100$ kV/cm, then the required plate length would be $\ell = 1/2B(E_m)^2 \sim 160$ cm -- not a very practicable length. For the transformer oil experiments reported here, the plate length was $\ell = 30$ cm which would imply a field of $E_m = (2B\ell)^{-1/2} = 228$ kV/cm for the first fringe. Breakdown fields, however, are typically 100 kV/cm so that $E/E_m = 0.44$ at the most. This results in a relative light intensity of $I/I_m = 0.09$. For such low relative light intensities ($I/I_m < 0.1$), an examination of figure 12 suggests there may be problems of measurement, since the relative field E/E_m is a sensitive function of the relative intensity I/I_m. Let us examine this further.

Because we are limiting ourselves to small relative intensities (N = 0), eq (26) which expresses E/E_m in terms of I/I_m reduces to

$$E/E_m = \{(2/\pi)\sin^{-1}[(I/I_m)^{1/2}]\}^{1/2} . \quad (29)$$

Provided the relative intensity is small ($I/Im \ll 1$), the above relation simplifies even further to

$$E/E_m \simeq (2/\pi)^{1/2} (I/I_m)^{1/4} . \quad (30)$$

Our above concern for sensitivity is expressed in the differential relationship

$$dE/E_m \simeq (1/8\pi)^{1/2}(I/I_m)^{-3/4}dI/I_m. \quad (31)$$

The negative power of the relative intensity becomes large as the intensity reduces to zero, and this might lead one to believe that low-light-level Kerr measurements are impracticable. This is not the case, however, because we are mainly interested in the sensitivity of measuring a field dE/E (not dE/E_m) as determined by a deviation in the measured light dI/I (not dI/I_m). To put this another way, whenever an intensity $I(y,z)$ is measured it will exhibit the same intensity profile $I_m(y,z)$, that is, $I(y,z)/I_m(y,z)$ = constant, only if the field is not changed from its uniform structure by space charge. If there is space charge, then we can expect some change $dI(y,z)$ in the light intensity which can be related to the change in the field dE due to space charge. Thus the quantity of interest is dE/E related to dI/I by a sensitivity function $g(I/I_m)$. Using eq (24) the general relationship $dE/E = g(I/I_m)dI/I$ becomes

$$dE/E = (1/2\pi)(I/I_m)^{1/2}(1-I/I_m)^{1/2}(E/E_m)^{-2}dI/I, \quad (32)$$

where E/E_m is given by eq (26). Since we have restricted ourselves to $n \ll 1$, we can use eq (29) for E/E_m to obtain

$$dE/E = (1/4)(I/I_m)^{1/2}(1-I/I_m)^{-1/2}\{\sin^{-1}[(I/I_m)^{1/2}]\}^{-1}dI/I. \quad (33)$$

Here $g(I/I_m)$ is restricted to $I/I_m < 1$. Further restricting ourselves to small intensities so that $I/I_m \ll 1$, we obtain the simple relation

$$dE/E \simeq (1/4)dI/I. \quad (34)$$

Here $g(I/I_m) = 1/4$. This shows that for low light levels in the Kerr effect, a small change in the electric field will manifest itself by a factor of four larger change in the light intensity. The comparison of the exact coefficient of dI/I in eq (33) to the approximate coefficient in eq (34) is expressed in figure 13 along with a comparison of the exact and approximate expressions for E/E_m in eqs (29) and (30), respectively. Clearly, for intensities $I/I_m < 0.1$, eqs (34) and (30) hold rather well and the small-I approximation is useful for even an extended range of I/I_m values. Therefore, throughout the transformer oil work we will use the approximate expressions eq (30) for estimating the relative field E/E_m from the relative intensity I/I_m, because usually the relative intensity is $I/I_m = 0.1$ or below unless breakdown fields are explored.

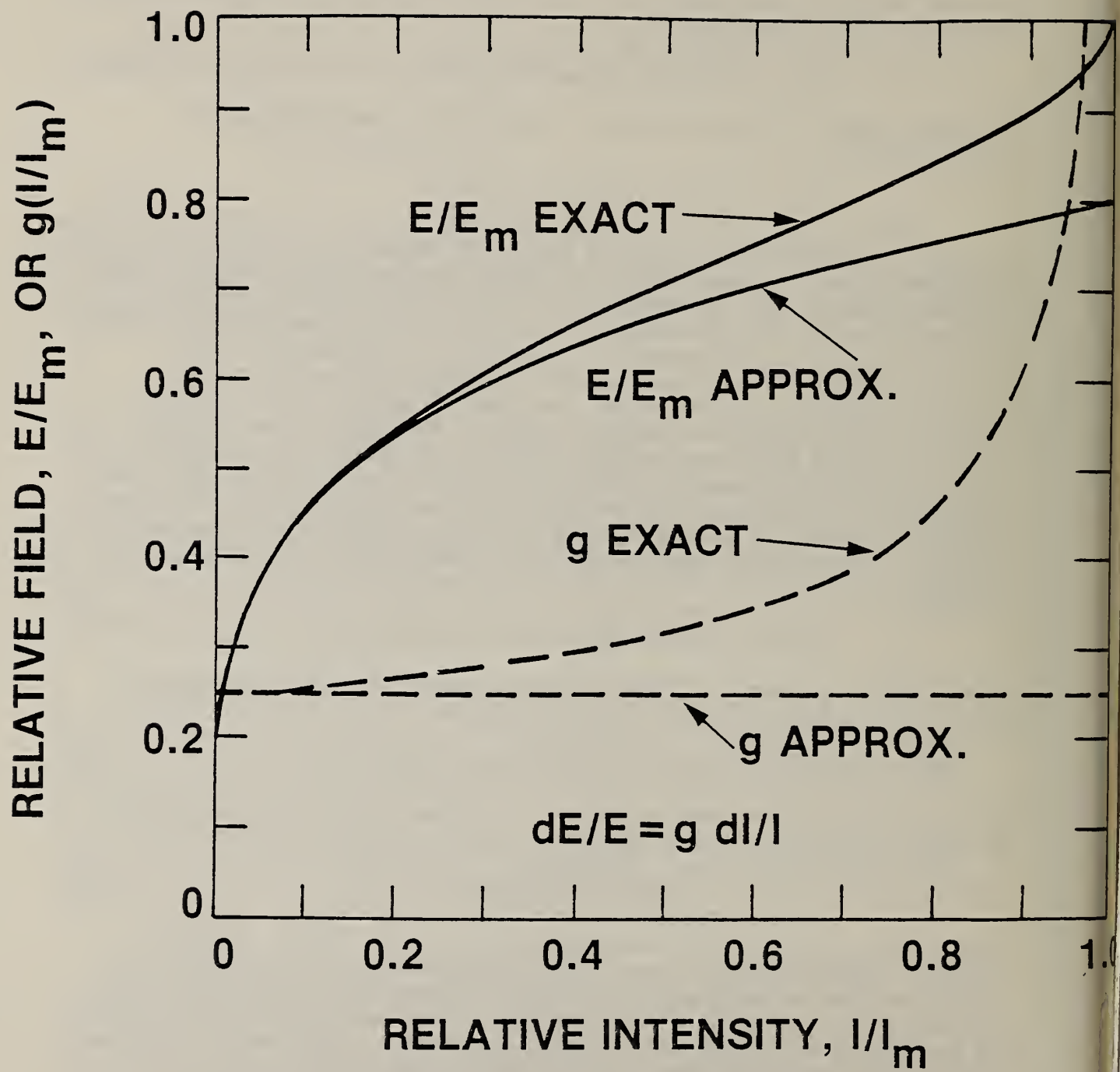

Fig. 13. Exact and approximate calculations are presented as a function of relative intensity $I/I_m \leq 1$. The approximate form for the relative field is good to 10% up to $I/I_m \sim 0.8$, whereas the forms of the sensitivity function $g(I/I_m)$ show a deviation of 10% near $I/I_m = 0.25$.

Even for relatively large intensities $I/I_m \sim 0.8$, the absolute error in using the approximate form of relative field is about 10%. If the field were distorted 10% at these levels, our error in estimating the amount of distortion would only be 1% as a result of using the approximate expression.

B. EQUIPMENT

The diagram of the apparatus is shown in figure 14, and the type of information obtained with the commercially available detector system is shown in figure 15. The first part of the detector is an electrostatically-focused image intensifier which illuminates a silicon target. The target is a microscopic array of photodiodes separated by ~8 μm. A 25-μm diameter electron beam scans this array to read the charge on the photodiodes and recharge them. Light causes the photodiodes to reduce the amount of charge remaining on them which is detected by the electron beam current. This current information is integrated for one line of scan, digitized and stored in the computer's memory. The resulting intensity profile I(z) can be position resolved into about 500 parts each with a dynamic range of 10^4 and ±2% linearity. Such a detector resolution often exceeds the resolution provided by the image producing optics. The detector can be pulsed and synchronized with the 60-Hz line allowing accumulative scanning for many 60-Hz waveforms. A computer console controls the scanning of the detector as well as the data collection, storage, manipulation, and output. Because of the sensitivity of the detector even in pulsed mode, neutral density filters are needed to decrease the input light levels.

When the apparatus is used to observe Kerr fringes in nitrobenzene, the procedure is much like conventional photography. Since both bright and dark fringes are present, the intensity profiles are easily interpreted to produce electric field profiles. Additionally, the low viscosity of nitrobenzene and other optical properties provide relatively stable intensity profiles which are not dramatically affected by turbulence during steady-state high-voltage operation, either 60 Hz or dc. Such luxuries are not afforded using transformer oil as the Kerr fluid.

The properties of transformer oil -- apparently an index of refraction which is very sensitive to temperature -- cause it to manifest turbulence by intensity fluctuations. This and the low light levels associated with the Kerr response requires complicated data-handling methods to acquire reliable data.

C. SPACE CHARGE IN NITROBENZENE

The nitrobenzene test cell, in which the nitrobenzene is dehydrated and filtered during the course of the measurements, had parallel plates 9.5 cm square and separated by 0.6 cm. The nitrobenzene is pumped through powdered alumina to remove much of the water and a mechanical filter which removes most of the particles over 2 μm in diameter. Because fluid motion degrades the image, the filtration is only performed before each measurement sequence and not during the accumulation of data.

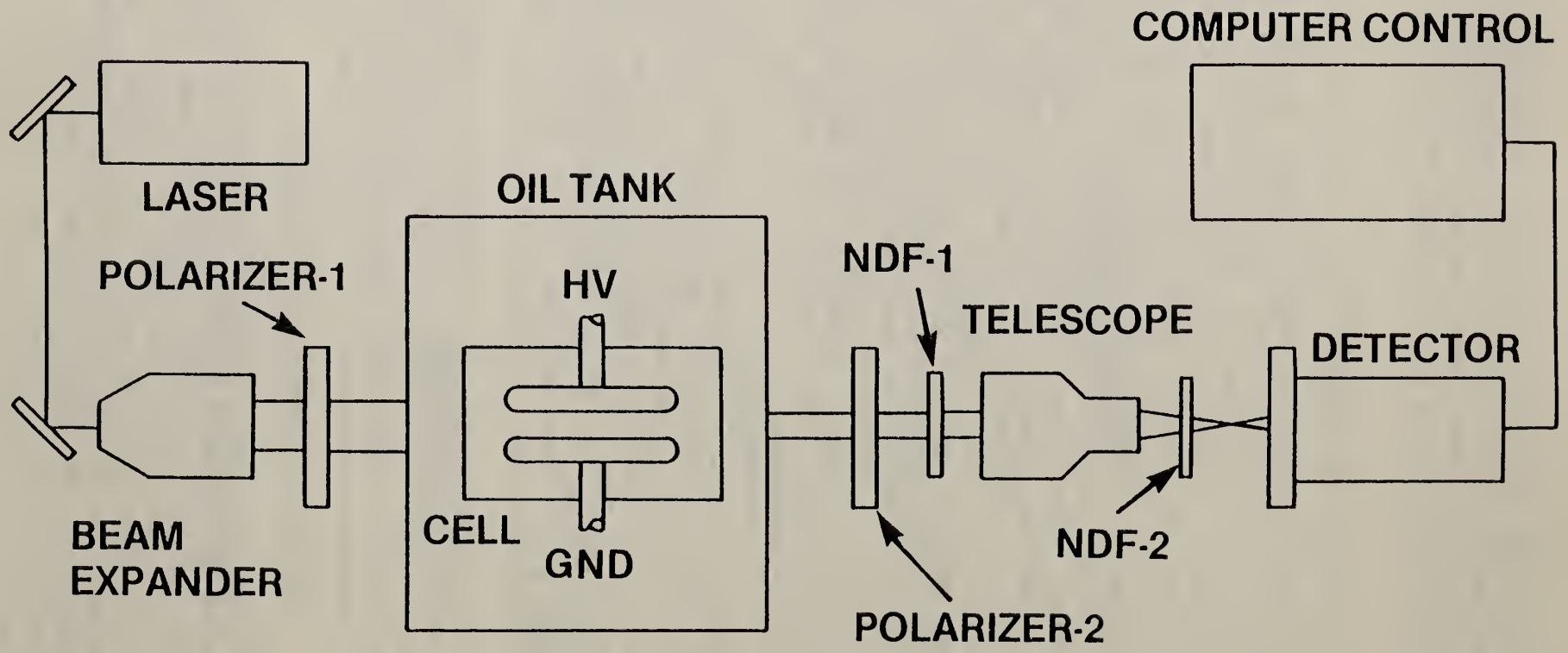

Fig. 14. Apparatus. An expanded laser beam provides illumination of the cell which is placed in an oil tank between crossed polarizers. A telescope provides proper image magnification, and neutral density filters are used to regulate the light intensity. The transmitted light is measured by a computer-based, intensified, silicon-vidicon detector.

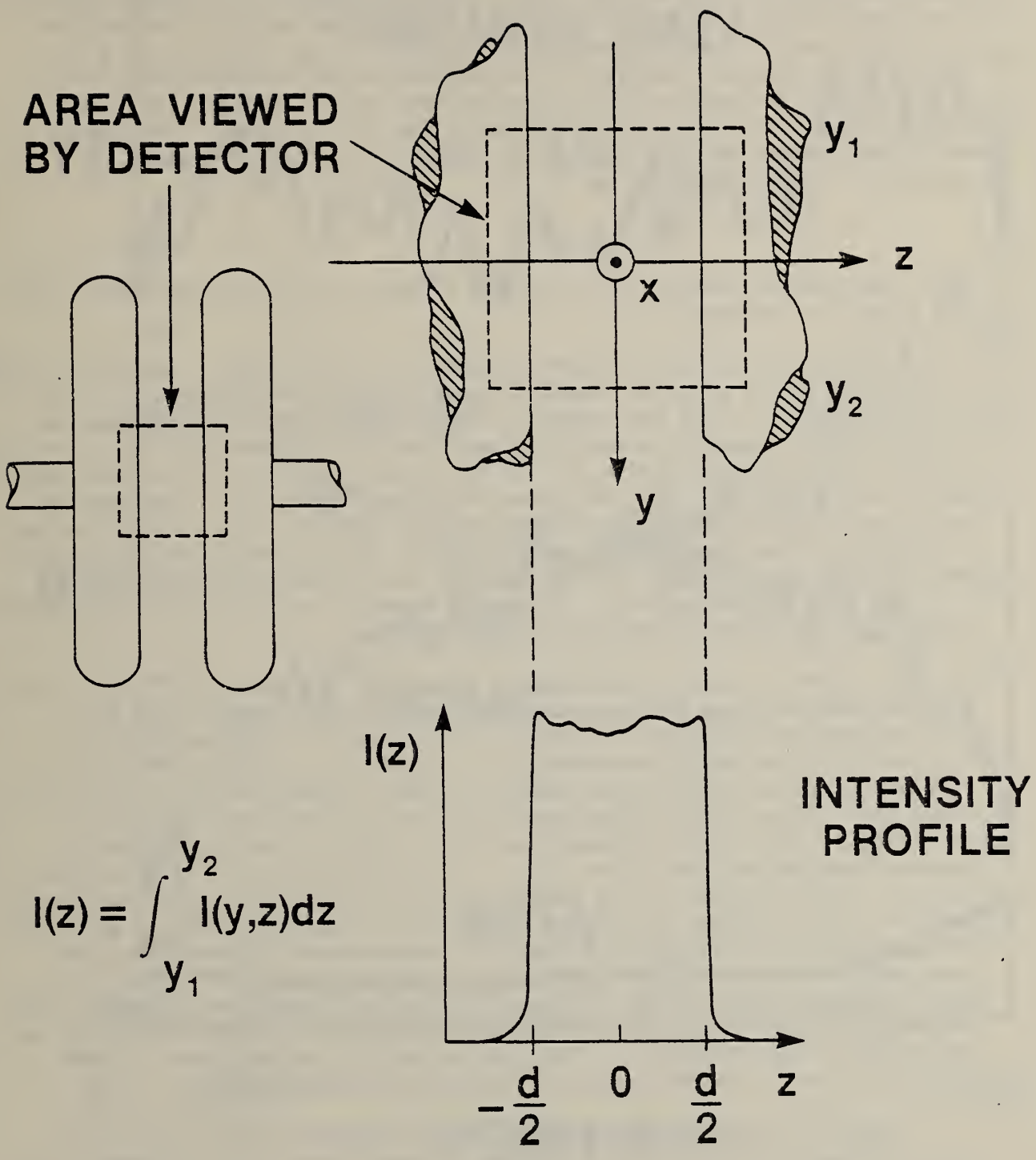

Fig. 15. The intensity profile I(z) generated by the computerized detection system is produced by scanning the viewed detector area and integrating the intensity for each scan parallel to the y axis.

To analyze the 60-Hz ac Kerr patterns, the distortions of the electric field arising from the fringe fields are determined. In an ideal parallel-plate Kerr cell, i.e., where the field is confined entirely between the plates of length ℓ and separation d, the Kerr fringe number n is given by eq (23). However, because of the fringe fields extending beyond the plates, there is some question as to whether or not these fringe fields will produce a significant distortion in the Kerr pattern. The change in fringe number Δn associated with a field distortion ΔE can be determined from eq (23) to be

$$\Delta E/E = \Delta n/2n \quad . \tag{35}$$

This field distortion arising from the fringe field can be measured using the detection system.

In figure 16, several intensity-profiles are shown for impulse voltages. The profile for 41 kV, for example, shows an intensity change of $\Delta I/I_m \approx 0.3$ on the average. Since the intensity is related to the fringe number by eq (24), this change in intensity gives rise to a fringe shift of $\Delta n = 0.2$. Using a fringe number of $n = 27 \pm 3$, the effective field distortion becomes $\Delta E/E = 0.004$ or 0.4%. Not only does this low distortion illustrate the approximately uniform field provided by this system, but it also provides an example of the measurement precision. In the following 60-Hz ac data, the fringe number is less than 10 so that the fringe-field contribution ($\sim 0.4\%$) will not be evident. Thus, any nonuniformity may be attributed to electric field distortions due to space charge.

The 60-Hz ac data is obtained by recording an intensity profile for 1 μs at some selected point on the 60-Hz waveform. The profiles for 100 consecutive waveforms are added to form the final intensity profile for that position on the waveform. In figures 17 and 18, profiles are displayed for the positive and negative peaks, respectively. Each profile shows the fringe pattern associated with the peak voltage. Because the intensity is not uniform between the plates, it is clear that there is space-charge distortion of the field. Since the relative field strength E/E_m is related to the fringe number n via eq (23), figure 19 shows the relative field between the plates as inferred from the intensity profiles. For both positive and negative peaks, a space-charge threshold may be seen near $n = 1$ or $E = E_m$. There is a pronounced decrease in the field near the anode and a slight increase in the field near the cathode. Also noteworthy is the fact that the space-charge density seems to saturate as the applied field increases. The charge density, proportional to the field gradient as shown by eq (28), may now be determined.

Figure 20 shows the approximate charge density ρ measured at the positive peak as a function of applied voltage. Here it is assumed that $E_m = 12.7$ kV/cm and $\kappa = 35$ for nitrobenzene. These curves are rough indications of space-charge behavior, not precision calculations based on eq (28); however, a saturation space charge of -400 nC/cm^3 or more is indicated.

Any net light intensity at the positive-negative zero crossing (PNZC) of the 60-Hz waveform reveals that the space charge decays more slowly than the voltage decay of the waveform [8]. Figure 21 shows PNZC profiles

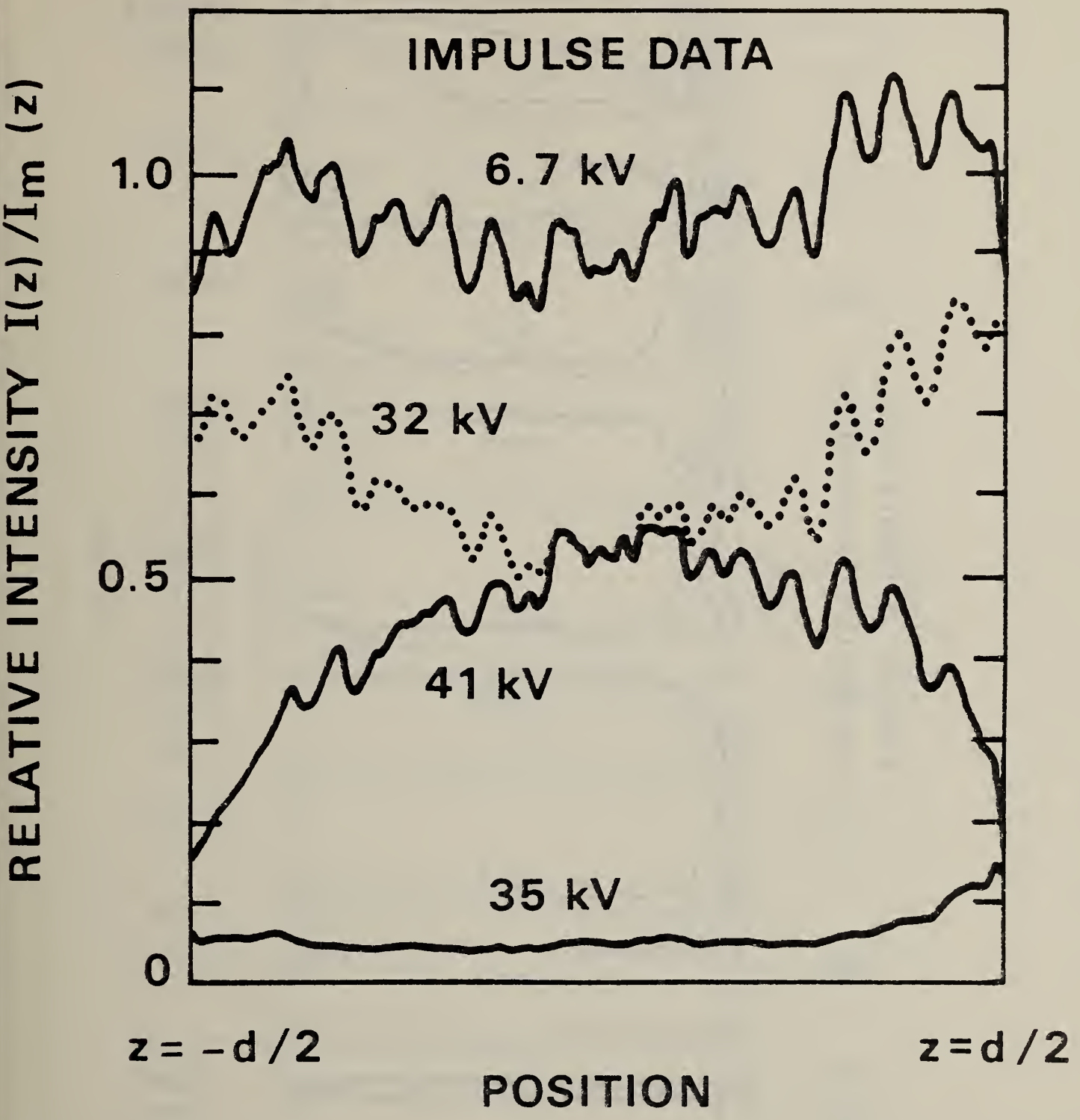

Fig. 16. Relative intensity profiles for impulse voltage applied to a nitrobenzene Kerr cell. The extent to which the profiles deviate from being uniform from plate to plate provides a measure of the nonuniformity of the field. The smaller, higher frequency modulations of the profiles are due to nonuniformities in the light sources and small changes within the liquid.

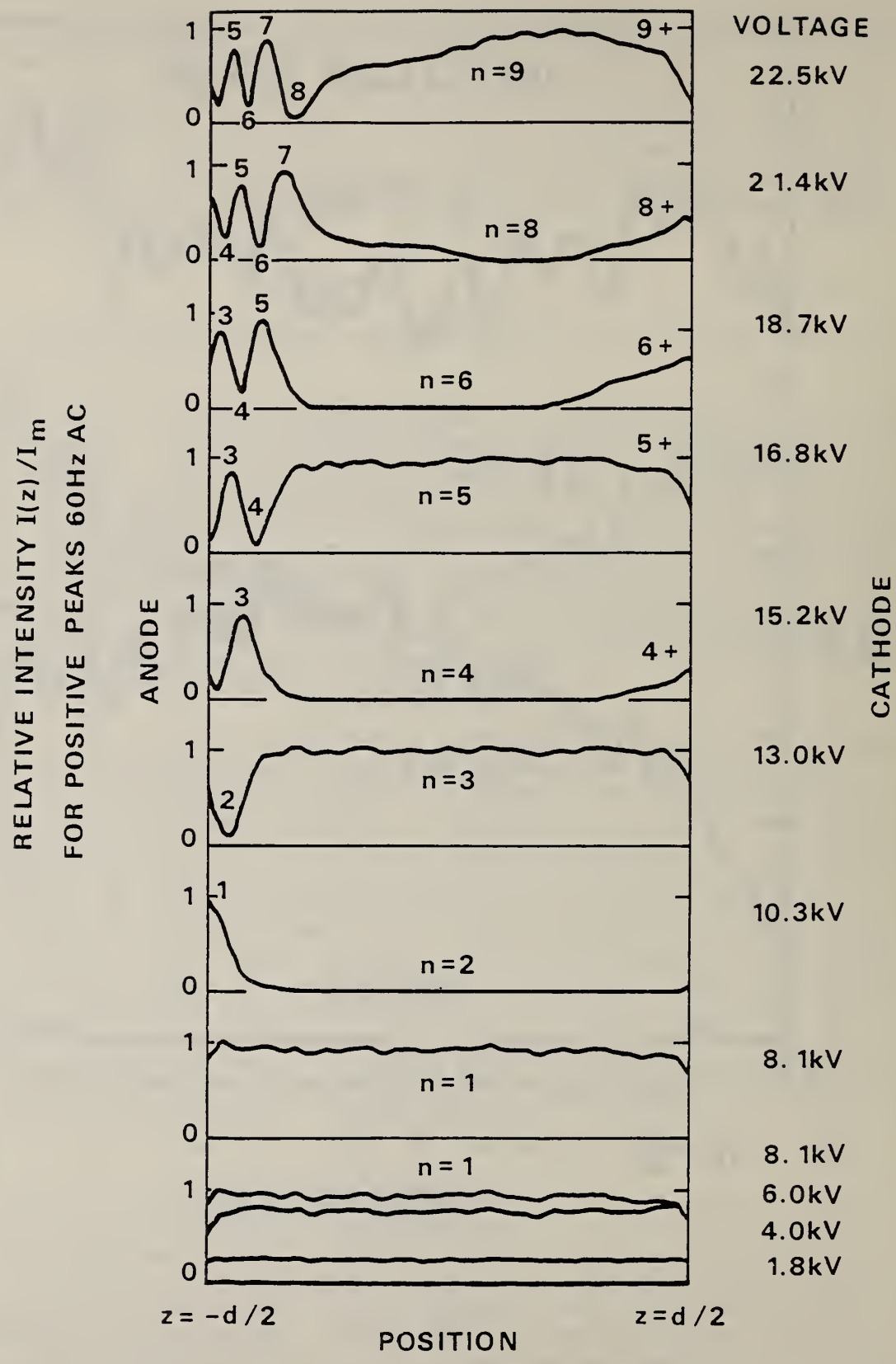

Fig. 17. Relative intensity profiles at the peak of the 60-Hz ac waveform vs several peak voltage levels. Note that distortions do not become obvious until the fringe number n exceeds one. The numbers near the profiles denote the fringe number.

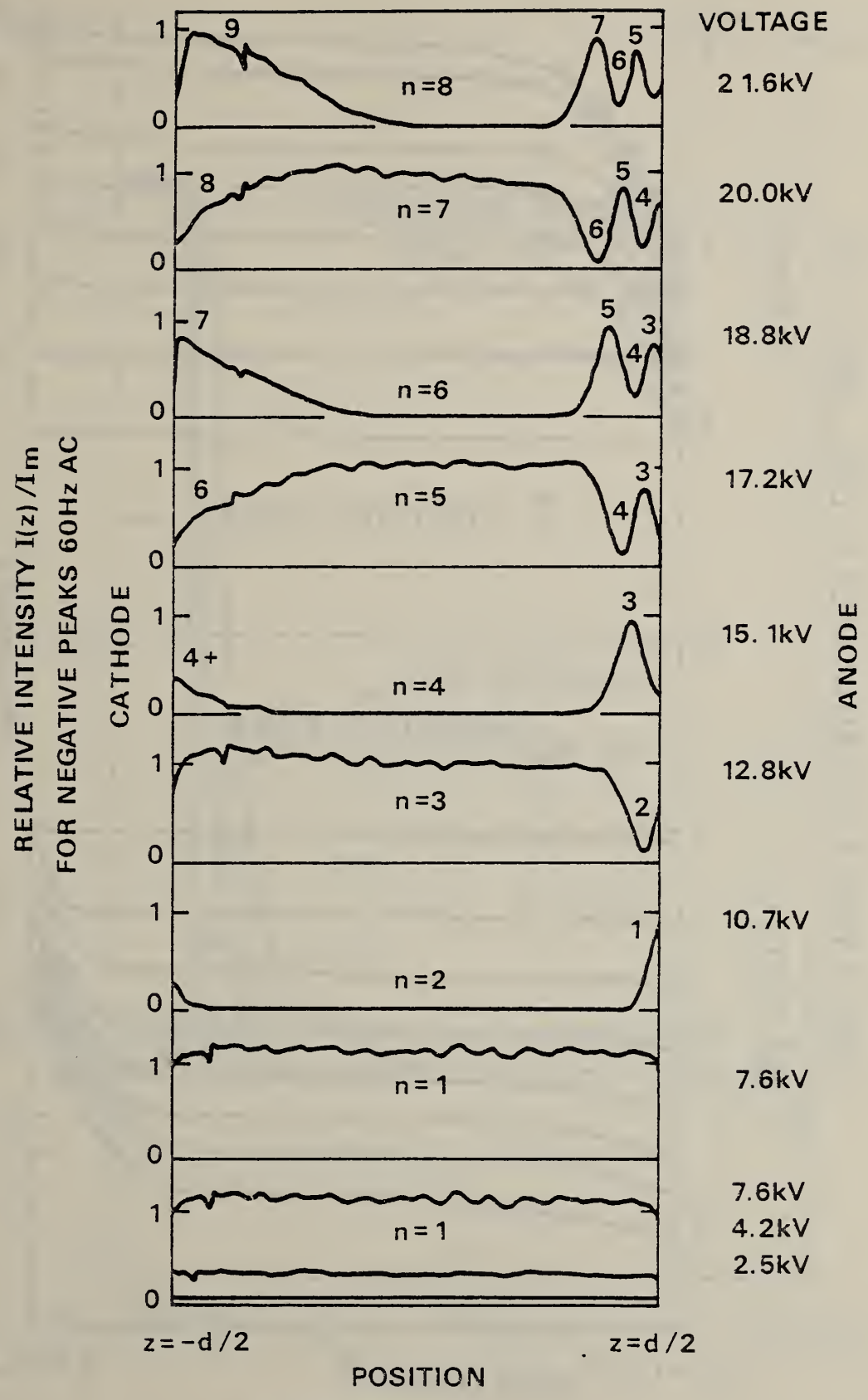

Fig. 18. Relative intensity profiles at the negative peak of the 60-Hz ac waveform vs peak voltage level. The numbers near the profiles denote fringe number.

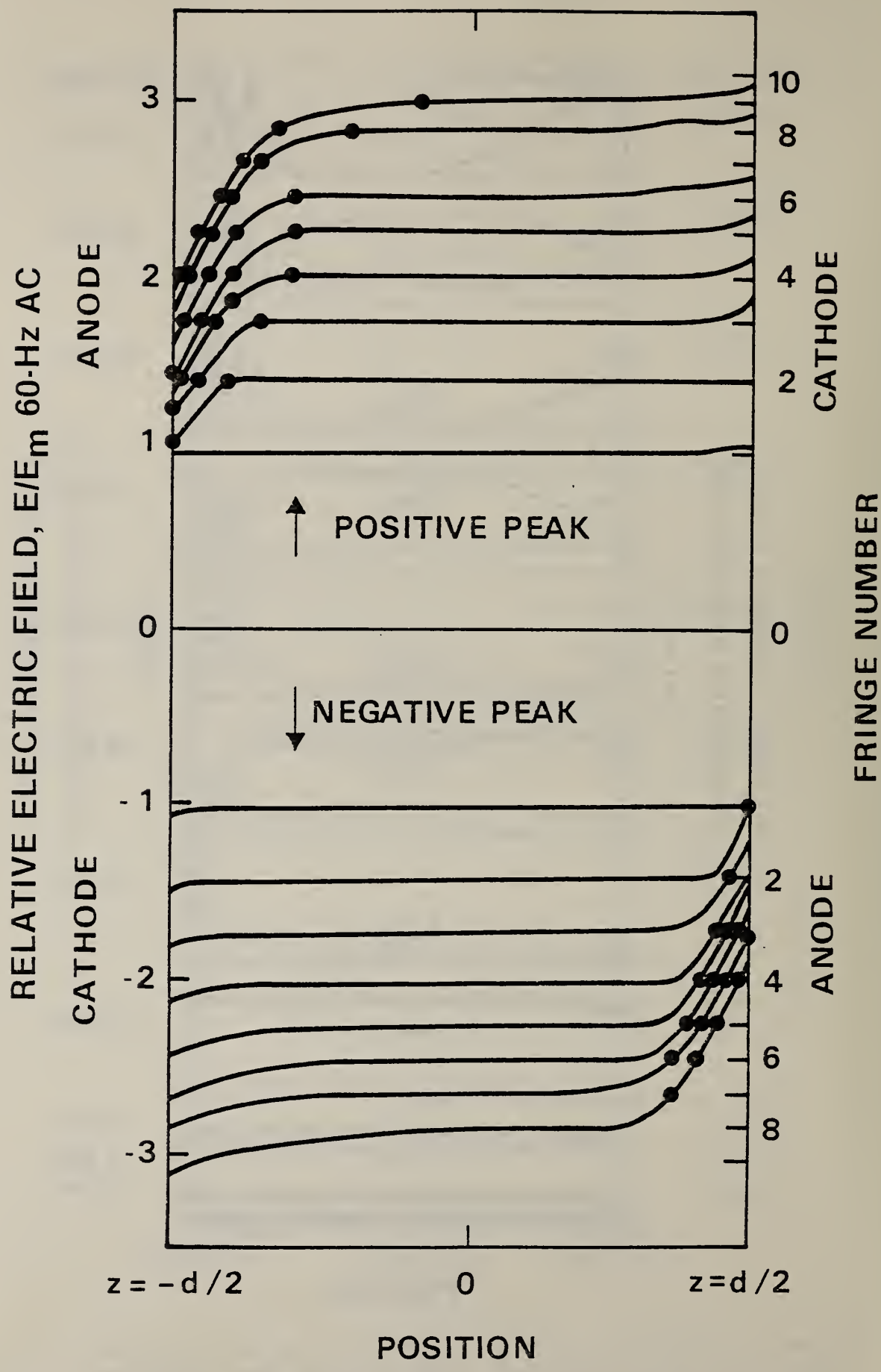

Fig. 19. Relative electric field at the positive or negative peak of the 60-Hz waveform as a function of position for the voltages in figures 17 and 18.

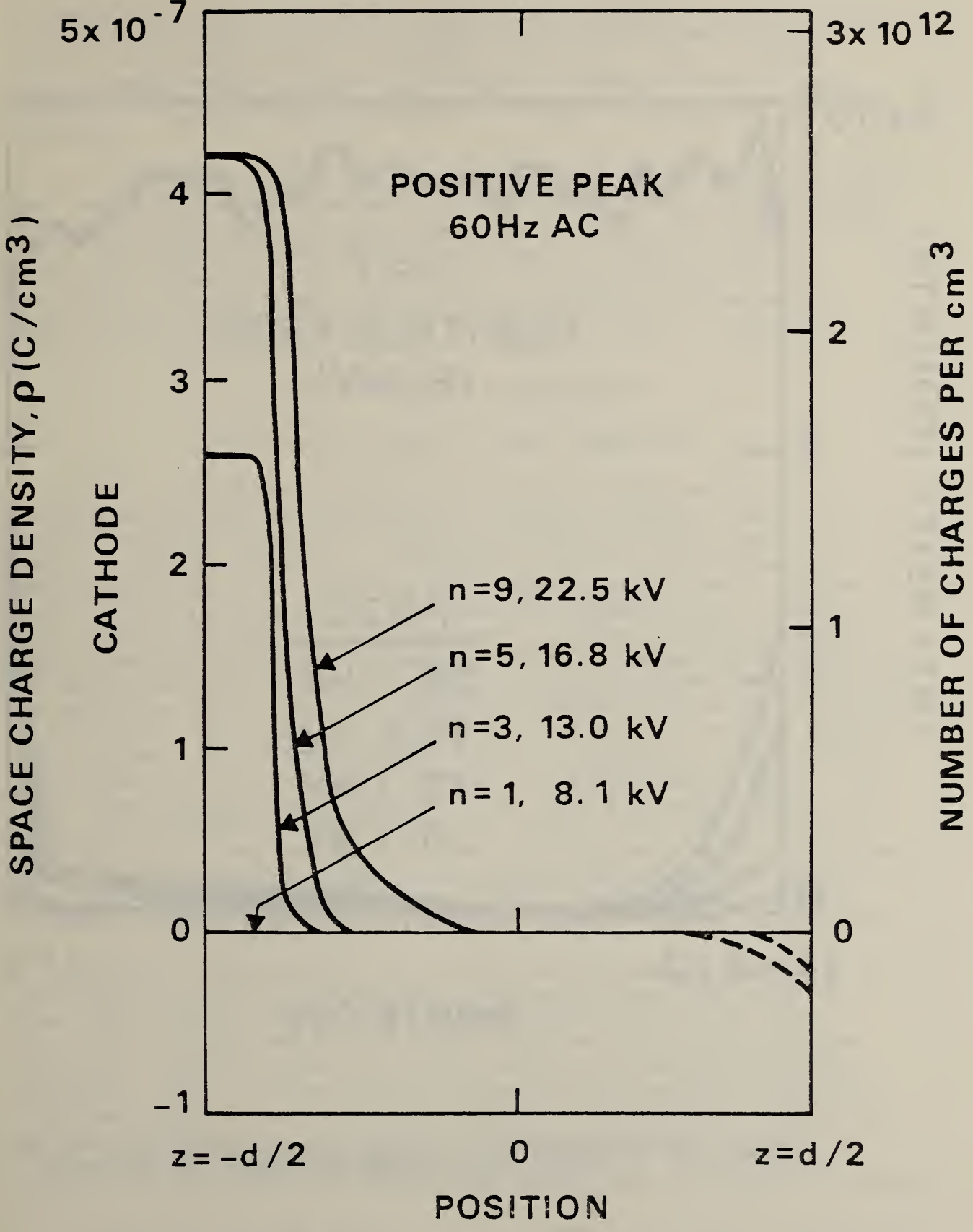

Fig. 20. Space-charge density in nitrobenzene. These approximate curves are inferred from the relative electric field plots in figure 19. Note that the highest density shown refers to 3.7 x10^9 molecules, assuming one charge per molecule.

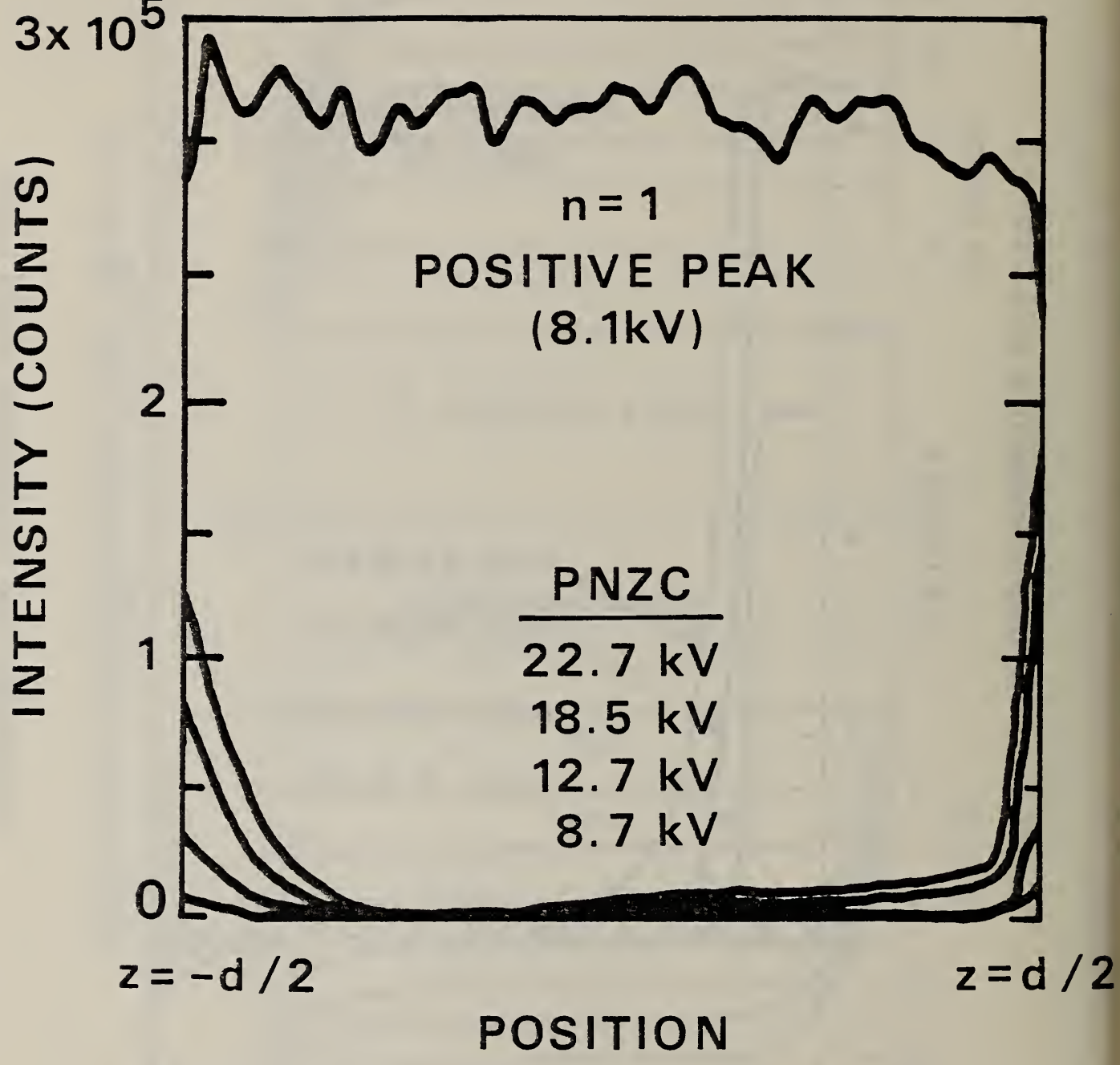

Fig. 21. Positive-negative zero-crossing profiles compared with the n = 1 profile. The grounded electrode is at the left.

as compared to the n = 1 profile. Note the peaks near the plates. It is instructive to examine the voltage dependence of these peaks to see if saturation of space charge at the PNZC also occurs. Figure 22 shows a plot of these intensity peaks as a function of voltage squared. A saturation of space charge is clear as a plateau is approached for higher voltages.

As a further illustration of space charge, it is instructive to record the intensity profiles at selected points from the negative peak, through the zero crossing to the positive peak (see fig. 23). These profiles are not significantly different from those shown in figures 17 and 18. Differences between the positive peaks of figures 17 and 23 may be a result of increases in space charge due to contamination from water diffusing out of the nylon walls of the cell or a result of the lack of precision associated with setting the voltage.

D. ELECTRIC FIELDS IN TRANSFORMER OIL

1. Contaminated (Wash) Oil, Room Temperature

Electro-optical measurements of the electric field were made in transformer oil employed previously as a wash for radiators used in power transformers after their construction was completed. One problem which is more significant in transformer oil than in nitrobenzene is the degeneration of the intensity profile due to turbulence. Each time the detector records a profile, it stores the intensity data in memory. The number of records which are averaged to produce an intensity profile may be controlled. Figure 24 shows the effect of increasing the number of records per profile from 10 to 100. The intensity profiles are produced by applying ac 66.8 kV peak to plates with length ℓ = 30 cm and separation d = 0.64 cm. Timing was such that the positive peak of the 60-Hz waveform was observed. If the intensity per record, at any point z, were normally distributed with a standard deviation of σ, one would expect that N scans would show a standard deviation $\sigma_n = \sigma/\sqrt{N}$. Such a situation is not observed presumably because the observation time, even for 10,000 scans, may not be sufficient to obtain a normal distribution because of long-time turbulence fluctuations or flow pattern changes within the cell due to heating. To reduce the effects of turbulence, each intensity profile below is a composite of 10,000 scans which requires 2.8 min to accumulate.

Figure 25 shows intensity profiles at 70.5 kV peak voltage 60-Hz ac -- six positive peak (PP) profiles and three negative peak (NP) profiles. These data have not been adjusted by subtracting a background signal. The "glitch" at the left side of the NP profiles is an artifact of the detector. Figure 26 shows the averaged data with background profiles subtracted. The error bar represents the standard deviation associated with the profiles. There does not appear to be any measurable distortion in these profiles, i.e., it appears that space charge has no effect on the field distribution. To check this conclusion, it is important to examine the relative field strength E/E_m and not just the intensity profiles.

An estimate of the incident profile is made by aligning the polarizers and recording the $I_m(z)$ profile. This turns out not to be an adequate means to establish the true $I_m(z)$ profile because of the imperfections

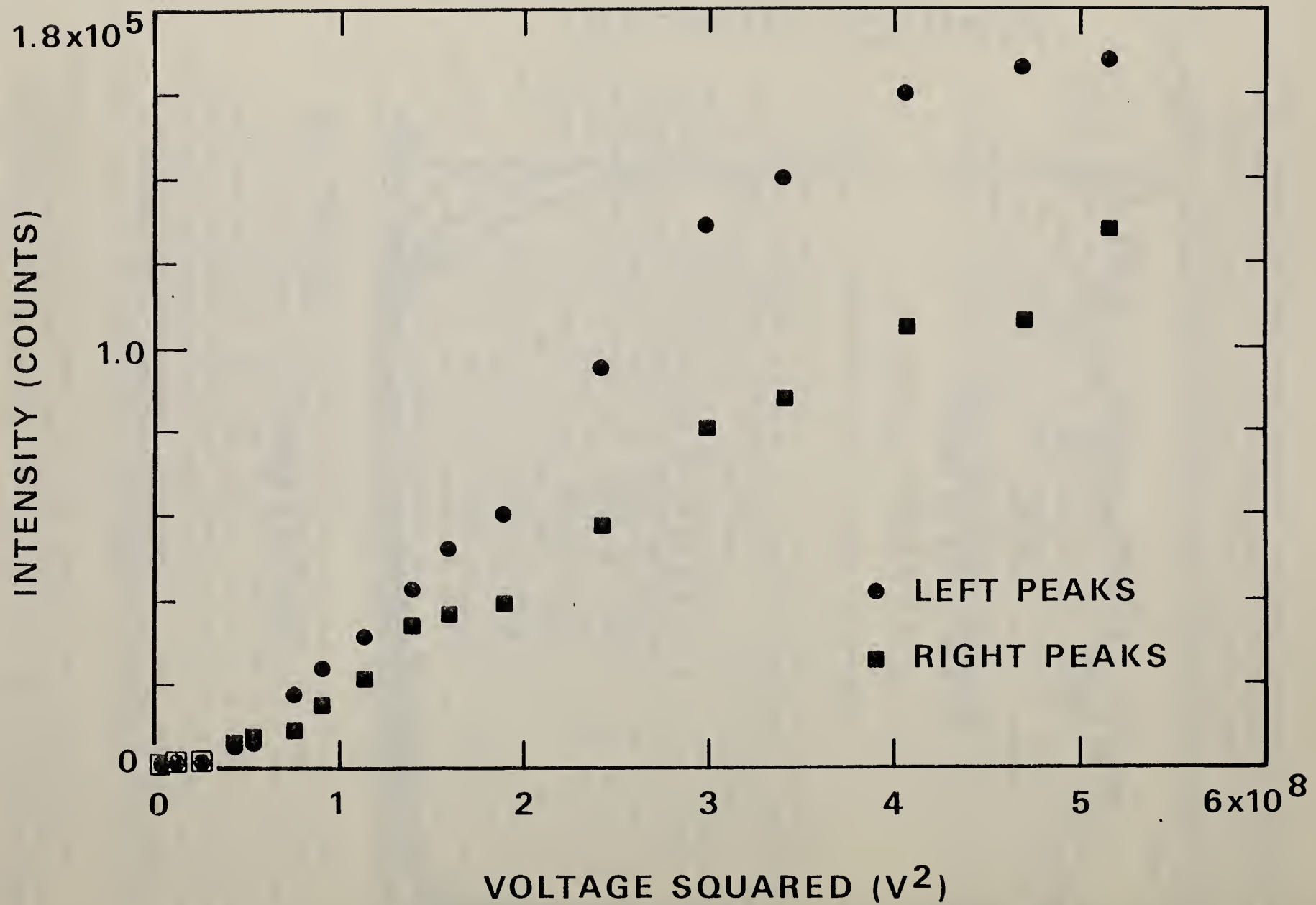

Fig. 22. The height of the transmittance peaks at the positive to negative zero crossing as measured at the plates as a function of the peak voltage squared. The grounded electrode is at the left. (V^2 is used as the abscissa rather than V or V^4 in order to keep in line with customary Kerr-effect plots.)

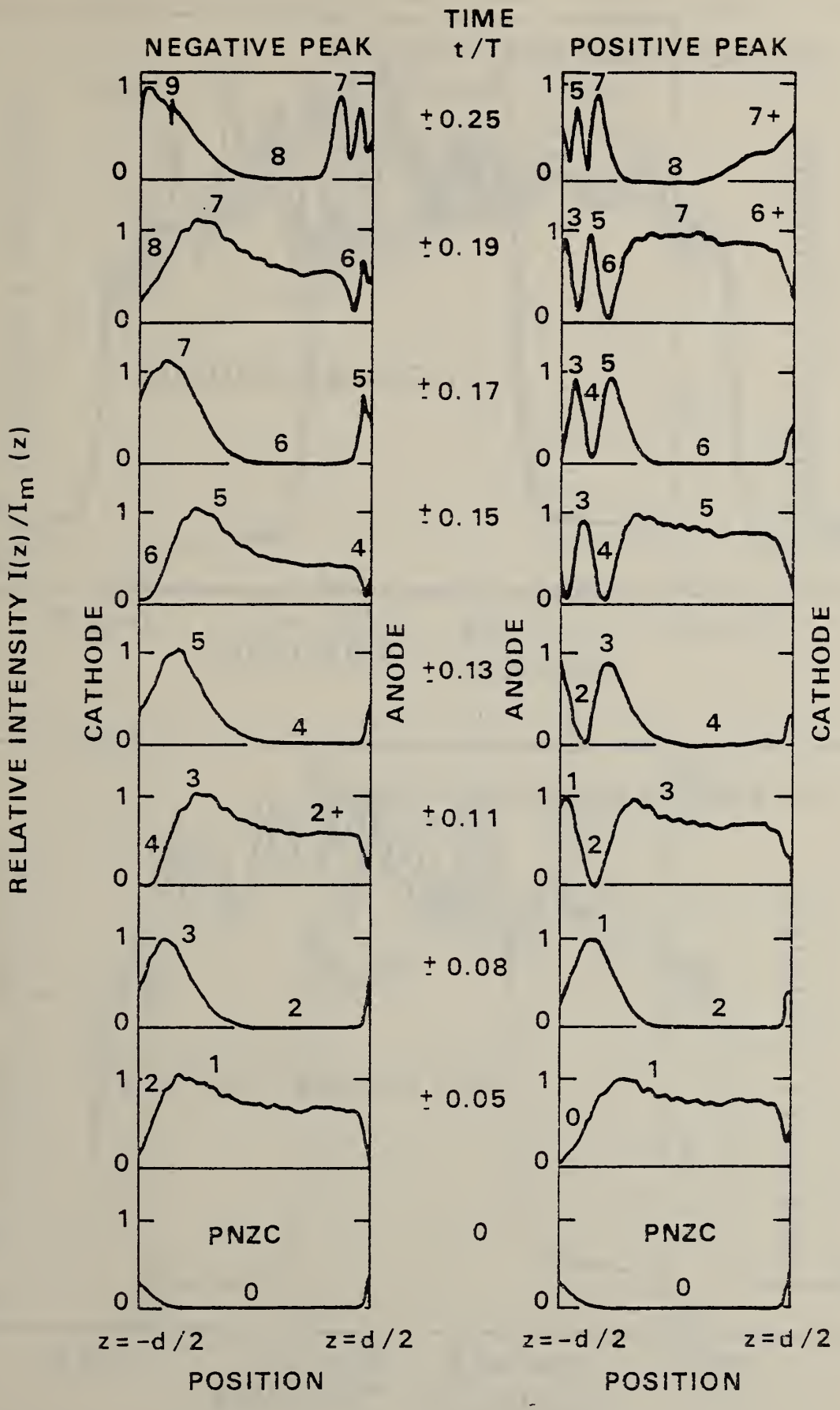

Fig. 23. The change in relative intensity selected voltages between a negative and a positive peak. The peak applied voltage was about 22 kV.

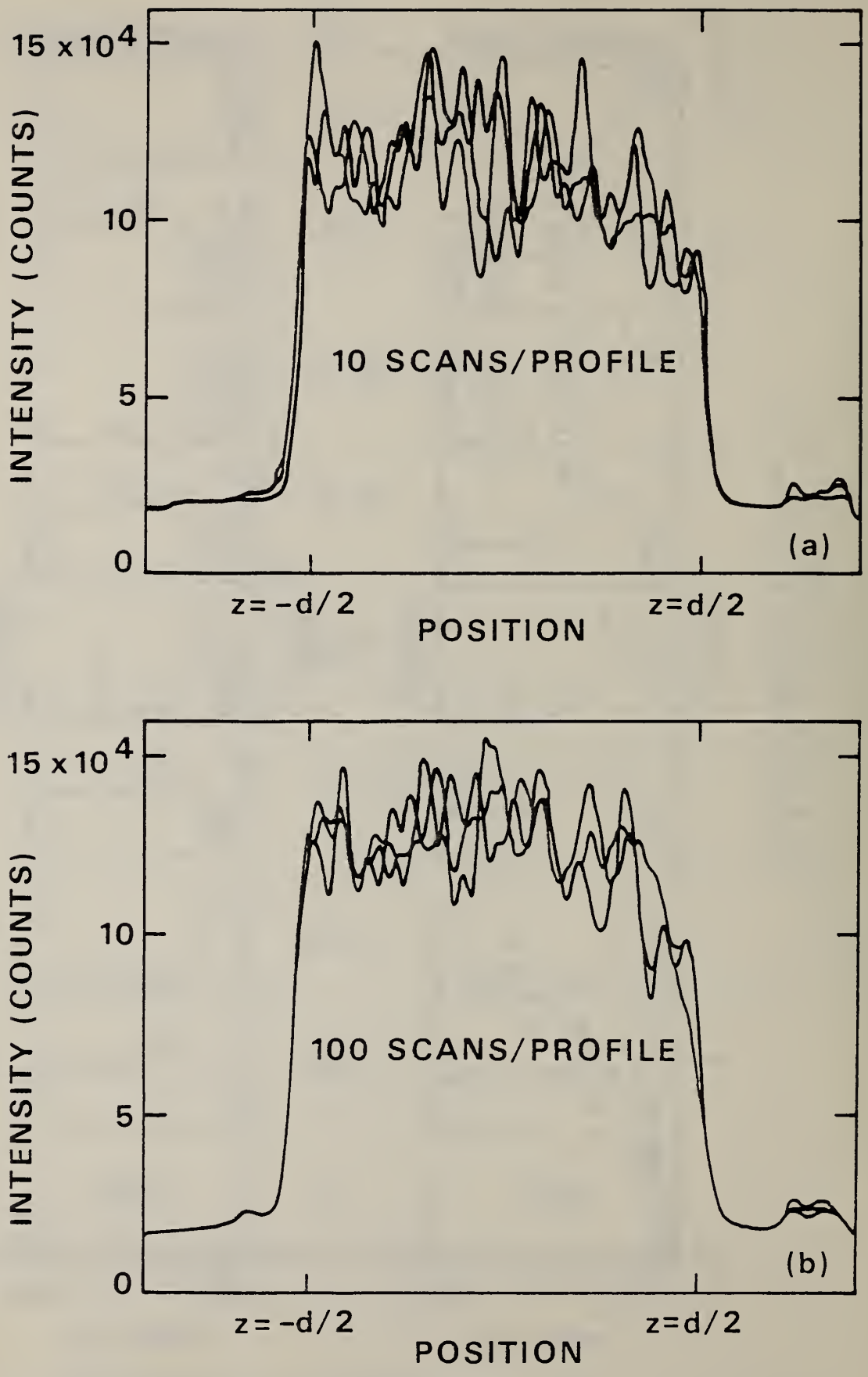

Fig. 24. Comparison of the measured intensity averaging 10 detector records and 100 detector records.

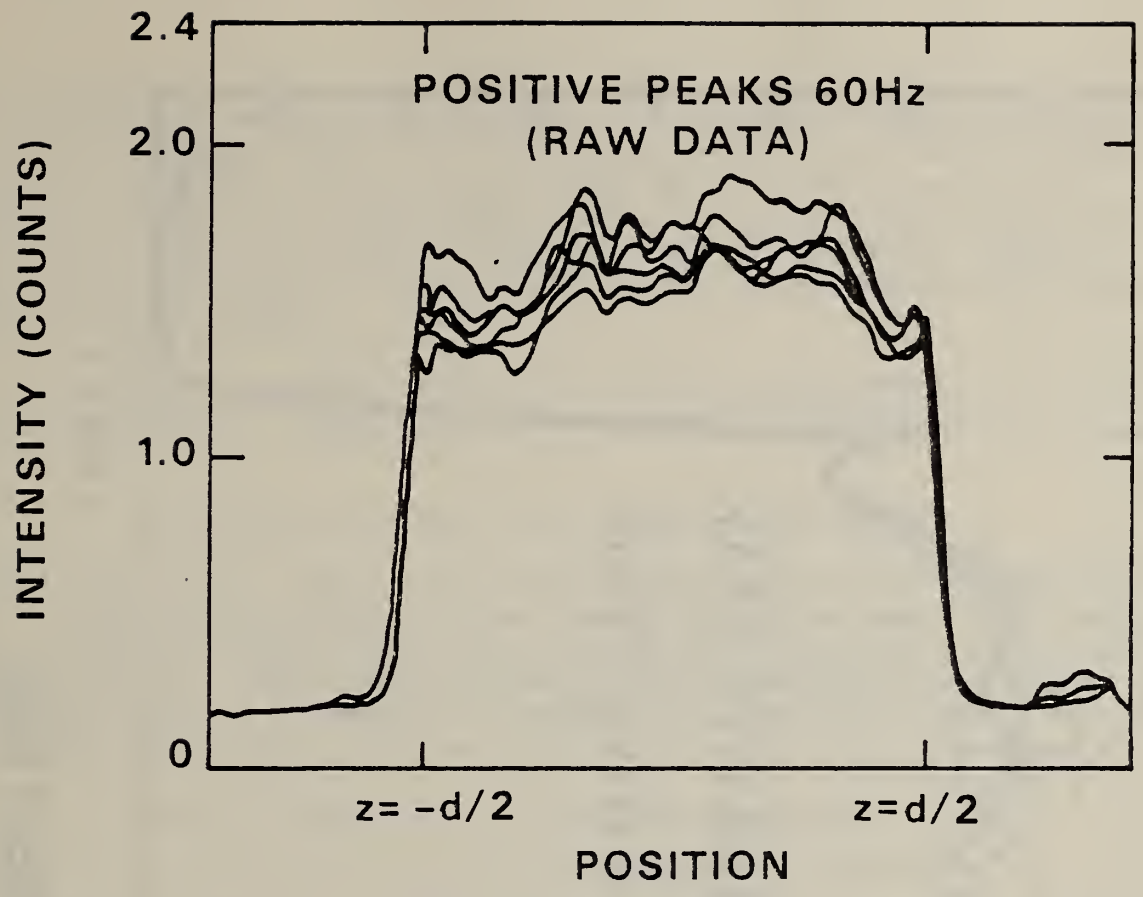

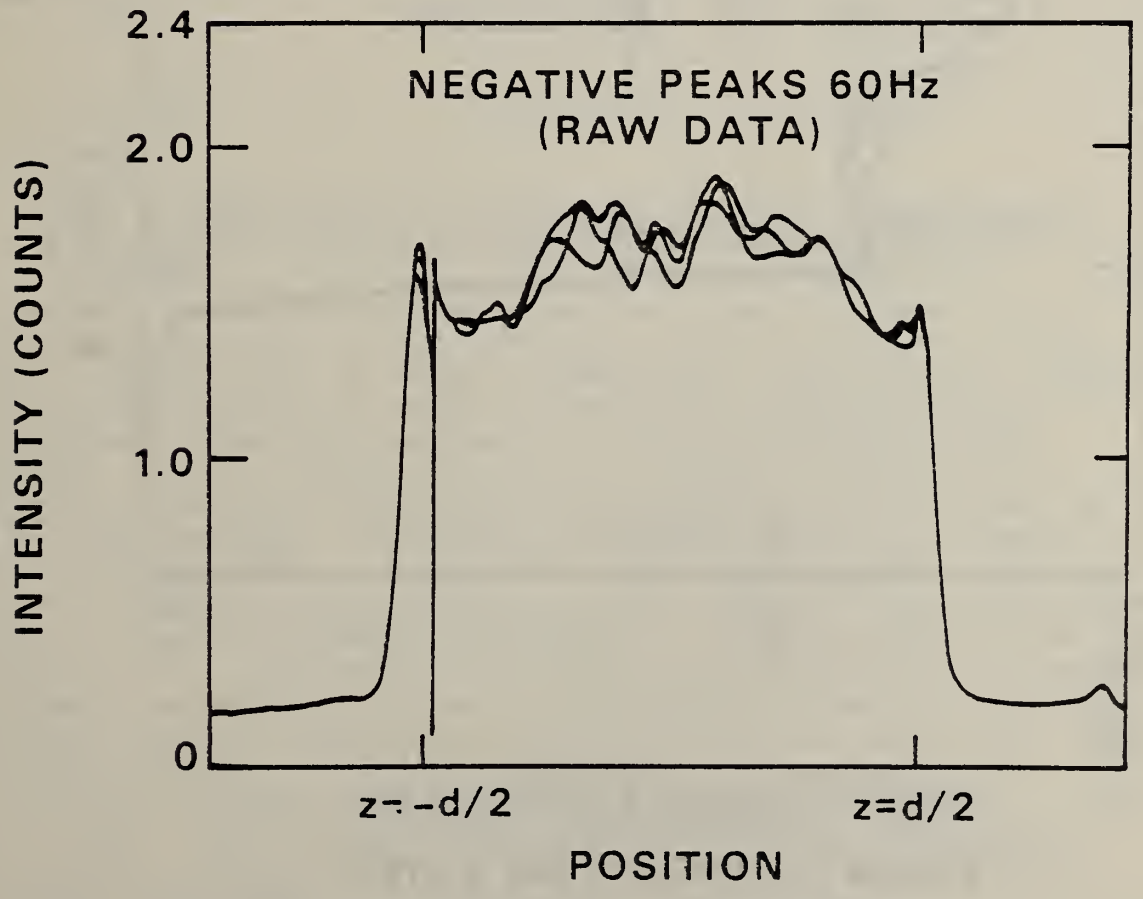

Fig. 25. Intensity profiles taken at the positive peak and negative peak of the 60-Hz waveform. 10,000 scans were averaged to produce the profiles. The peak voltage was 70.5 kV.

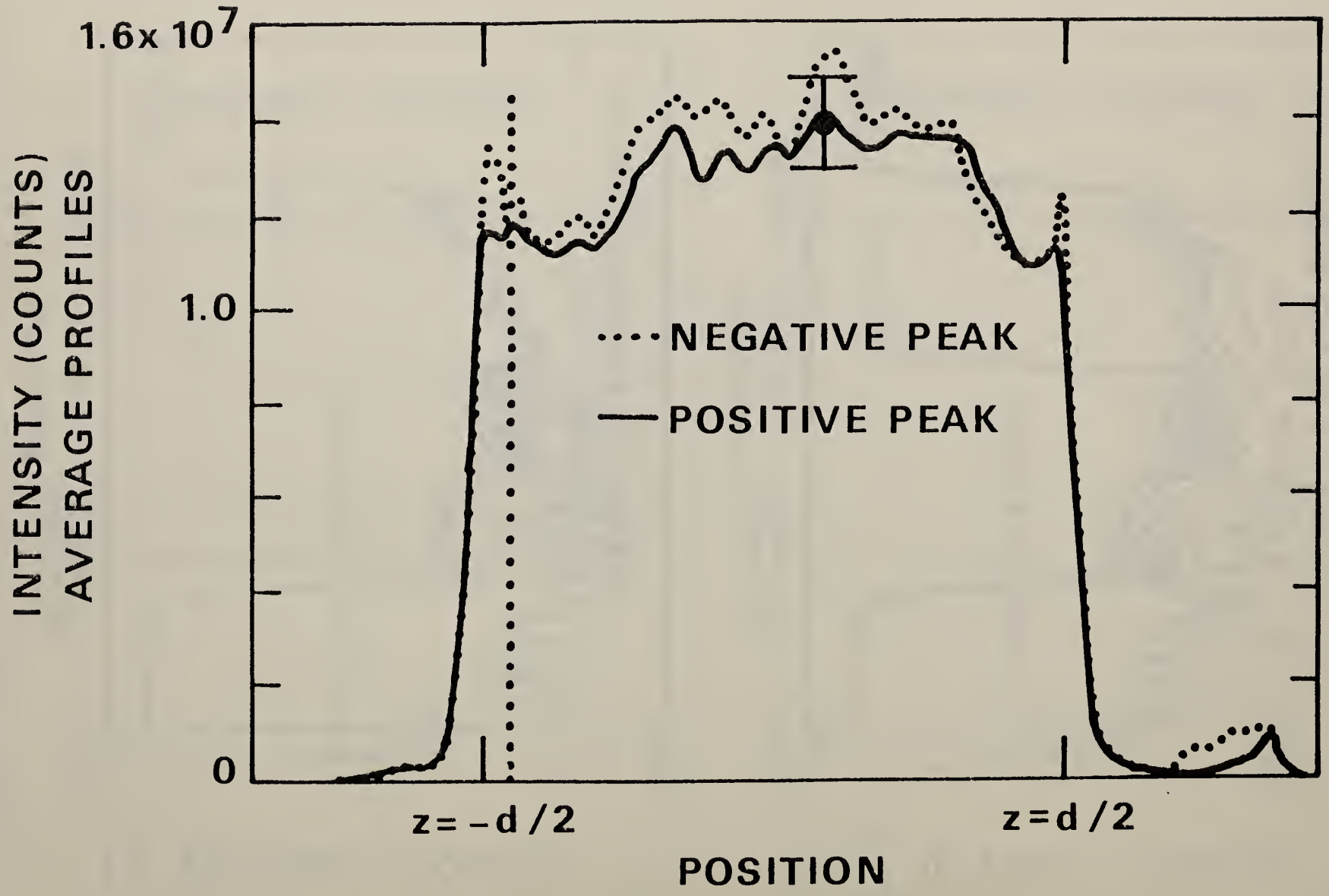

Fig. 26. Comparison of the average positive and negative peak profiles with typical standard deviation associated with these measurements.

in the optical elements. A more sophisticated process is needed which will be presented and used in later data presentations. The determination of $E(z)/E_m$ is accomplished via the approximation in eq (30) and the results are shown in figure 27. Thus the error bar in figure 27 represents the standard deviation of the field measurements and is about 3% of the relative field value. These data were taken with a field of 110 kV/cm. The cell readily broke down with fields of 129 kV/cm, so we were operating near the breakdown field strength.

The conclusion reached here is that even for room-temperature transformer oil which is heavily contaminated, space-charge field distortions are less than 3%.

2. Contaminated (Failed) Oil, Elevated Temperature

Although the oil used in the previous investigation was contaminated, there was some concern whether or not the typical contaminants were found in it. Some transformer oil was then tested which came from a transformer which had failed. Electro-optical Kerr-effect measurements were made on this oil at room and elevated temperatures. The contamination level of this oil is summarized in table 4.

Table 4. Summary of particulate contamination

Particle size[a] μm	Number of particles/ml Contaminated oil	Normal oil
3 - 150	1221	40 - 70
50 - 150	60	0.1 - 0.2

[a]About 90-98% of the particulates were cellulose (from the paper or pressboard in the apparatus) with the remaining being iron or copper.

An analysis similar to that performed previously was made for the intensity profiles taken at several temperatures. For these data, however, 100 scans were averaged for each I(z) profile and three I(z) profiles were combined to give the resulting I(z) profile from which E(z) is determined. The resulting E(z) profile was composed of an average of 300 profiles taken at the positive peak of the 60-Hz waveform. This was done at each temperature. Throughout these measurements, a voltage of about 42 kV was applied to the parallel plates with a gap of d = 0.64 cm so that the applied field was 66 kV/cm -- well under the usual breakdown voltages. Figure 28 summarizes the electric field measurements in the contaminated oil. The electric-field profiles shown here are normalized to emphasize and more easily quantify the relative distortions. At room temperature, this oil exhibited no measurable field distortion, that is, the electric field was uniform to within ±2% of its average value. Near 53°C, the field was again uniform to within about ±3% of its average value. Near 57°C the field was again uniform to within about ±3%; there may, however, have been some enhancement at the anode and a decrease of the electric field strength at the cathode.

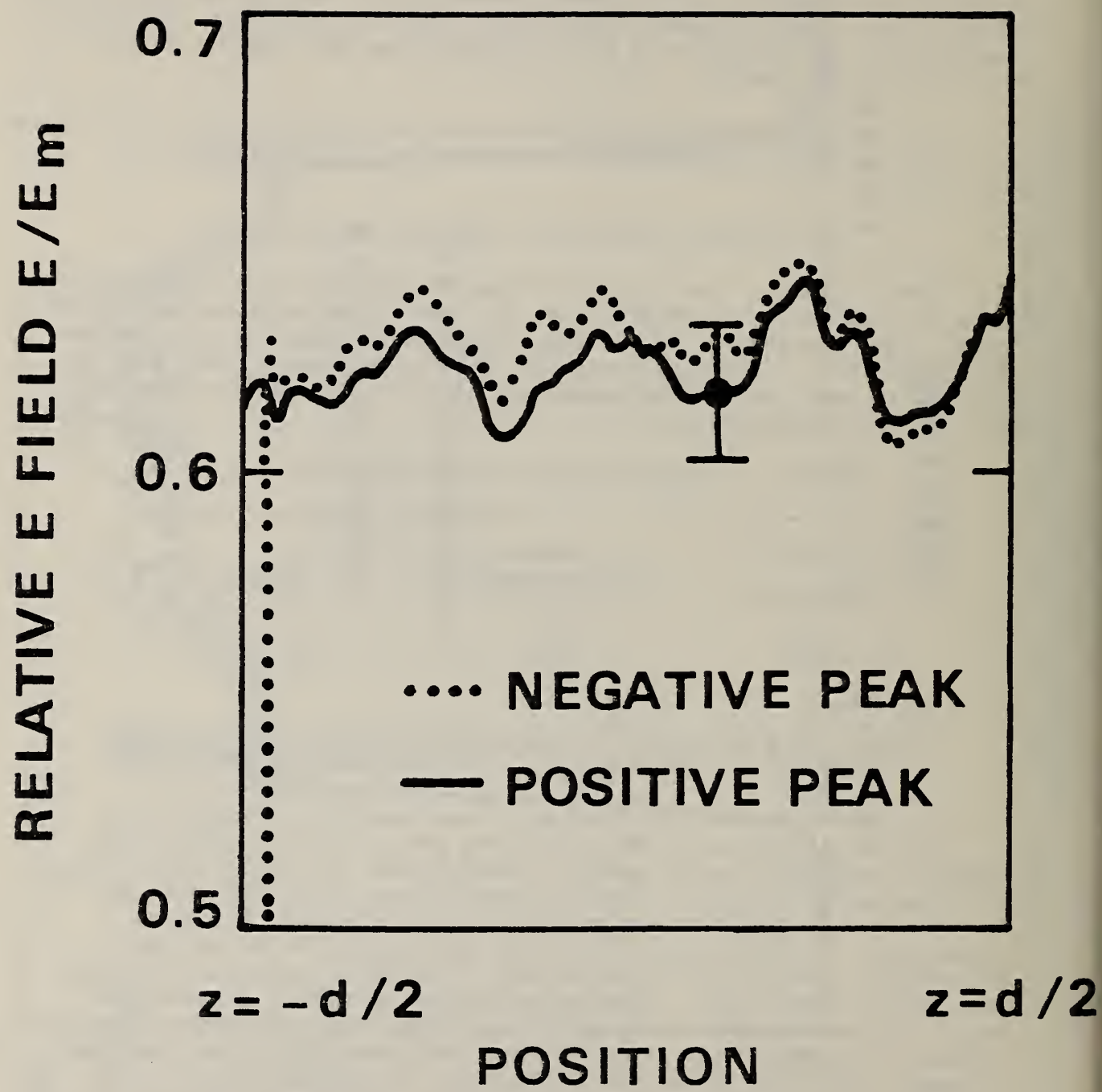

Fig. 27. Relative electric field for the positive and negative peaks and associated standard deviation .

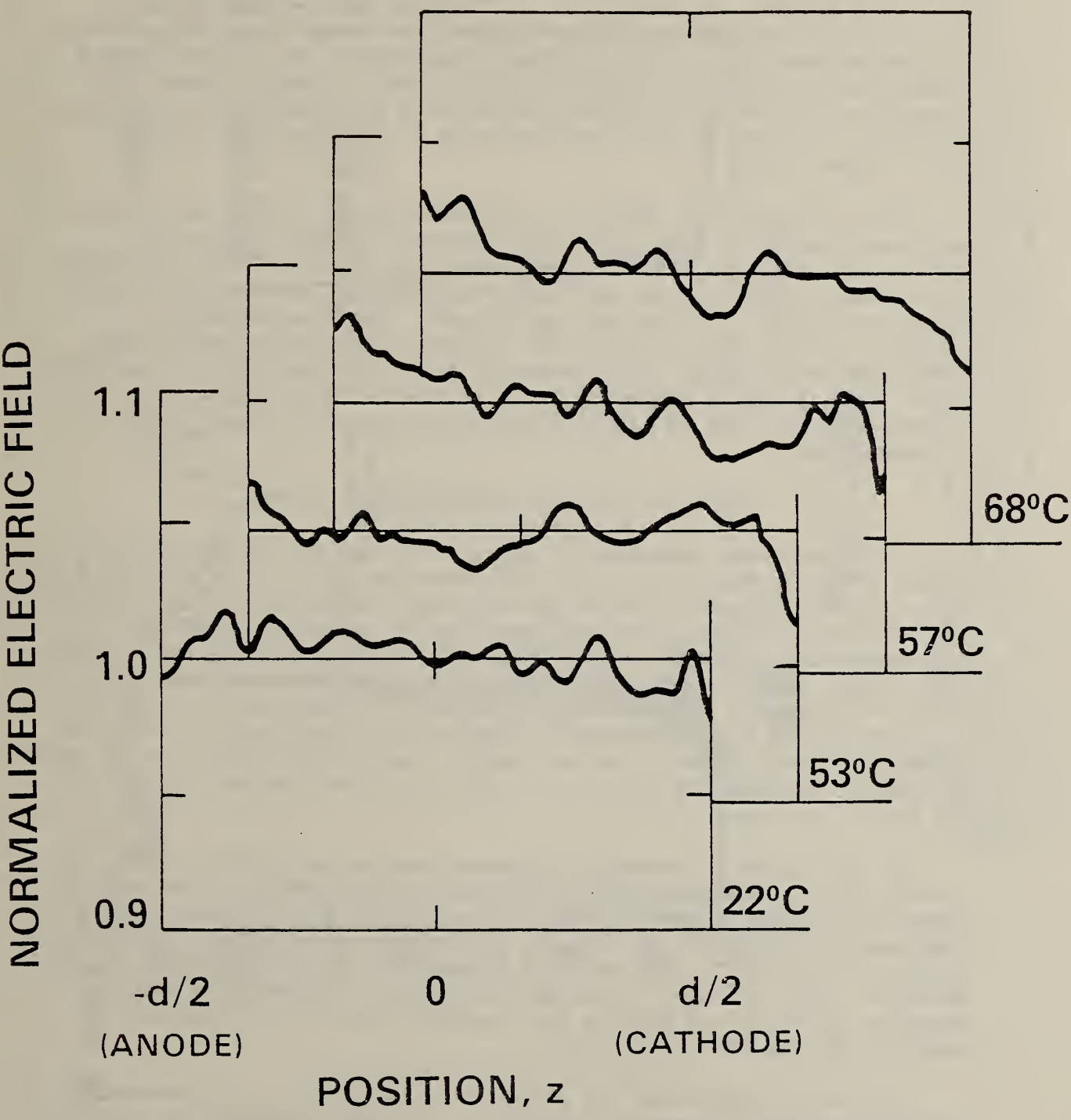

Fig. 28. The normalized field as a function of position between parallel plates in transformer oil at four different temperatures. The data at 68°C suggests that the space-charge density may be making a significant (~5%) contribution to the electric field.

For the temperature near 68°C an apparent distortion was observed in the electric field profile. The maximum 6% or more change in the field from one plate to the other was about 5% of the average electric field between the plates. If this is space-charge field distortion, and not an artifact of the apparatus, then the space-charge density which could produce such a distortion would be about -1 nC/cm^3. It must be stressed that this is a preliminary measurement and must be further substantiated before confidence in such a result is established. In comparison, the amounts of space charge which are found in nitrobenzene are easily a factor of 400 times larger than the value listed above for oil (see fig. 20).

With this possible indication of space charge, it was desirable to make measurements at even higher temperatures -- 100°C and higher. However, the cell was made from high-pressure, laminated phenolic plate (paper base, grade xx) and could not withstand the application of high voltage at 100°C. (The failure was probably due to water vapor.) However, profiles were obtained at 75°C and room temperature. These profiles were similar to those shown in figure 28, only with an opposite slope. Such a result suggests that even the 6% field distortions indicated by the data in figure 28 may not be real but an artifact of the measurement.

3. Clean Oil, Elevated Temperatures, AC, DC

To extend these measurements above 100°C, several materials were tested in transformer oil up to 170°C under the application of high voltage. On the basis of these tests, a new cell, cell holder, positioning device, and tank were designed. The cell was made of stainless steel with machinable glass ceramic, acetal or polytetrafluoroethylene (PTFE) plastic high voltage feed-throughs and electrode supports and silicone rubber and/or PTFE seals. The insulated, aluminum, oil tank has a sealed top and vents to the laboratory air through an activated charcoal filter to eliminate hot-oil odors. The cell can be positioned in the tank by means of controls outside the tank. Up to 6600 W of heat may be applied to the tank.

At this point a "standard" procedure was established to record the profile data. We summarize the main features in table 5. The profiles (denoted by memory number in table 5) associated with an actual run are displayed in figures 29 through 31. These data were taken at an oil temperature of 76°C. Each curve is a composite of 1000 scans of the detector. When voltage is applied, the phase is adjusted so that the detector (on for 6 μs) obtains the intensity profile for the positive peak (PP) of the 60-Hz waveform.

In order to determine the electric field $E(z)/E_m$, it is necessary to know the relative intensity $I(z)/I_m(z)$. It is not adequate to align the polarizers and determine $I_m(z)$ because the polarizers are not perfect and small perturbations in the intensity pattern -- almost invisible to the eye -- become important. Measurements with the polarizers aligned, however, provide a value for the magnitude of I_m. The profile shape of $I_m(z)$ is obtained by slightly rotating the polarizers from their crossed position to obtain a measurable intensity. The intensity profile does

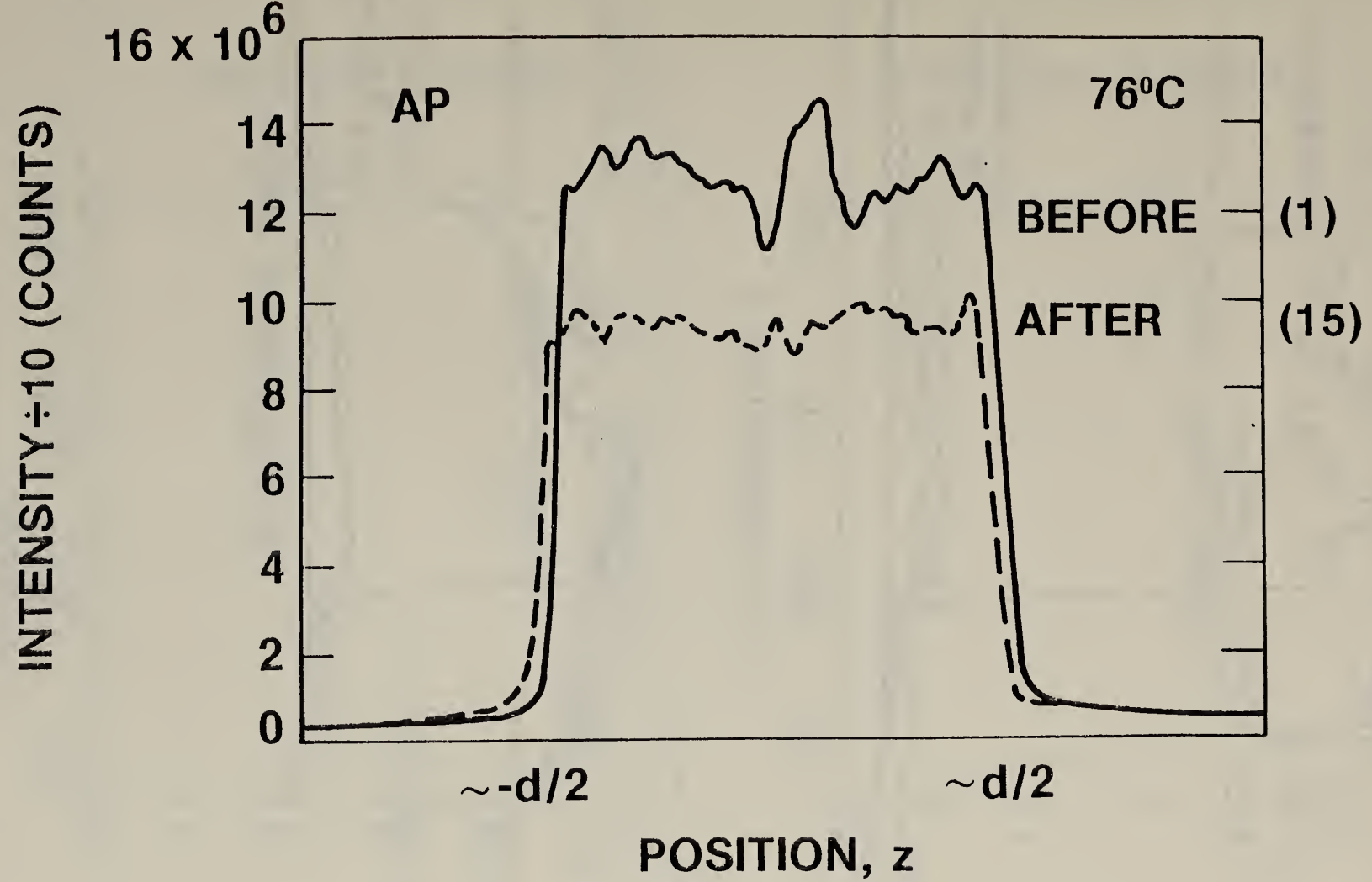

Fig. 29. Intensity profiles for aligned polarizers. These are only used to establish the magnitude of I_m and not the shape. The intensity after voltage application has decreased probably due to increased particulate contamination and/or malfunction of illuminating laser.

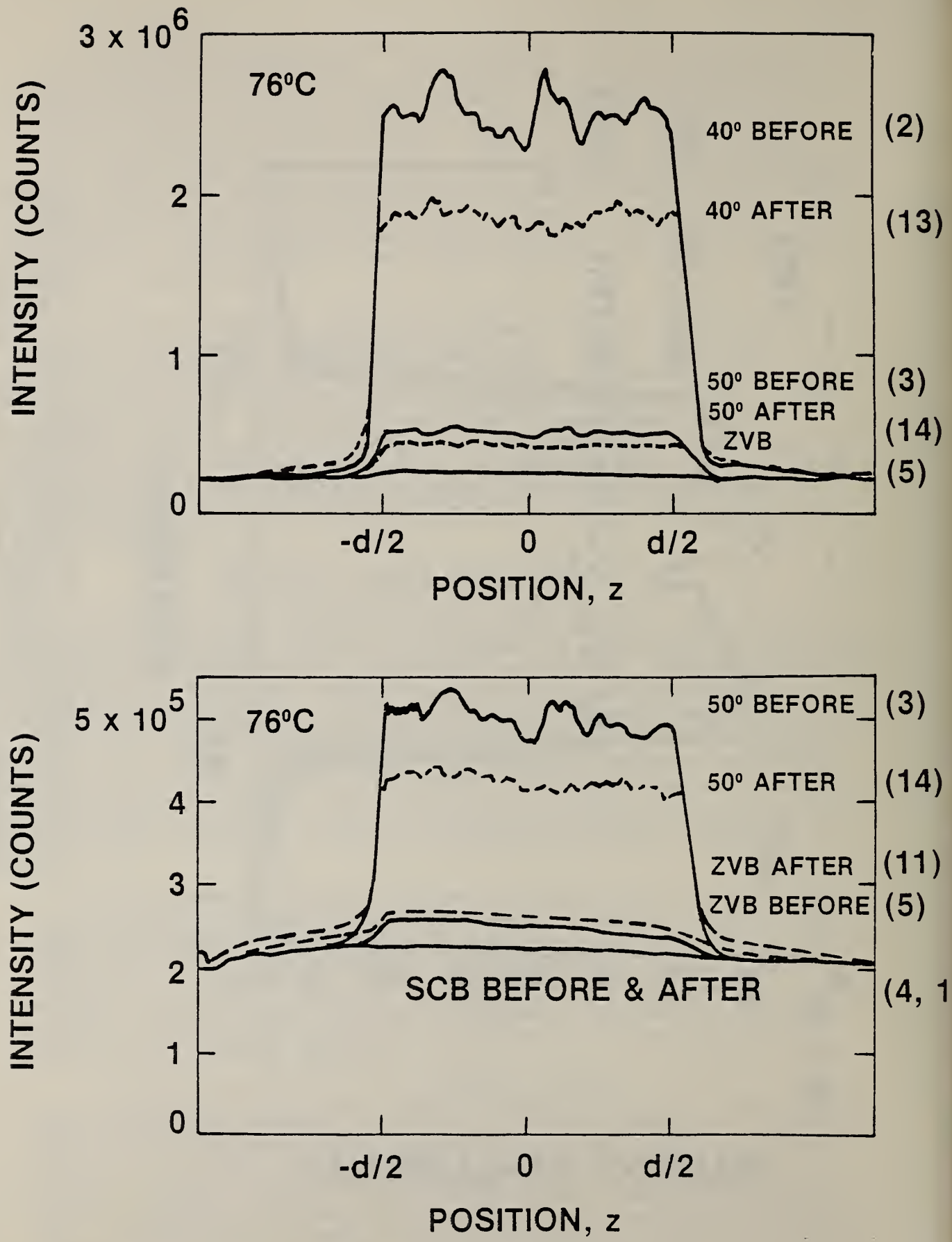

Fig. 30. Comparison before and after voltage is applied to the curves used to establish the I_m profile and the background curves. The numbers in parentheses refer to the profile number in table 5.

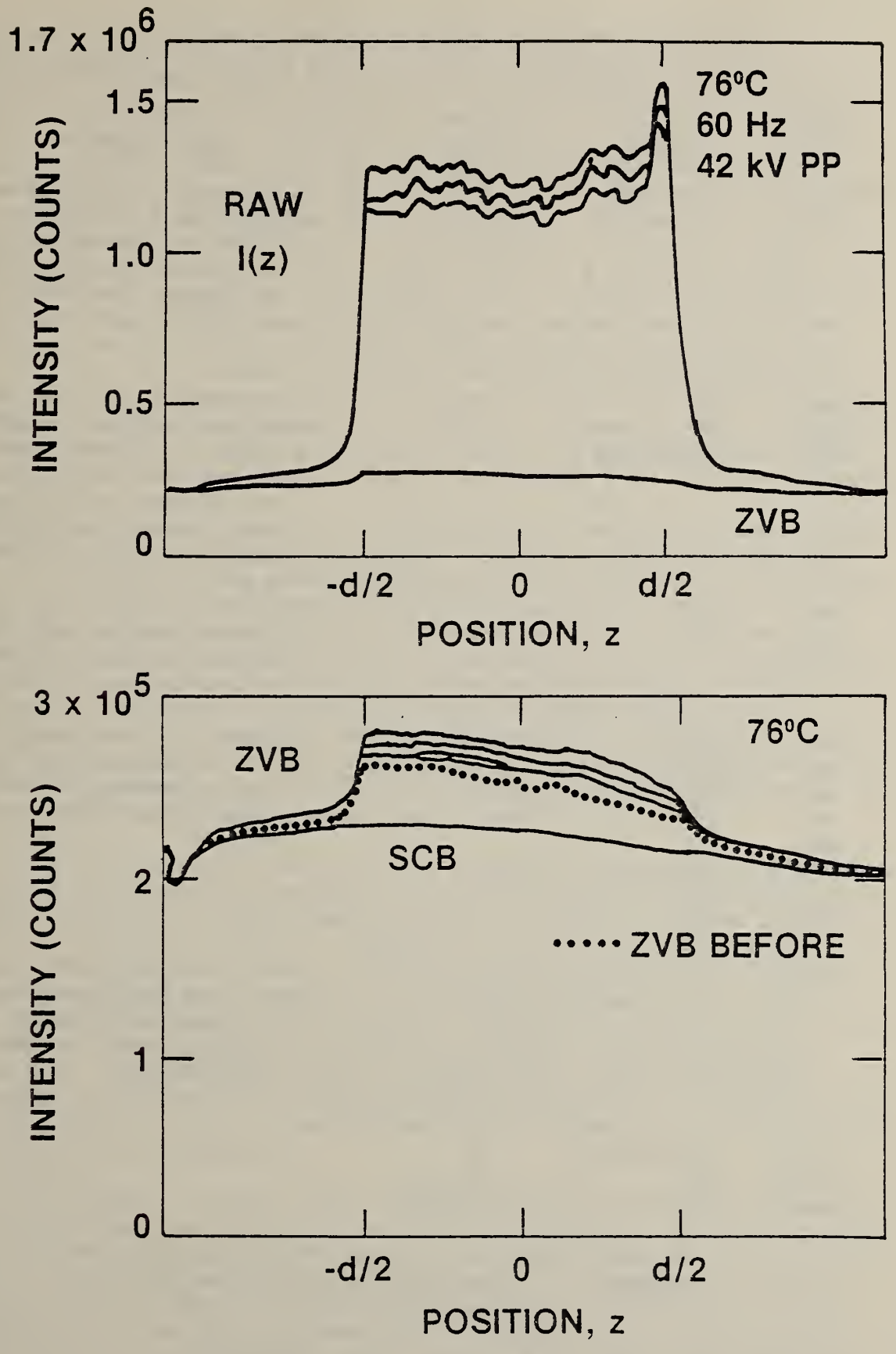

Fig. 31. Unprocessed (raw) data at 41 kVPP of 60-Hz waveform and zero-voltage backgrounds. Each curve is an accumulation of 1000 scans.

Table 5. Data collection sequence

Profile No.	Symbol	Figure No.	Description
M1	AP (#1NDF)	29	Polarizers are aligned and a 1.0 neutral density filter is placed at NDF-1 in figure 14. This filter is removed after this profile is obtained.
M2	40°	30	Polarizers almost crossed.
M3	50°	"	Polarizers almost crossed.
M4	SCB or NSB	"	A shutter is closed ahead of the detector to determine the detector background, and/or the illumination is blocked to give a no-signal background.
M5	ZVB	"	With the shutter open a background is obtained with no voltage applied. Polarizers are crossed.
M6	V_1	31	A profile is obtained with the voltage on, then off, for a sequence of at least three times; four are shown here.
M7	ZVB	"	
M8	V_1	"	
M9	ZVB	"	
M10	V_1	"	
M11	ZVB	"	
M12	V_1	"	
M13	ZVB	"	
---	V_2, V_3, etc.		The above on-off sequence is repeated for each voltage level or phase (for 60-Hz).
M14	SCB or NSB	30	As above.
M15	40°	"	
M16	50°	"	
M17	AP (#1NDF)	29	As above M1

not change in shape significantly for ±10° about the crossed polarizer setting. Because of a scale error the polarizers are crossed when polarizer P2 (see fig. 14) is set at 47.5° with respect to the vertical plates. The incident profile $I_m(z)$ is determined from the 40° and 50° profiles before and after the application of voltage (profiles M2, M3, M15, M16) by first subtracting off the zero-volts background (ZVB, intensity through crossed polarizers, e.g., profile M5), then normalizing each curve to 1, averaging the four profiles, and then multiplying the result by the average magnitude of the AP profiles -- the magnitude of I_m. The result is shown in figure 32. Any average of a profile is made along the "level" portion of the profile, i.e., the level region defined by where the the profile breaks off its steep intensification from low background levels. (If the 40°-50° profiles are dramatically different after the data is collected than before, the profiles taken before the voltage data may be ignored since this would indicate that the application of voltage modified the intensity distribution. Whenever this is the case, it is also obvious in the ZVB profiles --- the ZVB profiles change after the voltage has been applied but they do not change from that point onward.)

To obtain the net signal profile for the Kerr effect at some voltage, the three or, in this case, four voltage profiles (profiles M6, M8, M10, M12) are averaged and the average background (an average of ZVB, profiles M7, M9, M11, M13) is subtracted from it; the result is in figure 33. Usually the profile is set to zero at the assumed position of the plates ($z = \pm d/2$) so the place location can be determined easily throughout the remaining data handling (see fig. 33). The relative intensity profile $I(z)/I_m(z)$ is obtained by a pointwise division of the two profiles (see fig. 34). It is only the information contained between $-d/2 \leq z \leq d/2$ that is of interest. Finally, using the approximate relation between E/E_m and I/I_m expressed in eq (30), $E(z)/E_m$ may be calculated (see fig. 35). The data handling process is summarized in table 6.

It is rather evident that there is a possible intensity shift problem during the course of an experiment. This is evident in the dramatic change of intensity of the aligned-polarizer profiles in figure 29. Some of this is due to the gradual introduction of particles into the gap during the voltage application. The fact that the oil is well-filtered before the application of voltage is evidenced by the lack of forward light scattering from the laser beam as it passes through the cell. While the voltage is applied, particles (diameters > 2 μm) accumulate in the gap. These particles serve to scatter the light, increasing the background in the areas shadowed by the plates (fig. 31) and serve to depolarize the light, increasing the light transmitted through crossed polarizers (fig. 32).

An additional problem is the intermittent failure of the laser which could explain why the I(z) profiles in figure 32 are not all at the same level (though they are the same shape). In either case, it is not really important that we obtain absolute measurements at this time. If we needed to know the absolute space-charge density to ±10%, then it would be important to know the I/I_m accurately. However, since we are trying to obtain only an indication of space charge, approximate magnitudes are sufficient. The profile shapes, not their absolute magnitude, are important to detect the presence of space charge.

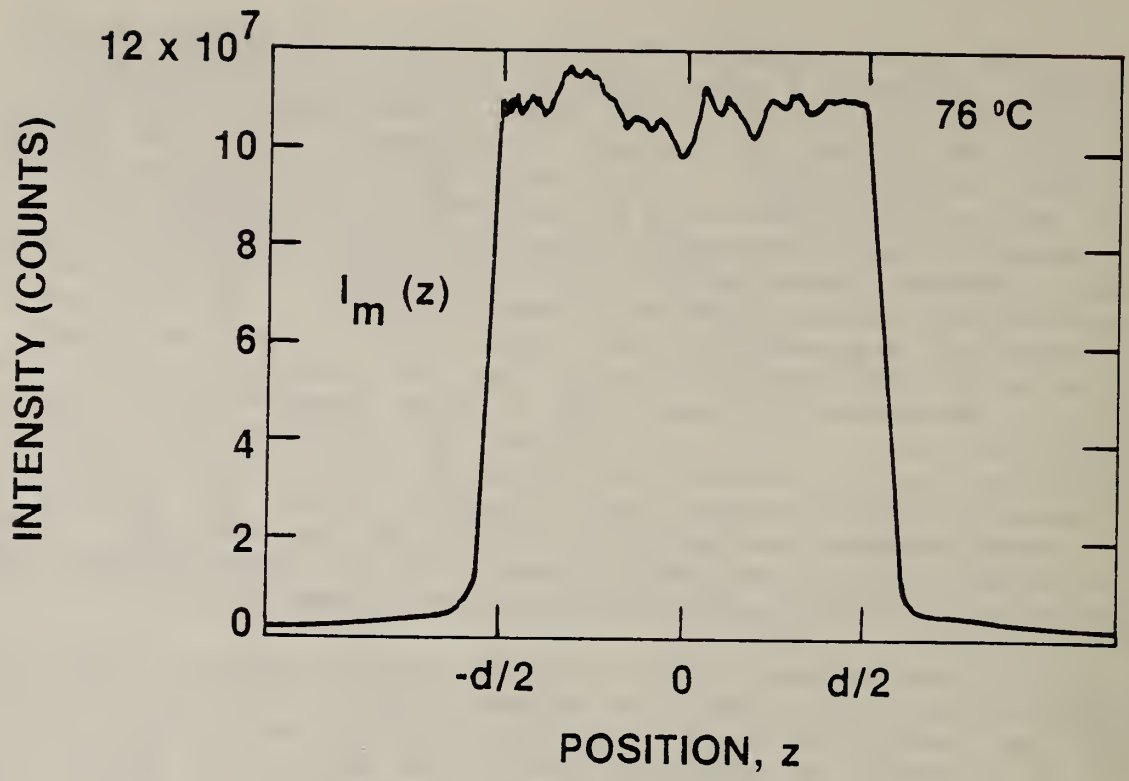

Fig. 32. The incident intensity profile $I_m(z)$.

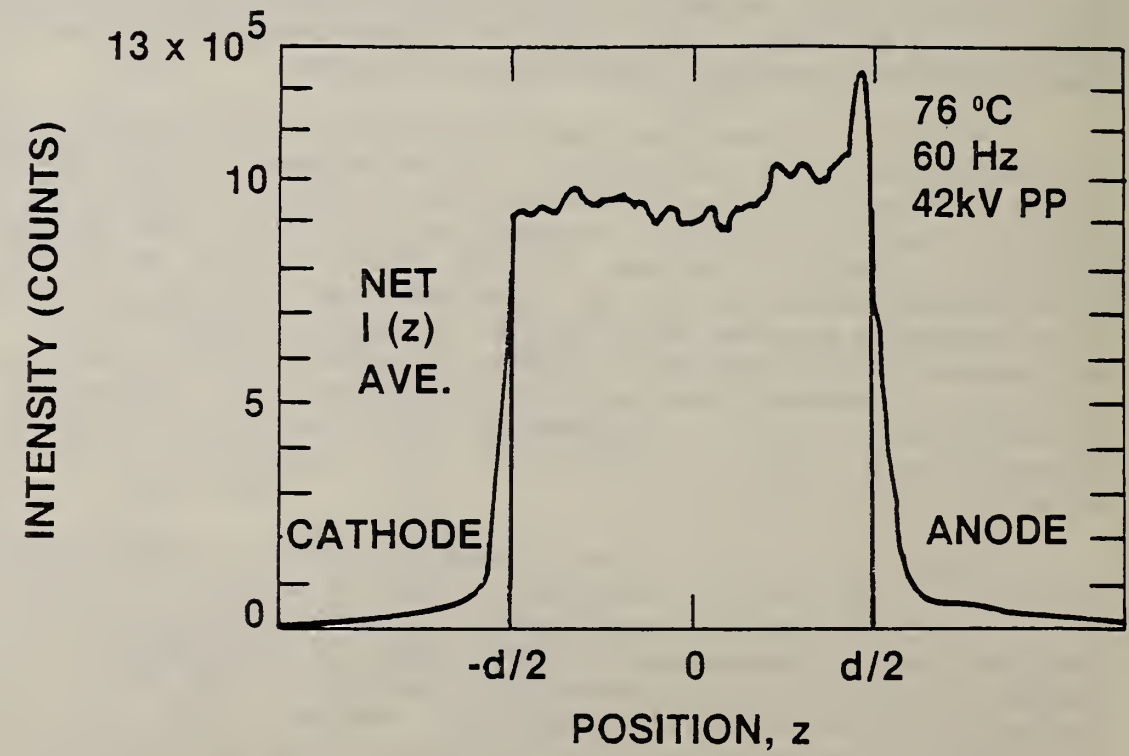

Fig. 33. The net, average Kerr profile I(z).

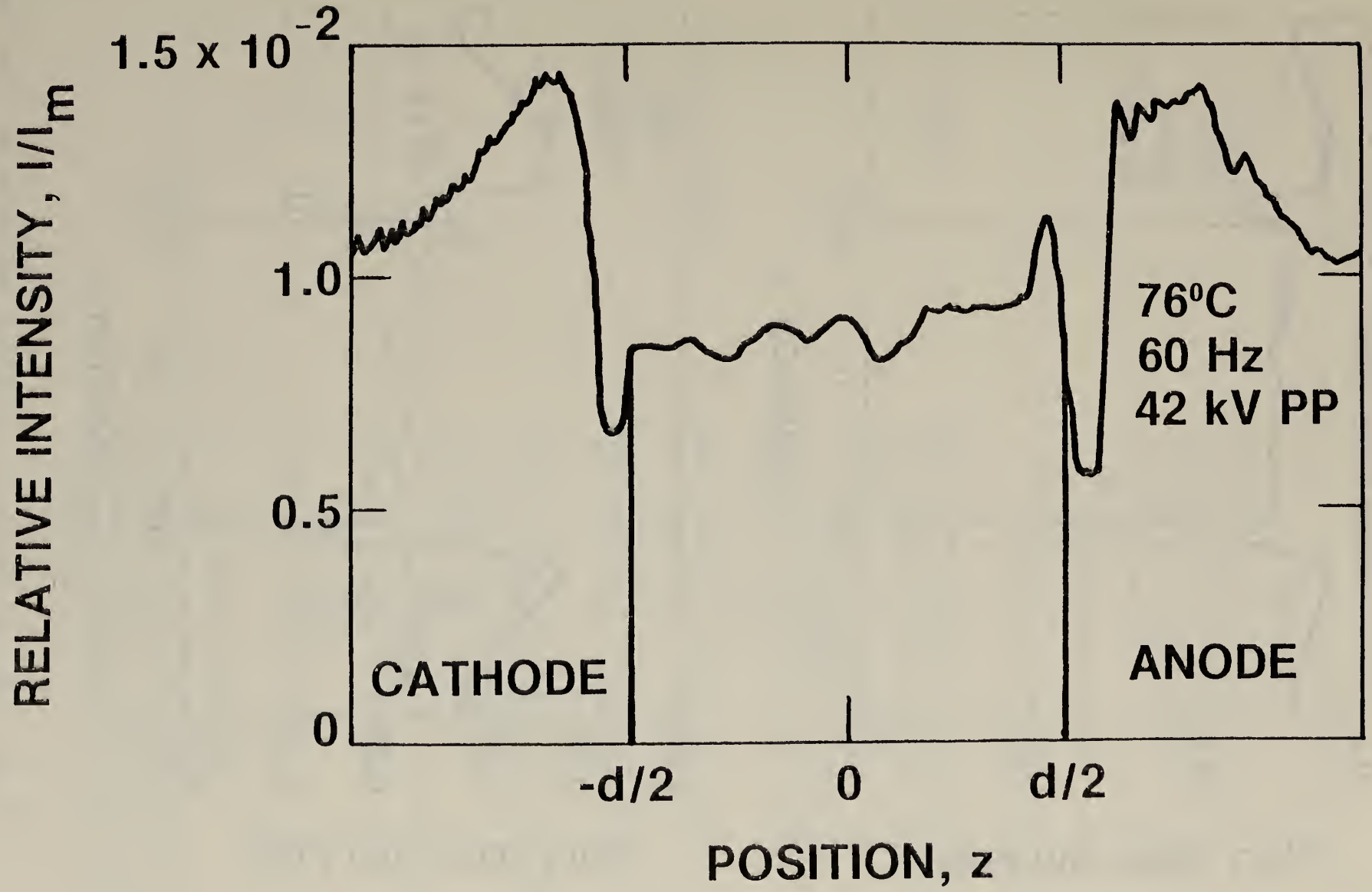

Fig. 34. The relative intensity profile $I(z)/I_m(z)$.

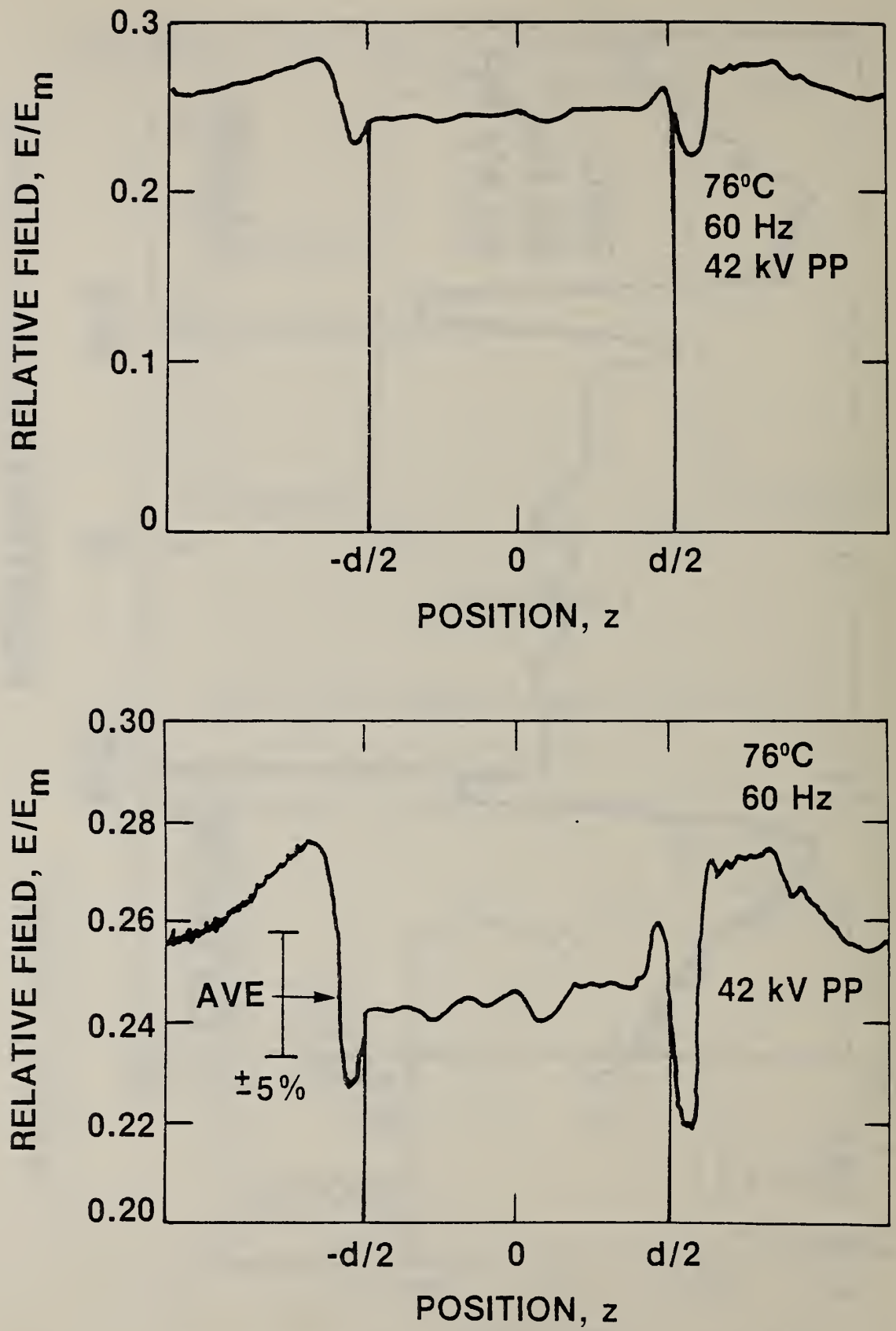

Fig. 35. Relative electric field $E(z)/E_m$; ±5% limits are shown about the average in the magnified view.

Table 6. Data handling

Result	Figure	Operation
I_m Magnitude		Subtract background (ZVB) from AP curves, obtain average values over level portion ($-d/2 \leq z \leq d/2$), average the values from before and and after the run. $I_m(1)/10$ = AVE(M1-M4-(M5-M4)/10) $\simeq 12.5 \times 10^6$ $I_m(2)/10$ = AVE(M17-M14-(M13-M14)/10) $\simeq 9.10 \times 10^6$ $\lvert I_m \rvert = (I_m(10) + I_m(2))/2 = 1.08 \times 10^8$.
I_m Profile (M18)	32	Subtract backgrounds (ZVB) from 40° and 50° curves (before and after run), normalize and average the four curves, multiply by $\lvert I_m \rvert$. M18 = $I_m(z) = \lvert I_m \rvert$[NORM(M2) + NORM(M3) + NORM(M15) + NORM(M16)]/4 where, e.g., NORM(M2)= M2/AVE(M2) where average is made over level portion ($-d/z \leq z \leq d/2$).
Raw I(z) Average (M19)		Obtain average of voltage-on profiles. M19 = (M6 + M8 + M10 + M12)/4
ZVB Average (M20)		Obtain average of voltage-off profiles. M20 = (M7 + M9 + M11 + M13)/4
I(z) Net (M21)	33	Subtracting the average of the voltage-on and voltage-off profiles is equivalent to averaging the subtraction of the voltage-on/off profiles. M21 = M19 - M20 Set I(z) = 0 at $z = \pm d/2$ to mark plates.
$I(z)/I_m(z)$ (M22)	34	Perform pointwise division of I by I_m M22 = M21/M18
$E(z)/E_m$ (M23)	35	Perform pointwise operation on I/I_M according to eq (30). M23 = (0.40528 * M22) (1/4) The average value with standard deviation ($-d/2 \leq z \leq d/2$) is 0.245 ±0.004 (1.67%). The maximum E/E_m is 0.261 (6.4% high from average), the minimum is 0.239 (2.3% low from average).

Now that we have established the electric field profile shown in figure 35, several comments are in order. First, if the nonuniformity of the field is due to space charge, then the field nonuniformities can be confined to less than 10% of the applied field. Second, the small peak to the left of z = d/2 is characteristic of a reflection off a plate or part of a diffraction pattern arising from optical alignment problems. It would be reasonable to ignore the peak on that basis thus reducing the field nonuniformity, but we will not do so since it has not been definitely established that such a peak is not due to space charge. Third, the overall slope of the profile is opposite to that obtained previously on contaminated oil -- compare figure 36 with figure 29. Either the nature of the space charge was different or the slope is due to systematic effects. Because of the data to follow, it is suspected that there are yet systematic problems associated with optical alignment which give rise to a nonuniform intensity profile which can be mistaken as a space charge.

In figures 36 through 38 we show $E(z)/E_m$ profiles for the positive peak (PP) of a 60-Hz waveform at oil temperatures of 86°C, 95°C, and 107°C respectively. Each curve in these figures represents an accumulation of I(z) for 3000 to 4000 cycles of the 60-Hz waveform. In figure 36, the 86°C E/E_m profile shows an enhancement at the cathode as we saw in the 76°C (fig. 35). Similarly, all the field nonuniformities can be contained within 10% of field maximum. In the 95°C data (fig. 37), we see a sharper apparent field enhancement at the cathode. It can, however, no longer be confined to 10% of the field maximum. If this were a trend and not a result of optical alignment, then at higher temperatures we would expect more enhancement -- an enhancement which would not depend upon small changes in alignment. The cell's position was changed during the course of these experiments, if not by thermal expansion of parts then by direct alignment changes. The 107°C E/E_m profiles in figure 38 show some enhancement at the cathode -- especially for the lower voltages -- but there is essentially no enhancement at the highest fields. This result suggests that the previous field nonuniformities are due to systematic effects and not due to space charge.

Referring to figure 38, there seems to be a trend toward field enhancement at lower voltages. However, when the intensity profiles are examined (fig. 39), we find that the low-voltage profiles are near background levels --- levels which could easily exhibit the nonuniformity of the polarizer's parallelism. Therefore, these low-intensity data cannot be trusted.

Another possible source of error is nonuniform optical activity of the cell-tank-polarizer system. It is conceivable that multiple reflections between non-parallel window surfaces, temperature dependent optical activity of windows, reflections off the plate surfaces, and/or index of refraction changes due to nonuniform heating of the oil between the plate could make the system nonuniformly sensitive to the polarization direction of the light passing through the cell. Such possibilities must be investigated before more sensitive measurements can be made; however, this hypothesis is verified to some extent since the profile shape seems sensitive to the alignment of the system with the laser beam.

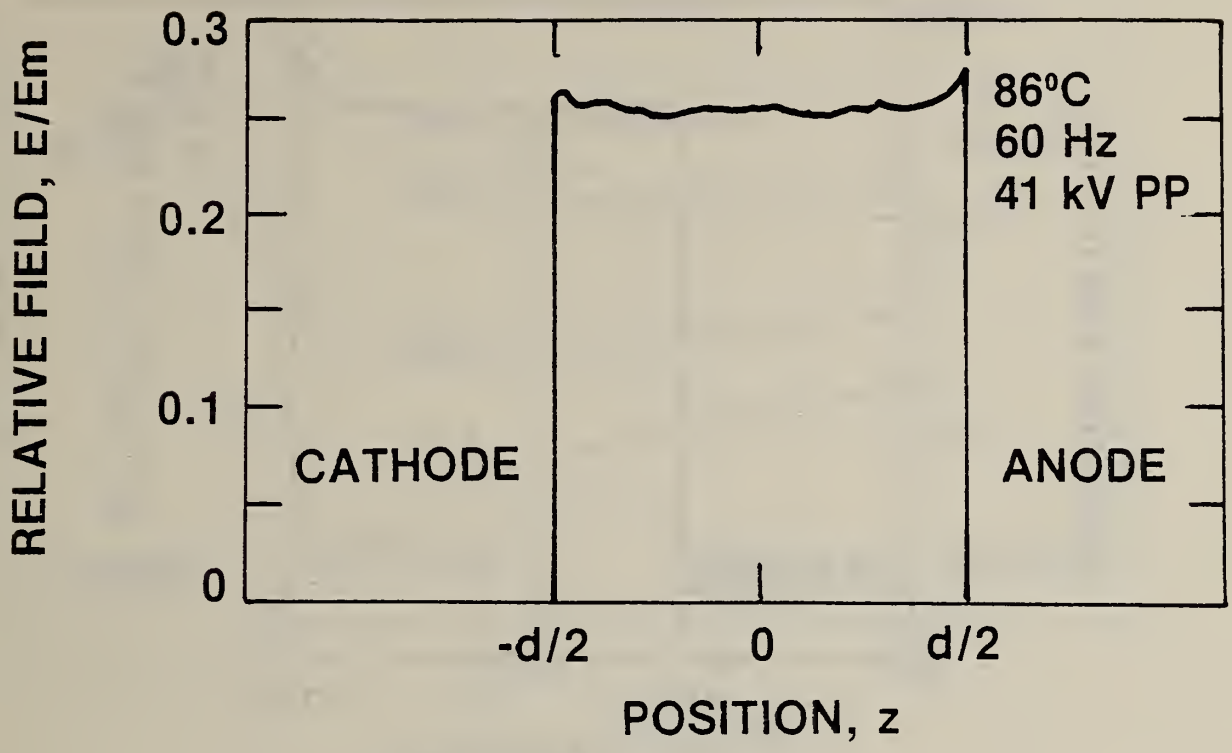

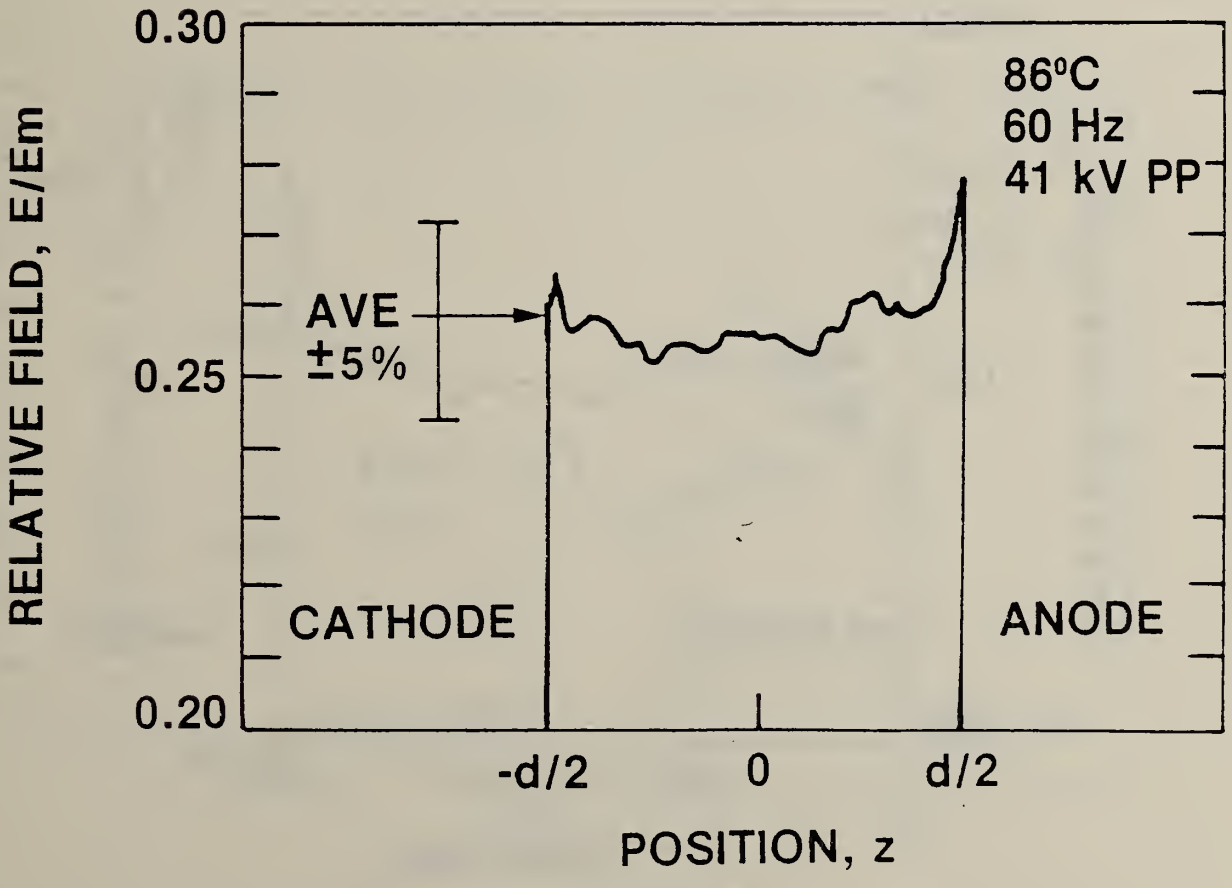

Fig. 36. Relative field for 86°C.

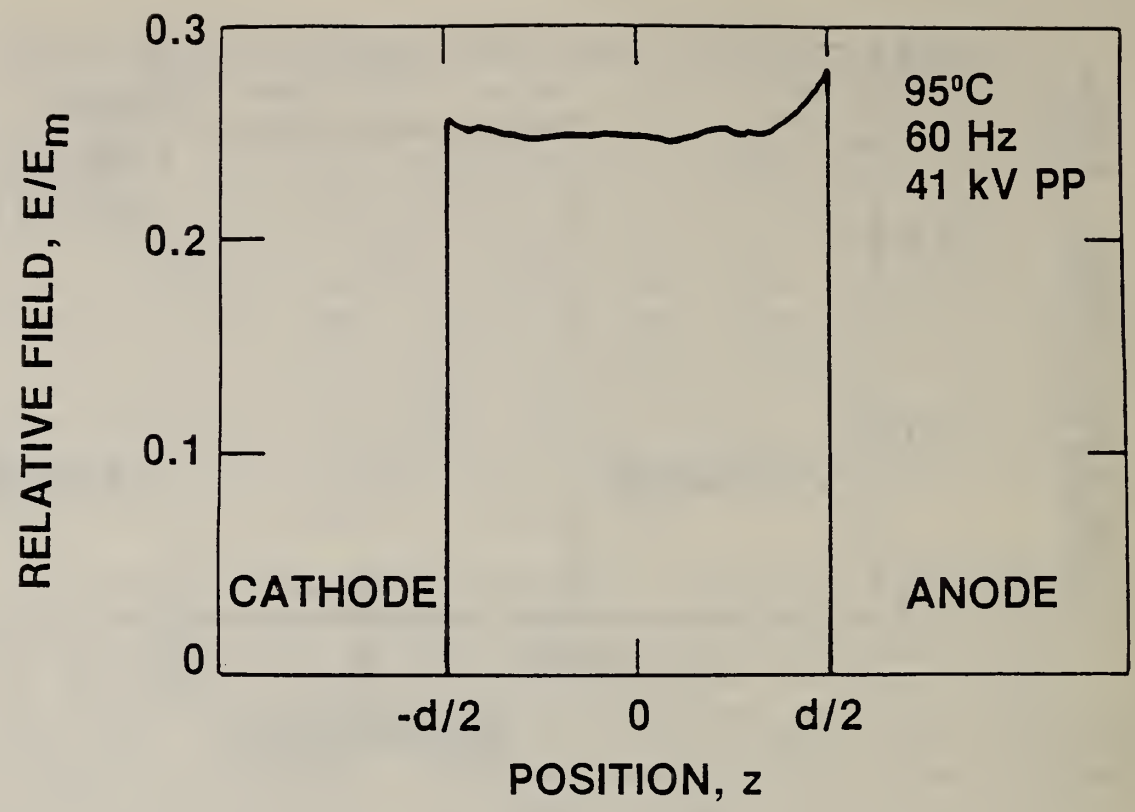

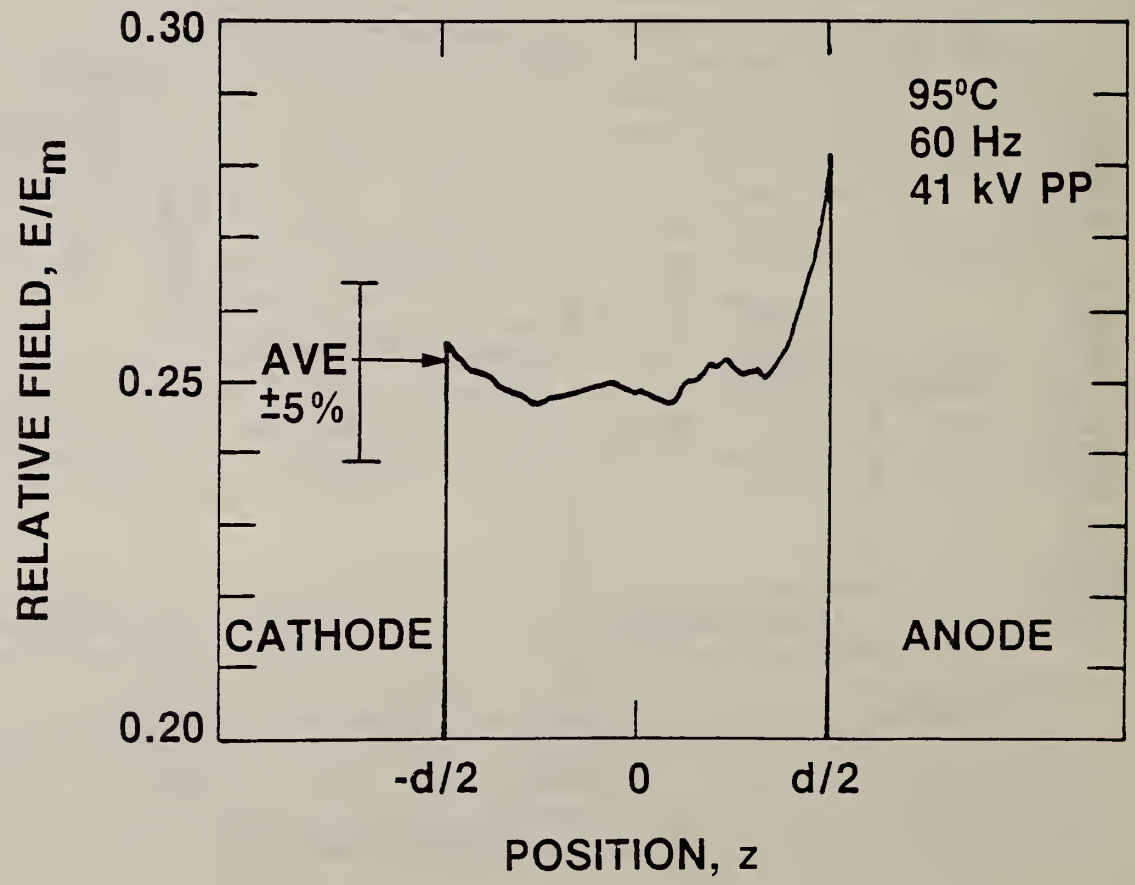

Fig. 37. Relative field for 95°C.

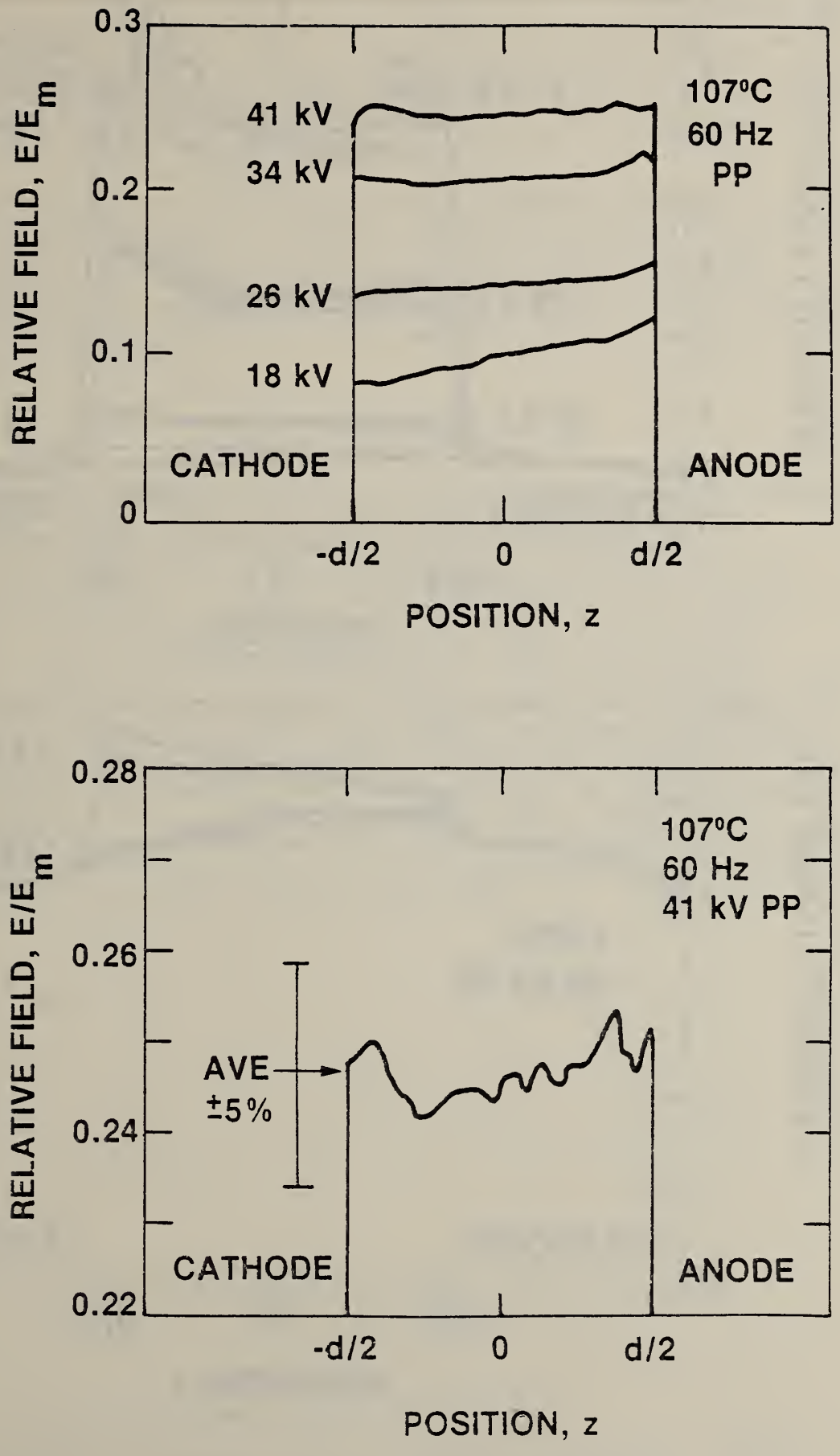

Fig. 38. Relative field for 107°C.

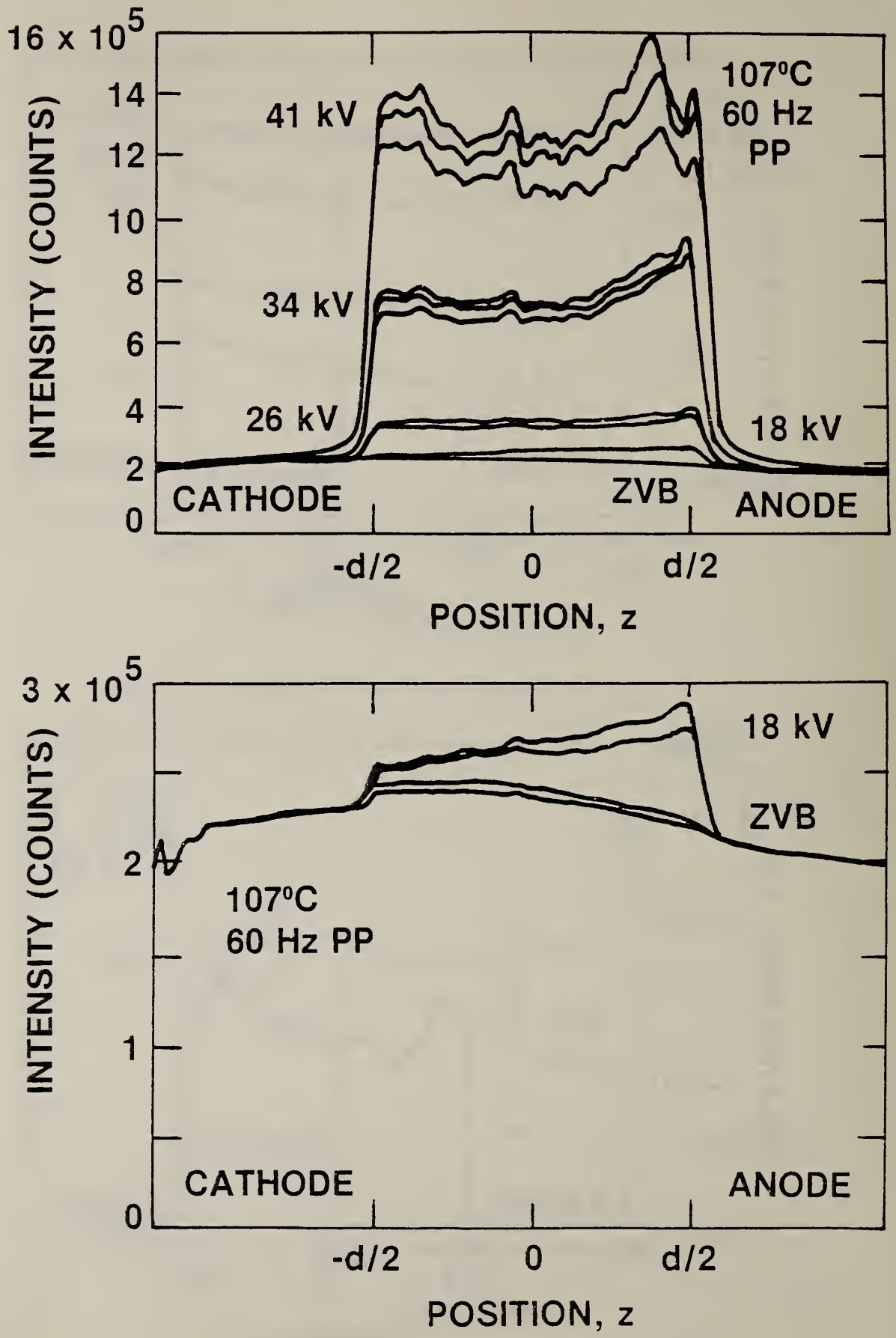

Fig. 39. Intensity profiles at various voltages for 107°C oil compared to background signal levels.

Previously we noted (figs. 21,22) that space charge in nitrobenzene persisted through the zero crossing of the 60-Hz waveform. This is not observed in the 107°C data at the positive-negative zero crossing (PNZC) of the 42kV 60-Hz waveform (see fig. 40). This also indicates that space charge may not be present in transformer oil.

The results taken for dc show dramatic intensification near the plates (fig. 41); however, the non-symmetric profile shows no polarity sensitivity which tends to rule out space charge in favor of optical alignment or activity problems. With increasing temperatures, the E/E_m profiles are U-shaped and rather symmetrical. However, the maximum distortion of the field at the highest voltage is still less than 10% of the field maximum (see fig. 42).

V. CONCLUSION

In this report we calculated the field modifications due to space or surface charges. Next, we examined data which showed that an interfacial system need not break down at the interface even in a contaminated system, and we discussed how the condition of the paper influences breakdown. We then turned our attention to space charge in liquids, and characterized the space charge found in nitrobenzene at 60-Hz ac. A saturation space charge of over -400 nC/cm^3 could be measured electro-optically at the cathode. Finally, these electro-optical measurement techniques were applied to transformer oil. There it was found that no field distortions greater than ±5% of the average field could be attributed to space charge. This was true for clean or contaminated transformer oil from room temperature to 100°C or above. These results will be refined and carried to higher temperatures; nonuniform electrode geometries, and interfaces in the future to quantify the contribution of space charge to the electrical characteristics of insulating liquids under practical conditions.

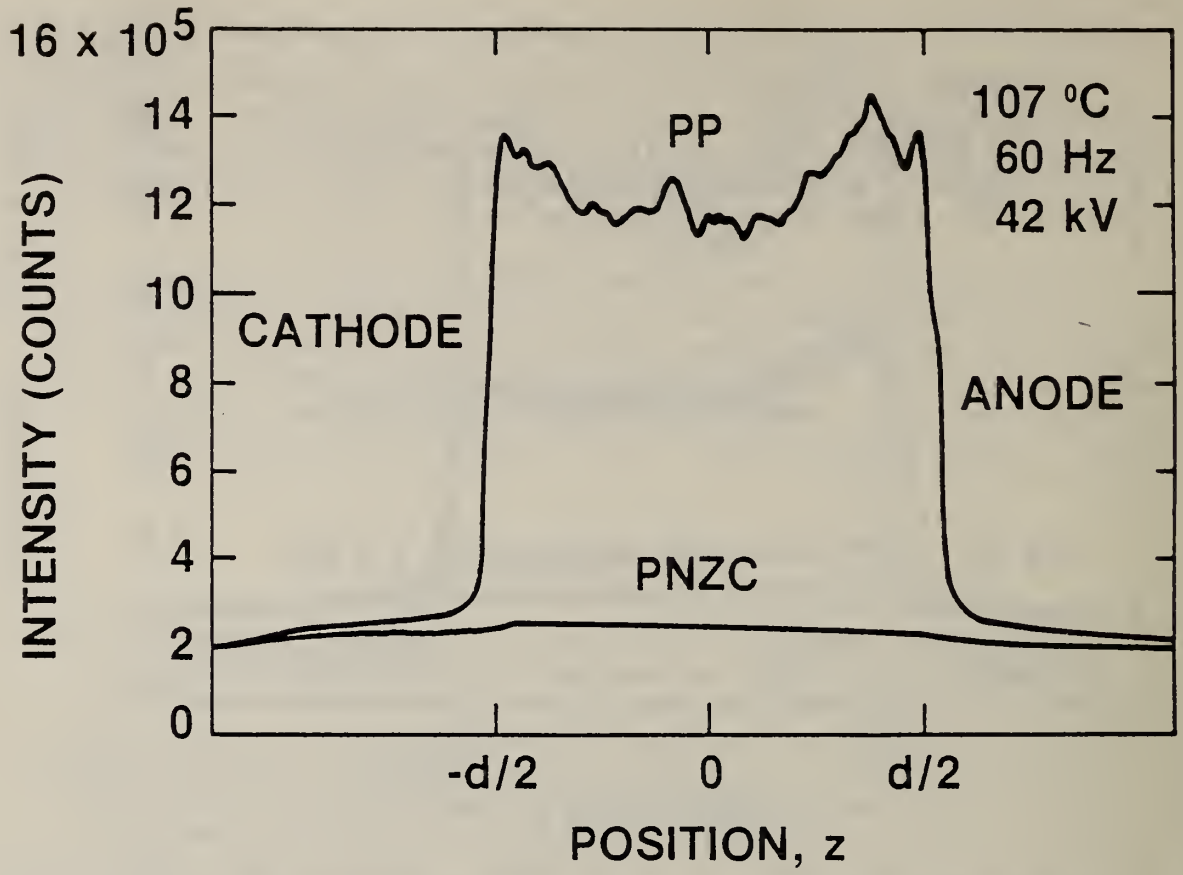

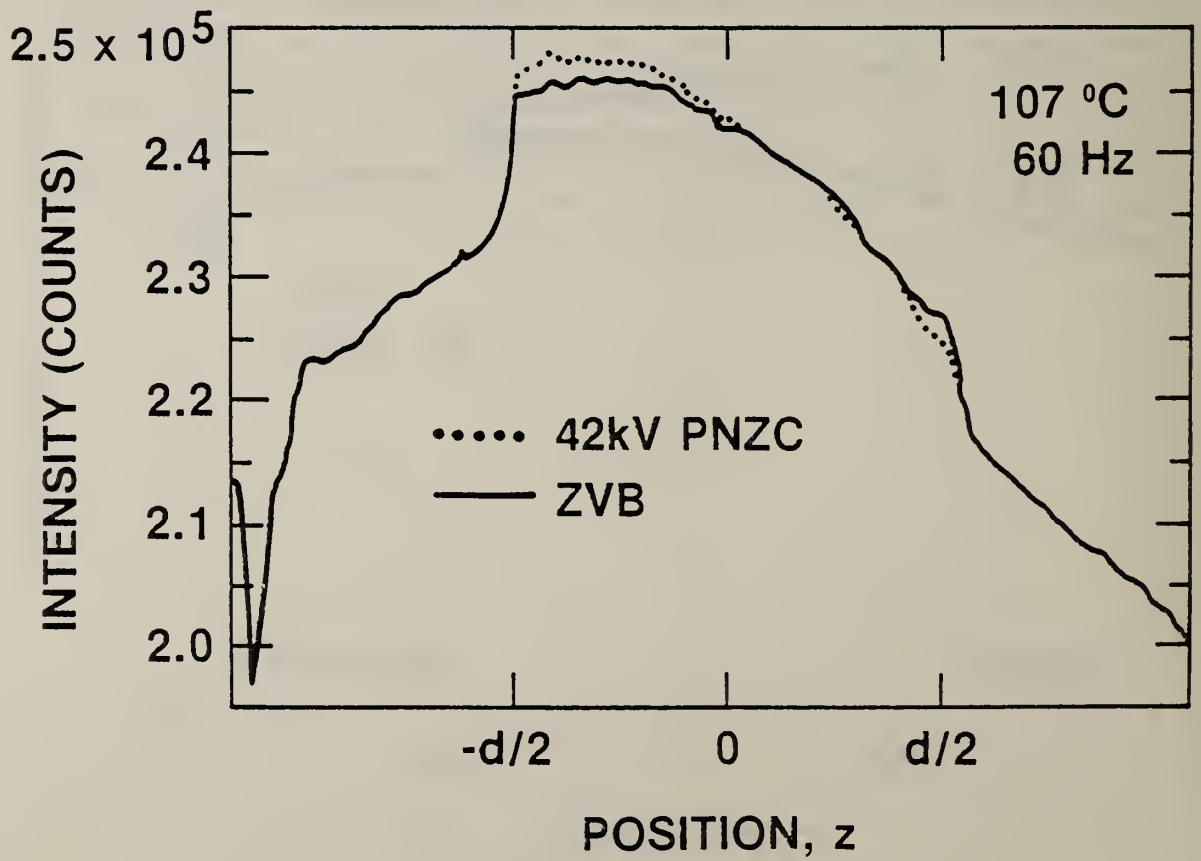

Fig. 40. Comparison of the 60-Hz intensity profiles taken at the positive peak (PP), the positive-negative zero crossing (PNZC), and the zero-voltage background reveals no significant space charge as would be found with observations of the 60-Hz zero crossing in nitrobenzene.

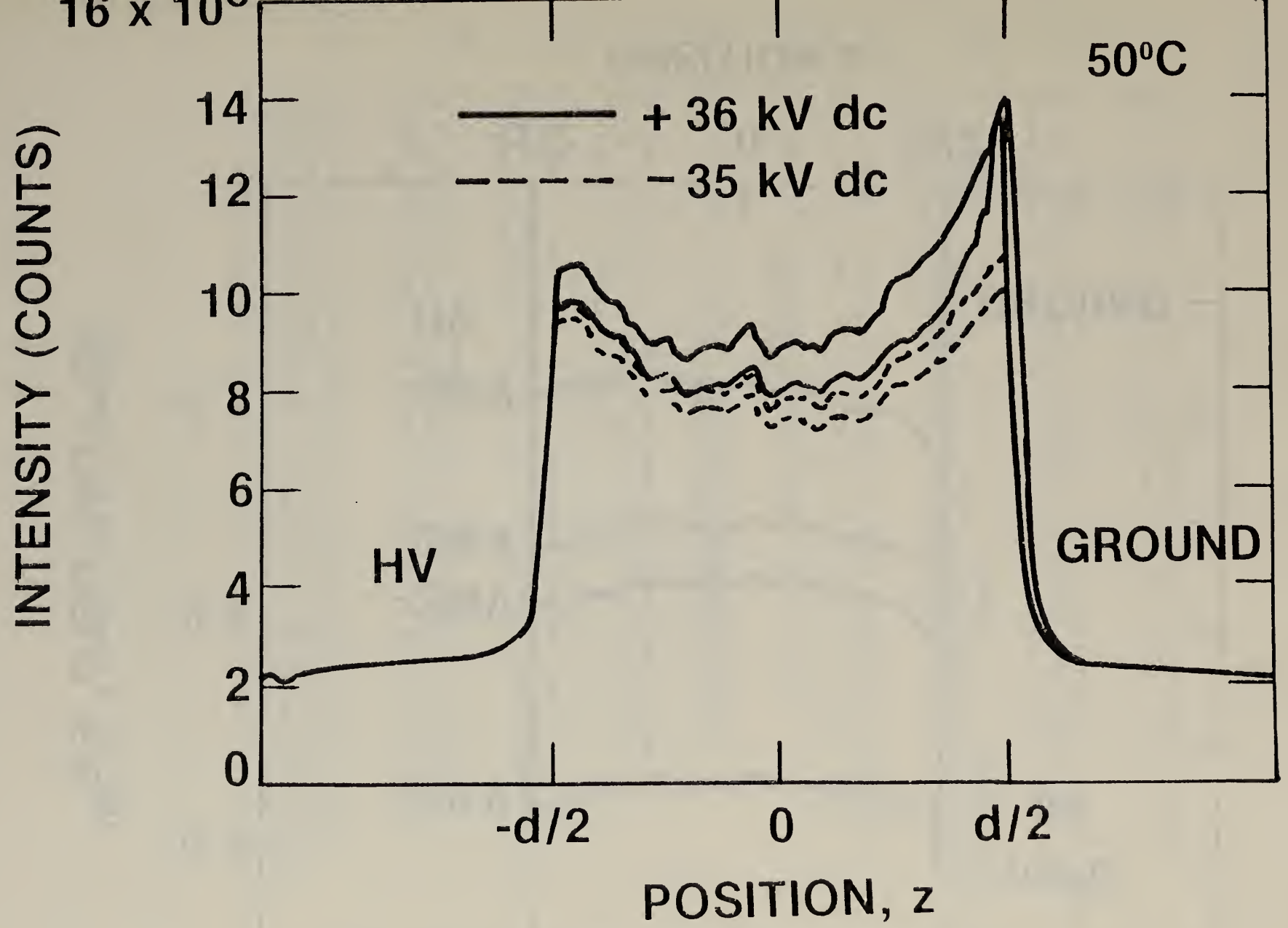

Fig. 41. Intensity profiles under application of dc. No polarity dependence of shape is obvious as would be expected if the deviations from intensity uniformity were arising from space-charge field distortions.

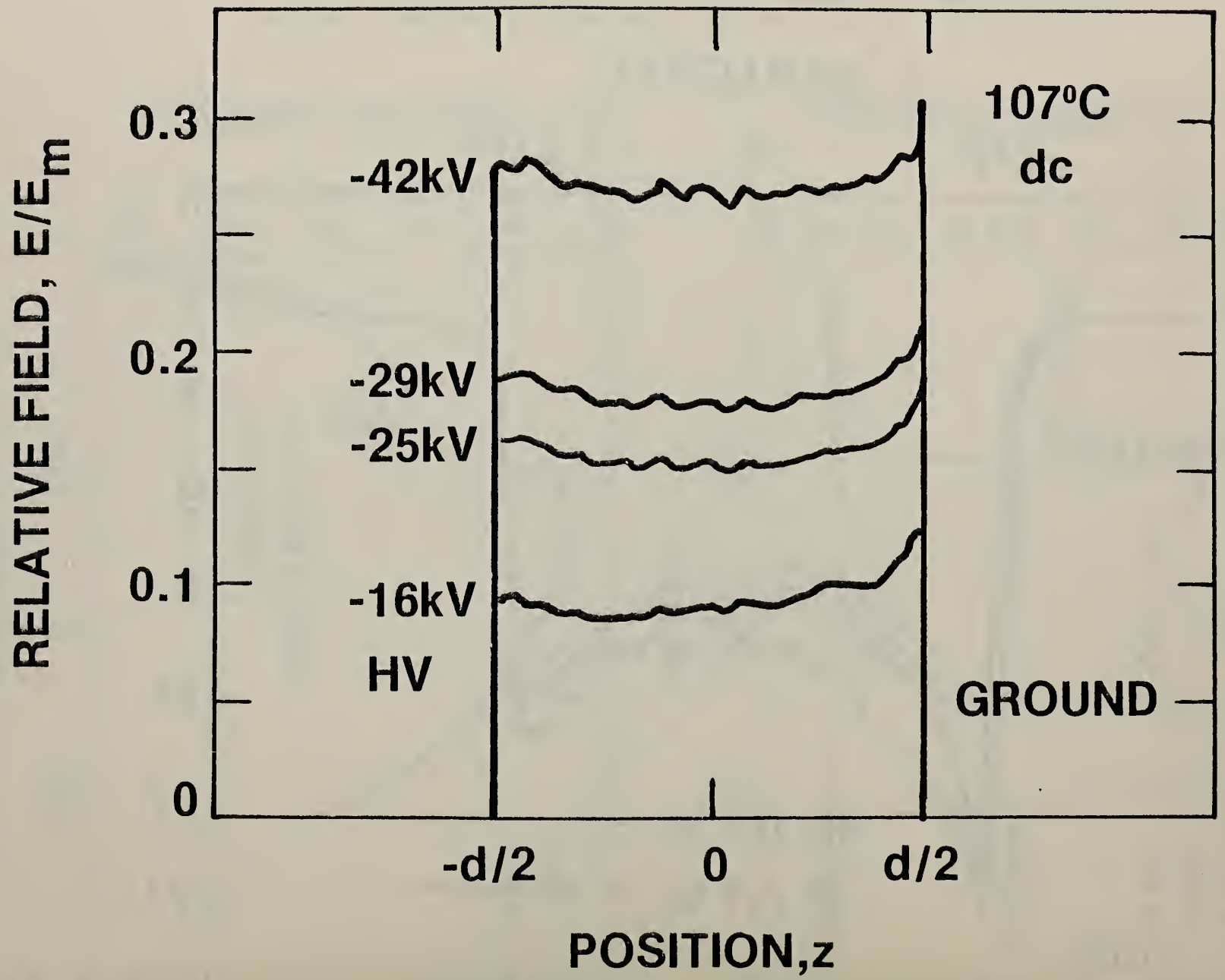

Fig. 42. Relative field profiles at 107°C under application of dc show slight intensification at each plate.

VI. REFERENCES

[1] J. E. Thompson, J. Lin, K. Mikkelson, and M. Kristiansen, Electro-Optical Surface Flashover Measurements, Appl. Phys. Let. Vol. 37, No. 6, 15 Sep. 1980, p. 574-576.

[2] J. E. Thompson, J. Lin, K. Mikkelson, and M. Kristiansen, Investigations of Fast Insulator Surface Flashover in Vacuum, IEEE Trans. on Plasma Science, Vol. PS-8, No. 3, Sept. 1980, pp. 191-197.

[3] R. E. Hebner, Jr., E. F. Kelley, J. E. Thompson, T. S. Sudarshan, and T. B. Jones, 1980 Annual Report: Optical measurements for interfacial conduction and breakdown, Nat. Bur. Stand. (U.S.), NBSIR 81-2275, 83 pages (May 1981).

[4] T. J. Lanoue, Insulation Studies for Power Frequency Improvement, Report on Contract ET-78-C-01-3058, U.S. Dept. of Energy, 1980.

[5] A. Zygmund, Trigonometric Series Vol. I , pp. 16, 19 (Cambridge U. Press 1959).

[6] P. Morse and H. Feshbach, Methods of Theoretical Physics, Part I, pp. 82, 456 (McGraw Hill Book Co., 1953).

[7] Fortran subroutine PLTMG developed by R. Bank and A. Scherman of the University of Texas, and amplified and modified by J. Blue and C. Wilson of NBS.

[8] E. F. Kelley and R. E. Hebner, Breakdown between bare electrodes with an oil-paper interface," Nat. Bur. Stand. (U.S.), NBSIR 80-2071, 33 pages (June 1980).

[9] E. C. Cassidy, R. E. Hebner, Jr., M. Zahn, and R. J. Sojka, Kerr-Effect Studies of an Insulating Liquid Under Varied High-Voltage Conditions, IEEE Trans. Elec. Insul., Vol. EI-9, No. 2, June 1974, pp. 43-56.

[10] P. D. Thacher, Optical Effects of Fringing Fields in Kerr Cells, IEEE Trans. Elec. Insul., Vol. EI-11, No. 2, June 1976, pp. 40-50. (A rather complete analysis is given here to determine perturbations in the uniform-field Kerr patterns because of fringing fields of real vs. ideal plates as well as the effects of windows in the cell.)

NBS-114A (REV. 2-8C)

U.S. DEPT. OF COMM. BIBLIOGRAPHIC DATA SHEET (See instructions)	1. PUBLICATION OR REPORT NO. NBSIR 82-2629	2. Performing Organ. Report No.	3. Publication Date January 1983

4. TITLE AND SUBTITLE

1981 ANNUAL REPORT: OPTICAL MEASUREMENTS FOR INTERFACIAL CONDUCTION AND BREAKDOWN

5. AUTHOR(S)

R. E. Hebner, Jr., E. F. Kelley, and J. N. Hagler

6. PERFORMING ORGANIZATION (If joint or other than NBS, see instructions)

NATIONAL BUREAU OF STANDARDS
DEPARTMENT OF COMMERCE
WASHINGTON, D.C. 20234

7. Contract/Grant No.

8. Type of Report & Period Covered
Final

9. SPONSORING ORGANIZATION NAME AND COMPLETE ADDRESS (Street, City, State, ZIP)

Prepared for
Department of Energy
Division of Electric Energy Systems
Washington, DC 20585

10. SUPPLEMENTARY NOTES

☐ Document describes a computer program; SF-185, FIPS Software Summary, is attached.

11. ABSTRACT (A 200-word or less factual summary of most significant information. If document includes a significant bibliography or literature survey, mention it here)

This report presents measurements and calculations contributing to the understanding of space and surface charges in practical insulation systems. Calculations are presented which indicate the size of charge densities necessary to appreciably modify the electric field from what would be calculated from geometrical considerations alone. Experimental data is also presented which locates the breakdown in an electrode system with a paper sample bridging the gap between the electrodes. It is found that with careful handling, the breakdown does not necessarily occur along the interface even if heavily contaminated oil is used.

The effects of space charge in the bulk liquid are electro-optically examined in nitrobenzene and transformer oil. Several levels of contamination in transformer oil are investigated. Whereas much space charge can be observed in nitrobenzene, very little space charge, if any, can be observed in the transformer oil samples even at temperatures near 100°C.

12. KEY WORDS (Six to twelve entries; alphabetical order; capitalize only proper names; and separate key words by semicolons)

breakdown; composite insulation; dielectrics; electric field calculation; electro-optics; high voltage; insulation; interfaces; Kerr effect; liquids; solids.

13. AVAILABILITY

☒ Unlimited

☐ For Official Distribution. Do Not Release to NTIS

☐ Order From Superintendent of Documents, U.S. Government Printing Office, Washington, D.C. 20402.

☒ Order From National Technical Information Service (NTIS), Springfield, VA. 22161

14. NO. OF PRINTED PAGES
82

15. Price
$11.50